

**Numerical Modeling and Analysis of Static and Ballistic Behavior of
Multi-layered/Multiphase Composite Materials Using Detailed
Microstructural Discretization**

A Thesis

Submitted to the Faculty

of

Drexel University

by

Jovan M. Jovicic

in partial fulfillment of the
requirements for the degree

of

Doctor of Philosophy

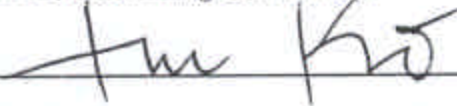
April 2003

Thesis Approval Form

This thesis, entitled _____
_____ Numerical Modeling and Analysis of Static and Ballistic Behavior of Multi-layered/Multiphase
_____ Composite Materials Using Detailed Microstructural Discretization _____ and authored
by _____ Jovan M. Jovicic _____, is hereby accepted and approved.

Signatures:

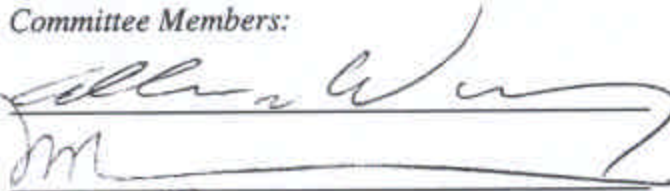
Chairman, Examining Committee:

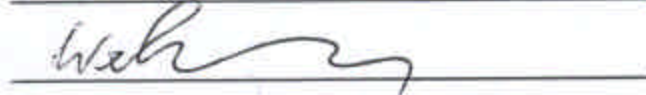
_____  _____

Supervising Professor:

_____  _____

Committee Members:

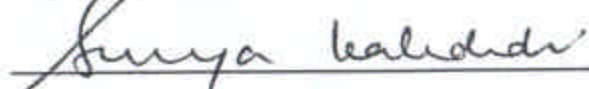
_____  _____

_____  _____

Graduate Advisor:

_____  _____

Department Head:

_____  _____

Dedications

This work is dedicated to my wife Vesna, mother of our sons Stefan and Filip. She has encouraged me through this work and provided tremendous emotional support. Vesna willingly sacrificed part of her life, allowing me to pursue my dreams, and I can only hope to someday make that up to her. Her presence in my life has made all of this possible.

I would also like to dedicate this thesis to my parents. To my father Milenko, whose life and work has always been, and still is, my continual inspiration, and to my mother Kostadinka, for all her endless love and support.

Acknowledgements

First and foremost, I want to thank Dr. Frank K. Ko, my advisor, for providing me with the wonderful opportunity to complete my doctoral studies under his exceptional guidance. He not only provided me with the necessary funding to complete my doctoral studies, as well as to attend several conferences in the area of composite materials, but without his patience, constant encouragement, guidance and knowledge, this work would not have been possible. Through weekly meetings and his open door policy, which I'm sure I've misused at times, Dr. Ko made an immense contribution to this dissertation and my academic growth, as well as my professional and personal life.

I would also like to express my gratitude towards my co-advisor Dr. Antonios Zavaliangos, who I'm grateful for his practical experience and technical knowledge that made an invaluable contribution to this dissertation. I appreciate the time he invested in advising me and for his openness, honesty, and sincerity.

I owe thanks to all of the people at the Fibrous Materials Research Center who have always been willing to provide assistance, give advice, and be a friend. Their friendship made my doctoral studies an enjoyable experience.

All of the people at the Department of Materials Science and Engineering of Drexel University also deserve thanks for their help and many fruitful discussions.

The time I spent at Drexel University has made a lasting impression on my life.

Table of Contents

List of Tables	vi
List of Figures	vii
Abstract	xii
1. INTRODUCTION.....	1
2. BACKGROUND AND OBJECTIVES	5
2.1 Textile Composites	7
2.2 Analytical and Numerical Models of Textiles and Textile Based Composites	14
2.3 Modeling Results of Impact Behavior on Multi-layered Composite Materials	21
2.4 Problem Statement	26
2.5 Thesis Objective	29
3. KEY ASPECTS OF NUMERICAL MODELING OF DYNAMIC EVENTS	32
3.1 Some Considerations in Numerical Modeling	33
4. STRUCTURE-PERFORMANCE MODELING OF 3D TEXTILE COMPOSITES	41
4.1 A New Efficient Algorithm for Structured Finite Element Mesh Generation of Fabric Geometry Models- (FE-FGM).....	44
4.2 Numerical Models of Textile Composite Unit Cells	51
4.3 The Influence of Fabric Architecture on Textile Composite Mechanical Properties	55
5. MATERIAL MODELS	65
5.1 Introduction of Failure Models	69

5.1.1 A Cracking Model for Ceramic Facing	70
5.1.2 A Brittle Tensile Failure Model	77
5.2 Element Failure Model for Polymer Matrix Composite	78
6. PROJECTILE MODELS AND CHARACTERISTICS	87
7. NUMERICAL MODELING OF IMPACT BEHAVIOR OF TEXTILE COMPOSITES.....	93
8. NUMERICAL MODELING OF IMPACT BEHAVIOR OF INTEGRATED MULTI-LAYERED/MULTIPHASE COMPOSITE MATERIAL	110
8.1 Comparison of Experimental and Numerical Results.....	129
9. CONCLUSION	137
10. FUTURE WORK (RECOMMENDATIONS).....	140
Bibliography.....	143
Appendix A: Computer Code Example	152
Vita.....	181

List of Figures

2.1 Textile Modeling Hierarchy.....	9
2.2 Classification of Fiber Architectures.....	10
2.3 Linear, Planar, and Three-Dimensional Fibrous Structures	11
2.4 Common Weave Patterns	12
2.5 3-D Braided Structure	13
2.6 Velocity as a Function of Areal Density for Multi-layered Design Composite	24
2.7 Damaged Areas on the Facing and Backing Layers of Panel After Ballistic Impact.....	25
2.8 Polymer-Reinforced Textile Composite.....	27
2.9 Polymer-Reinforced Composite With Ceramic Spheres.....	28
2.10 Ballistic Impact Modeling Parameters	29
2.11 Developed FE Models and Their Characteristics.....	30
3.1 Convergence of the Solution Study.....	40
4.1 Engineering Modeling Tool	43
4.2 Algorithm of a MAPLE Code	45
4.3 Yarn Architecture and Cross-Section.....	46
4.4 Relocation of a Node During a Mesh Sweep	50
4.5 Representative Unit Cell Models of Different Textile Composites	51
4.6 FE Model of a Woven Composite Unit Cell.....	53
4.7 Influence of Fabric Volume Fraction on Composite Elastic Properties.....	55
4.8 Shear Moduli as a Function of Volume Fraction.....	56

4.9	Young's Modulus as a Function of Laminae Stacking Sequence	57
4.10	In-Plane Elastic Properties for Angle-ply Laminated Composites	58
4.11	Stiffness as a Function of Volume Fraction for Different Textile Composite Architectures	59
4.12	The Effect of Unit Cell Architecture on In-plane Mechanical Properties	59
4.13	Out of Plane Elastic Properties as a Function of Textile Architecture	60
4.14	Stiffness of a Braided Textile Composite as a Function of Braiding Angle	60
4.15	The Influence of Yarn Cross-section on Woven Composite Mechanical Properties	61
4.16	Elastic Properties as a Function of Fabric Architecture	62
4.17	Variations of the Stress as a Function of Axial Strain	63
4.18	Fabric Crimp Effect on Textile Composite Mechanical Properties	64
5.1	Mode I Fracture Energy Based Cracking Behavior	74
5.2	Crack Opening Dependent Shear Retention (Total) Model	76
5.3	Crack Opening Dependent Shear Retention (Incremental) Model	77
5.4	A Brittle Tensile Failure Model	78
5.5	Stress-Strain Curve Using the Ductile Mode	79
5.6	Material Orientation Systems	81
5.7	Fail-Free Zone in Ceramic Layer Under the Projectile	84
5.8	Depth of Penetration as a Function of Ceramic Material Model	85
5.9	Effect of Ceramic Material Model on Velocity Time History	85
6.1	Projectile Models Used in Simulations	88
6.2	Geometric Characteristics of Different Projectile Shapes	88

6.3	Effect of Projectile Rotational Speed on Velocity Time History for Impact on 6.35mm Monolithic Ceramic Plate.....	90
6.4	Effect of Projectile Shape on Velocity Time History for Impact on 6.35mm Monolithic Ceramic Model.....	91
6.5	FE Simulation of Ballistic Impact on Monolithic Ceramic Plate.....	92
6.6	Comparison Between FE Model of a Deformed Projectile and the Projectile Fragments After Ballistic Test	92
7.1	FE Model of a Fabric Phase of Woven Composite Plate	93
7.2	FE Model of Angle-ply (0°/90°) Plate Under the Impact of Cylindrical Projectile.....	94
7.3	Boundary Condition Influence on the Target Ballistic Resistance	95
7.4	The Role of Textile Reinforcement in Composite Ballistic Resistance.....	96
7.5	Effect of Impact Velocity on Velocity Time History	97
7.6	Effect of Composite Fabric Architecture on Velocity Time History	98
7.7	Conical Deformation and Rupture of the Plain Woven Composite Plate at an Impact Velocity of 250m/s	99
7.8	Effect of Reinforcing Architecture on Impact Energy Transfer in Composite Structure	100
7.9	Maximal Principal Stress Distribution in Fabric Phase of Composite During the Initial Stage of Impact.....	101
7.10	Equivalent Plastic Strain Contours in Matrix Phase of Angle-ply Textile Composite (v=250m/s)	102
7.11	Stress Concentrations in the Woven Fabric During Projectile Penetration	103
7.12	Stress Concentrations at Fabric Crossover Points During the 250m/s Impact on Woven Composite	103
7.13	Equivalent Plastic Strain Contours at Front Side of Woven Phase of Textile Composite (v=250m/s)	104
7.14	Equivalent Plastic Strain Contours at Back Side of Woven Phase of Textile Composite (v=250m/s)	104

7.15 Square Shape of a Hole in Fabric Phase of Woven Composite After 250m/s Impact.....	105
7.16 Equivalent Plastic Strain Contours in the Matrix Phase of Woven Composite Target.....	106
7.17 Equivalent Plastic Strain Contours in Woven Phase of Textile Composite ($t=7.5\mu\text{sec}$, $v=1000\text{m/s}$).....	107
7.18 Equivalent Plastic Strain Contours in the Matrix Phase of Woven Composite ($v=1000\text{m/s}$)	108
7.19 Circular Shape of a penetration Area in Fabric Phase of Woven Composite After Impact of 1000m/s	108
8.1 MDC Material Concept.....	111
8.2 Schematic Representation of Simulated Impact Sites.....	112
8.3 FE Mesh of Integrated Design Composite Model.....	114
8.4 Ceramic Facing Model Composed of Two Layers of 6.35mm Spheres	114
8.5 Velocity Time History for Different Ceramic Models.....	115
8.6 Absorbed Energy of Different Ceramic Plate Models	116
8.7 Contours of Von Mises Stress During the Simulated Impact Between Two 12.7mm Spheres.....	118
8.8 Effect of Different Impact Sites, on Velocity Time History for the 9mm Spherical Facing Ceramic Model.....	119
8.9 Absorbed Energy of Two Layers of 6.35mm Spheres with Different Stacking Sequence	120
8.10 Von Mises Stress Distribution During the Impact on Two Layers of 6.35mm Spheres Plate, Between Four and Two Spheres	120
8.11 Superimposed Un-deformed (Green) and Deformed Model (in White) Simulation Showing Considerable Projectile Re-direction During Impact	121
8.12 Absorbed Energy With Respect to Projectile Impact Position.....	122
8.13 Backing Composite Plate Role in Armor Ballistic Resistance	123

8.14 Effect of Ceramic Facing on Ballistic Resistance of Multiphase Models	124
8.15 Projectile's Yawing Results in Better Armor Penetration Resistance	125
8.16 Simulation of an Oblique Impact on Integrated Material System.....	125
8.17 Optimal Combination of Multiphase Composite Armor	126
8.18 Energy Time History for Angle-ply Composite with Monolithic Ceramic Facing.....	127
8.19 The Influence of Textile Architecture on Energy Time History.....	128
8.20 The Influence of Ceramic Facings on there Energy Dissipation Capability	129
8.21 Ballistic Testing Lab	130
8.22 Impact Test Setup	130
8.23 Armor Sample: Pre-test.....	131
8.24 Armor Sample: Post-test	132
8.25 High-speed Photograph of the Ballistic Impact	133
8.26 Material Damage in Different Phases of target During Impact Simulation.....	133
8.27 Contours of Von Mises Stress at $t=60\mu\text{sec}$ During Simulation of Ballistic Impact Test.....	135
8.28 Velocity time History of a Simulated Ballistic Test	135

List of Tables

3.1 Characteristics of Computer Codes for High Velocity Impact	37
4.1 Boundary Conditions	52
4.2 Properties of Constituent Materials	54
4.3 Comparison of Continuum Properties	54
5.1 Engineering Elastic Constants of Composite Material Constituents	83
5.2 Material Properties Used in Impact Models	84
5.3 Spectra [®] Fiber Modulus Strain Rate Dependency	86
6.1 Calculated Projectile Rotational Speed	89
8.1 Varying Parameters in Ballistic Impact Simulations	112
8.2 Characteristics of Different Ceramic Facing Model	116
8.3 Material Properties of a WHA Projectile	131

Abstract**Numerical Modeling and Analysis of Static and Ballistic Behavior of
Multi-layered/Multiphase Composite Materials Using Detailed
Microstructural Discretization**

Jovan M. Jovicic

Dr. Frank K. Ko and Dr. Antonios Zavaliangos

The goal of this work is to analyze the static and ballistic performance of multi material systems using a detailed finite element analysis. As more complex materials systems are introduced in engineering practice, the design engineer faces the dilemma of utilizing homogenization techniques or detailed numerical models. The latter offers a number of advantages, such as the ability to introduce separate constitutive laws and failure criteria for each phase, at the expense of computation cost. This is particularly important in ballistic performance of armor where the sequence of failure of each phase plays a major role in the energy absorption.

An automatic geometry generation algorithm for composite materials is presented that can generate complex composite geometries spanning several unit cells. This capability is utilized to study the following phenomena:

1. Static behavior of textile composites: A comparative study of textile composites with different reinforcement architecture that shows the origins of non-linearity and the dependence of elastic parameters on the geometry of the unit cell;
2. Impact behavior of textile composites: The role of textile architecture in impact energy absorption;
3. Ballistic properties of ceramic sphere composites with textile composite backings.

A detailed study of a new multi-layered design concept is presented using a full finite element discretization method that shows that although ceramic spheres embedded

in epoxy exhibit a slightly lower energy absorption than the monolithic ceramic at the same areal density, they provide the advantage of ease of complex shape conformable manufacturing. A comparison with ballistic experiments on such material demonstrates that the analysis captures several aspects of this phenomenon.

1. INTRODUCTION

In the continuing quest for improved functional performance, which may be specified by various criteria including less weight, more strength and lower cost, currently used materials frequently reach the limit of their usefulness. Thus, material scientists and engineers are always looking for an innovation in engineering which often means the smart use of a “new” material, not essentially new in the sense of developing, but new to a specific application.

One of the material types that is both, old and new is a *composite material*. It is old in the sense that most natural objects including the human body, plants, and animals, are composites. It is new in the sense that development of man-made materials such as lightweight honeycomb structures and polymers reinforced with glass fibers were started in the 1930s, marking the beginning of the current era of composite engineering materials.

Composites can be defined as a combination of materials, in a material system, composed of a mixture of two or more macro constituents that differ in form or material composition and are essentially insoluble in each other.

In the beginning, composite materials were introduced because of their high specific strength and specific stiffness compared to conventional engineering materials. As their unique advantages are being more widely appreciated, many different types of composites, having different types of matrix and reinforcement combinations, have been

developed. The fact is that even during this stage of the technology explosion, the unique advantage of a composite material, i.e. the ability to tailor their properties to the structural or materials system of which they are intended, has not been fully explored.

Many structural components, in order to meet service conditions, require materials performance that varies with location within the component. This design concept firstly, was introduced and solved by Nature in many structures of living organisms. Bone and bamboo, for example, are multiphase materials, multi-layered to concentrate the strongest elements of their structure where the stress is highest.

It is well known that a sudden transition in the structural component or in the material composition often results in a sharp local stress concentration, whether the stress is internal or externally applied. It is also known that these stress concentrations are greatly reduced if the transition within the structure from the one material to the other is made gradually.

These considerations are basic reasons for the development of a special class of composite materials that are functionally layered-*Multi-layered/Multiphase Design Composites* (MDC).

In order to optimize the overall performance of the component (structure), MDC materials can be used to produce structures featuring engineered gradual transitions in the microstructure and/or composition that vary with location within the part.

One of the possible applications of the Multi-layered/Multiphase Design Composite materials would be the development of light armor materials systems: body armors, helmets, and protection against projectile threats in structures such as helicopters,

tanks and aircraft, which would have a significant improvement in penetration resistance, impact energy dissipation, and damage containment.

The development of a Multi-layered/Multiphase Design Composite material for a certain application, while maintaining its physical and mechanical properties, is primarily an exercise of selecting its constituents; hard (ceramic) facing, fibers, resins and interfaces tailored to a specific purpose and is within the expertise of chemists, physicists and material scientists. On the other hand, the engineer who has to design a specific structure, such as airplane part or body armor is more concerned with the macroscopic properties of the material. He uses anisotropic theory of elasticity and/or plasticity and finite element analysis to design an optimum weight or optimum cost structure with the desired performance characteristics.

Accordingly, the aim of this study is to analyze both the static mechanical properties of textile-based composites and ballistic impact performance of complex structures, such as Multi-layered/Multiphase Design Composite materials. Moreover, the difference in performance between a full ceramic facing versus a set of ceramic spheres embedded in a light epoxy is evaluated. The latter is proposed as an alternative to a monolithic ceramic in order to provide the feasibility for flexible armor manufacturing without sacrificing its ballistic effectiveness.

An understanding of the fundamental dynamic response of the material/structural geometry interaction is essential to the development and assessment of new armor systems.

In order to develop a precise methodology for optimizing the multiphase design composite armors, an improved understanding of the relative significance of the design

parameters must be developed. One way to study the relative significance of these parameters is through computational modeling.

Using an experimental-like power of a computer, the finite element analysis is used to simulate the structural behavior of textile composites and multi-layered composite armors, and assess the effect of the material selection and fiber architecture. The modeling and simulation tool developed in this work, Finite Element Fabric Geometry Model (FE-FGM), provides a new understanding of how interrelated failure modes, such as subsurface damage, projectile penetration and fragmentation occur and evolve in systems subjected to extreme loading conditions. These failure modes are difficult, if not impossible to observe experimentally yet the developed computational modeling engineering tool provides new insights that can be used to design new materials and systems.

Thus, rather than developing new materials with higher stiffness, it might be more advantageous to create structures using the optimal placement of components.

In that sense, this work attempts to be a bridge between materials and mechanics, between micro architectural design of the MDC materials and their macro mechanical response to the high strain rate effects during the impact process.

As Herakovich says in his “Mechanics of Fibrous Composites” [1.1]: *“The fundamental laws of mechanics are timeless. What will change is the synthesis and fabrication of new materials, and the **designs**¹ that can be accomplished with materials exhibiting superior properties, properties that can be tailored to meet the demands of the application.”*

¹ Highlighted by author

2. BACKGROUND AND OBJECTIVES

As the weapon designers were constantly improving the terminal effects of their projectiles, the armors were becoming thicker and heavier. The increased weight of the armor reduced the mobility of its user. Hence, armor materials research strives to find solutions for the major problems associated with armors: penetrability, weight and cost [2.3, 2.11, 2.14, 2.29, 2.39, 2.52].

In the search for improved armors, ceramic materials were considered [2.5, 2.11, 2.27, 2.37-2.39, 2.41, 2.55-2.57, 2.59]. High stiffness and hardness make them suitable for protective applications. On the other hand, their brittle behavior and poor tensile strength cause failure and prevent them from absorbing any significant amount of energy during the impact. By supporting the ceramic facing with a ductile back-up plate however, the performance of the armor can be dramatically increased. The performance of a specific armor protective system is characterized by its ballistic limit velocity (v_{50}). This velocity is defined as the minimum impact velocity for perforation, or the maximum impact velocity for which the residual velocity is zero. For example, a single 11.4mm thick tile of AD-85 alumina, has a ballistic limit of 390m/s. The ballistic limit of an armor faced with 6.35mm AD-85 alumina, supported by 6.35mm aluminum, which has same areal density, rises to 650m/s, when impacted by an identical projectile [2.29].

This example shows the necessity for multimaterial armor systems consisting of a harder facing layer, which would shatter or blunt the armor piercing projectile. The backing plate not only absorbs impact energy but also contains the damage in the ceramics and spreads the energy over a larger area.

Due to their high impact resistance and low density, fabric armors are usually employed for personnel protection, and considerable research has been directed to the study of the ballistic behavior of laminated, woven, and braided fabrics [2.11, 2.14, 2.16, 2.22, 2.42, 7.1, 7.3, 7.7-7.10].

Three distinct directions in research of armor materials could be followed: analytical prediction of the ballistic limit, experimental techniques, and numerical modeling.

Predicting the ballistic resistance of composite materials from the first principles is a complex task that some researchers have tackled [7.1]. However, only for some simple cases in which the mode of failure is known, using simple considerations can allow an estimation of the ballistic limit.

Experiments with lightweight armor systems are essential to improve the understanding of the penetration mechanisms. Unfortunately, the complexity and briefness of the impact event make instrumentation and measurements very difficult, and experiment becomes expensive and time consuming. On the other hand, with such complex designs, the number of independent parameters is very large.

To complement and perhaps guide the necessary experimental evaluation of such system, it is essential to develop a computational methodology that may lead us to an improved understanding of the relative significance of the various design parameters.

The key difficulty of this approach is the associated computational complexity in terms of both geometry and material models.

In recent years, numerical modeling has been extensively used as an alternate tool in better understanding of impact phenomena [2.2, 2.5, 2.27, 2.40, 2.53, 2.55-2.57, 7.1]. However, due to the complexity of both the ballistic process and reinforcing architectures, these techniques also consider a lot of assumptions [7.1]. Based on different homogenization techniques, as a result for example, the effect of textile architecture, yarn-to-yarn friction, are usually neglected [2.27, 7.1, 7.5, 7.7, 7.10].

Before embarking on the task of modeling of impact performance of multi-layered/multiphase composite materials, an extensive literature survey on numerical modeling of textile composites in general, and dynamic properties of comminuted materials was carried out. Recent efforts on the identification and modeling of the unit cells for fabrics and textile composites were also reviewed. Some of the results of the literature survey are presented here with some critical analysis.

2.1 Textile Composites

Textiles for composites probably have been around since cotton fabrics were impregnated with resins to protect the fragile mummies in Ancient Egypt.

In recent years, an increased interest in textiles and textile composites has been observed. Their applications range from bio-medical components, automotive and marine structures to aircraft and space applications [2.4, 2.19, 2.23, 2.44, 2.58].

The importance and wide usage of the textile composites arise from the fact that they have low a fabrication cost and easy handling (comparable to laminated composites) on the one side, while favorable mechanical properties combined with low weight, on the other.

The textile composite system consists of strong anisotropic fibers (the reinforcement) that carry most of the applied load and are bonded together by a weaker, usually isotropic material (the matrix). Because the reinforcement can be aligned with the applied load, the resulting efficient system is only strong in the directions that it needs to be.

The performance of a fiber-matrix composite depends on orientation, length, shape, and composition of the fibers (Figure 2.1), mechanical properties of the matrix, and the integrity of the bond between fibers and matrix. Of these, orientation of the fibers is perhaps the most important. It determines the mechanical strength of the composite and the direction of greatest strength. Fiber orientation can be one-dimensional, planar (two dimensional), or three-dimensional.

The one-dimensional structure has maximum composite strength and modulus in the direction of the fiber axis. The planar type exhibits different strengths in each direction of fiber orientations; and the three-dimensional type is isotropic but has greatly decreased reinforcing values. The mechanical properties in any one direction are proportional to the amount of fiber by volume oriented in that direction. As fiber orientation becomes more random, the mechanical properties in any one direction decrease.

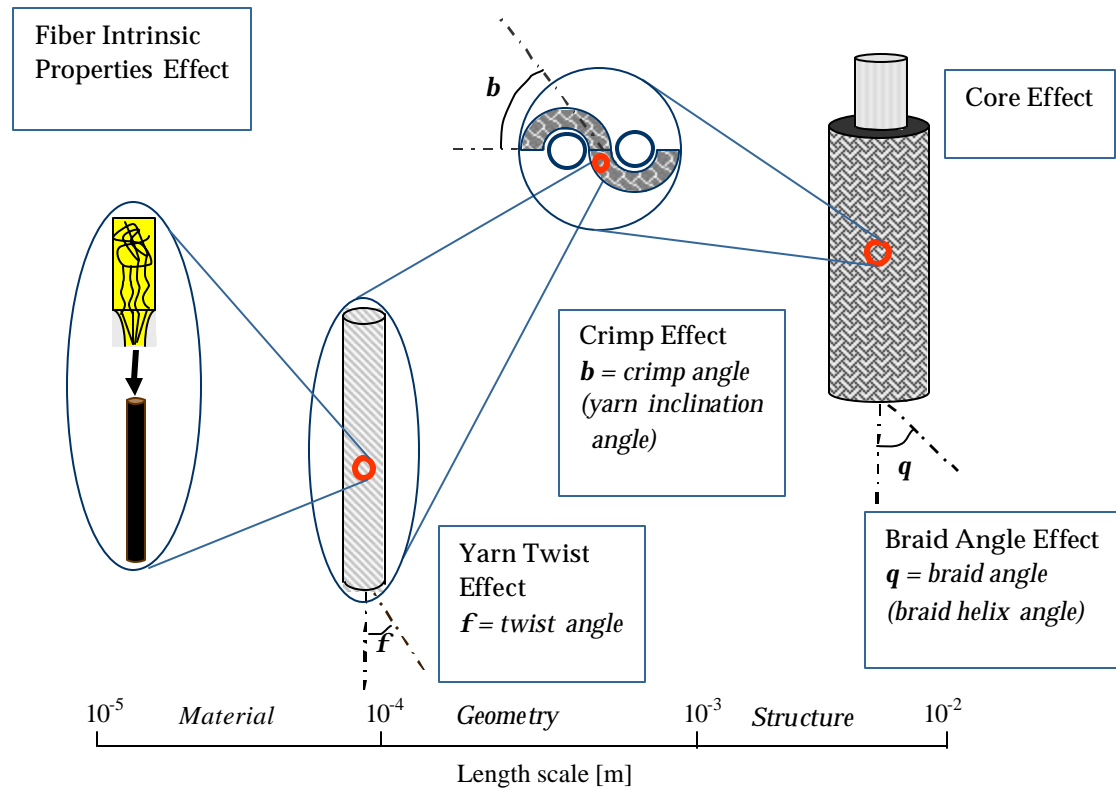


Figure 2.1: Textile Modeling Hierarchy

The interfaces are also very important yet less understood components of a composite material. In particular, there is a lack of understanding of the processes occurring at the atomic level of interfaces, and how these processes influence the global material behavior. There is a close relationship between processes that occur on the atomic, microscopic, and macroscopic levels. In fact, knowledge of the sequence of events occurring on these different levels is important in understanding the nature of interfacial phenomena. Interfaces in composites, often considered as surfaces, are in fact zones of compositional, structural, and property gradients, typically varying in width from a single atom layer to micrometers. Characterization of the mechanical properties of interfacial zones is necessary for understanding mechanical behavior [2.4].

Reinforcement of textile composites (usually called-fabric preform) is formed by various processes such as weaving, knitting or braiding, etc. (Figure 2.2, [2.20]).

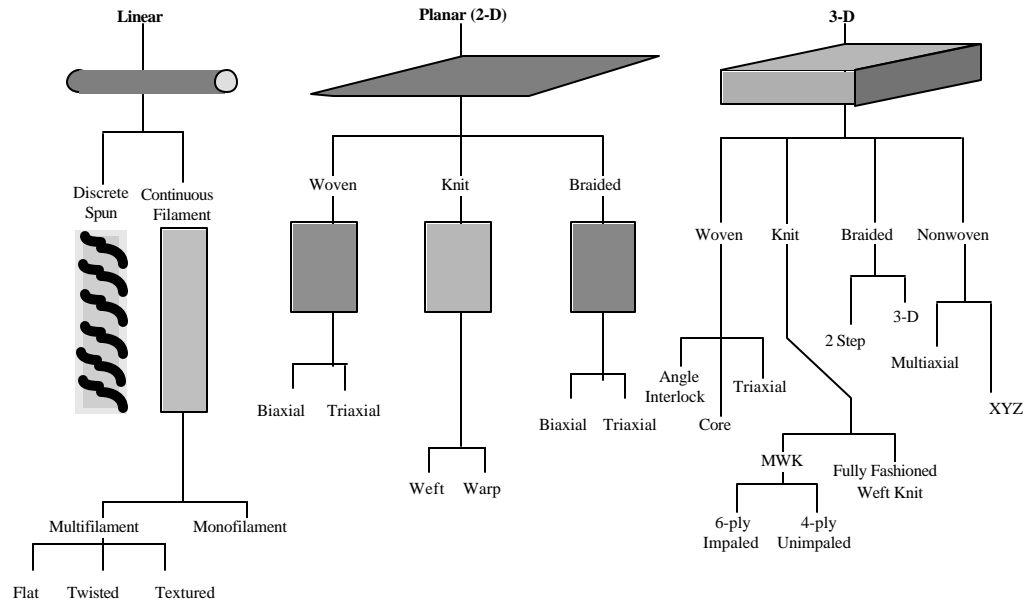


Figure 2.2: Classification of Fiber Architectures

Although there is a lack of a definitive criterion for separating textile preforms into the two-dimensional and three-dimensional types, one may say that they can be distinguished by yarn orientation distribution and by the number of yarn diameters in the thickness direction. A two-dimensional fabric consists of two or three yarn diameters in the thickness direction, while three-dimensional fabric has three or more yarn diameters in the thickness direction, forming a specific fiber network in which yarns pass from surface to surface of the fabric in all three directions (Figure 2.3 [2.20]).

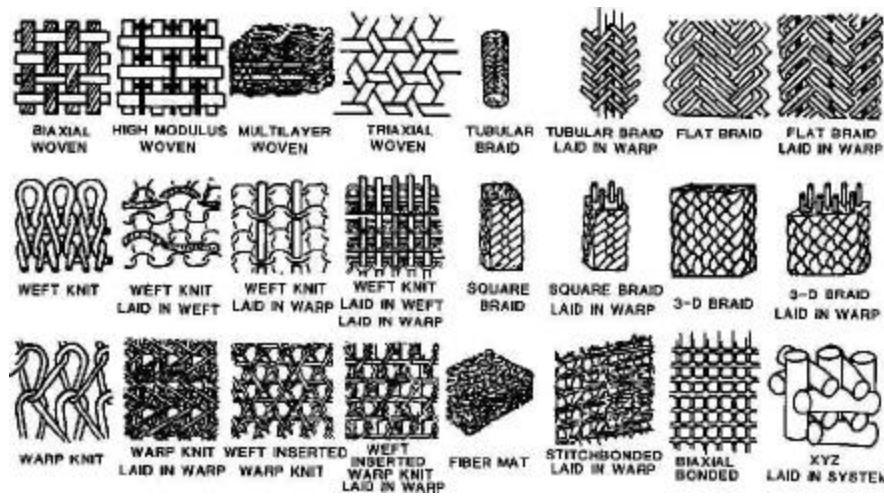


Figure 2.3: Linear, Planar, and Three-Dimensional Fibrous Structures

Traditionally, fibrous composites are manufactured by laminating several layers of **angle-ply** (unidirectional) fiber tapes impregnated with a matrix material. Changing parameters, such as the fiber and matrix material properties, fiber orientation in a layer, fiber volume fraction and layer stacking sequence, can result in the control of the effective properties of the composite.

Woven fabrics are fabricated by the interlacing of yarns. There are hundreds of possible fabric combinations, which can be divided into biaxial and triaxial woven structures according to in-plane fiber orientation. The three basic weave geometries from which many other patterns evolve are plane, satin and twill weave. Although weaving is usually thought of as a two-dimensional process, three-dimensional weaving is often employed. Three-dimensional woven fabrics are produced principally by a multiple warp weaving method. Five commonly used patterns are presented in the Figure 2.4.

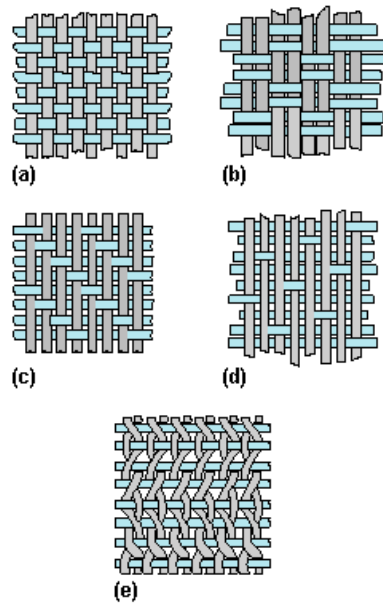


Figure 2.4: Common Weave Patterns: (a) Box or Plain Weave, (b) Basket Weave (c) Crowfoot, (d) Satin Weave, and (e) Leno Weave

Knitted fabrics are interlooped structures wherein the knitted loops are either produced by the introduction of the knitting yarn in the cross machine direction (weft knit), or along the machine direction (warp knit). As a result, a knitted structure is more open than either a woven or braided, due to the interloping of yarns. An advantage of knitted structures is the flexibility and ability to conform to complicated contours.

Braided fabric can be produced in flat or tubular form by intertwining three or more yarns together (2D braid). The braiding process is most effective for cylindrical geometries. It is used for missile heat shields, lightweight ducts, fluid-sealing components such as packing and sleeveings, and tubes for insulation. On the other hand, three-dimensional braiding is textile process in which a variety of solid, complex structural shapes can be produced in an integral manner, resulting in a highly damage-resistant structural perform. A unique feature of 3-D braids is their ability to provide through the thickness reinforcement (Figure 2.5), as well as their adaptability to the fabrication of a

wide range of complex shapes ranging from solid rods to I-beams to thick-walled rocket nozzles.

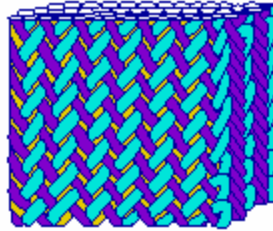


Figure 2.5: 3-D Braided Structure

Nonwoven structures are fiber to fabric assemblies produced by mechanical, thermal or chemical bonding, or by combination all three. The most general description of their fiber architecture is in terms of the probabilistic fiber distribution functions.

Although structural performance of textile composites under uniaxial loading yields to that of unidirectional composites, good impact resistance and the balanced in-plane properties of these materials, as well as ease of application, and the resulting low manufacturing cost make them superior for a variety of applications.

Because the mechanical properties of the textile structure are highly dependent on the constitution, especially on the fabric geometry and properties of the constituents, it is useful to develop models (both analytical and numerical) to determine the influence of various parameters.

2.2 Analytical and Numerical Models of Textiles and Textile Based Composites

One can say that models are tools of design and analysis, and the principal goal is to develop a model that is as realistic as possible in terms of its geometry and material characteristics, in the given constraints of time and money.

The development of accurate and realistic models for fabric composites is more difficult compared with unidirectional composites because of the geometric complexity of the fiber architecture. In a similar manner with laminated composites, the most common approach is to identify a Representative Volume Element (RVE, also referred to as a unit cell) that captures the major features of the underlying microstructure and composition in the material, and study its response under loading conditions that correspond to specific macroscopic loading conditions.

One of the greatest difficulties in developing detailed models of the mechanical response of textile composites is an accurate model of the reinforcing elements. In the case of elastic property predictions, the variation of fiber position may not have a critical role in performance. However, when considering highly localized stress events, such as those associated with cracks and holes, the exact position of the reinforcement probably dominates the failure mode.

Historically, efforts in textile composite mechanical analysis have focused mainly on the prediction of effective elastic material properties of a unit cell [2.4, 2.6-2.10, 2.13-2.15, 2.17-2.21, 2.23-2.26, 2.30-2.36, 2.44-2.51]. The approaches developed could be divided into three main categories:

1. Analytical models, based on the classical laminate theory,
2. Stiffness averaging and homogenization method, and

3. The finite element method.

Ishikawa and Chou have developed several micromechanical models for the stiffness and strength investigation of woven composites [2.4, 2.15]. In the **mosaic model**, the yarn crimp is neglected and so the composite is idealized as an assemblage of cross-ply units. The **crimp model** included the effect of the yarn undulation, but only in one (fill) direction. Although a good agreement between predictions and experimental results was reported, fiber continuity and non-uniform stresses and strains in the interlaced region were not considered in this model.

The **bridging model** [2.4] as an extension and combination of the crimp and the mosaic models, was used to analyze the load transfer between the interlaced regions of satin weave fabric composites.

The composite moduli in the **fiber inclination model** are obtained through volume averaging based on the simple state of iso-stress or iso-strain within the RVE Yang et al., [2.58] 1986. The moduli are calculated in the principal directions through laminate theory. The idealized unit cell treated all yarns as straight segments oriented in different directions. However, the interaction among the yarns was not taken into account.

The **layered plate model** has been developed by Dow et al. 1987 [2.4], for 2-D fabric composites. The cross-section consists of several sub-layers, each containing axial, transverse and crossover yarns. The yarn cross-sections are assumed to be circular. An upper bound is calculated by assuming an iso-strain condition. The strains are assumed to be constant along the laminate plate but vary linearly through the thickness. The effective stiffness is obtained by volume averaging the local stiffness. Similarly,

stresses may be assumed to vary linearly through the thickness and remain constant in the laminate plane.

Pastore and Ko [2.35] presented a **processing-science model** for textile composites in which a topological model of the braiding process was combined with geometrical and mechanical models. The process-science model provided the yarn geometry and fiber volume fraction. From this information, mechanical properties of the 3D braided fabric reinforced composites were calculated through a laminate theory. For the nonlinear stress/strain relationship, the total stiffness of the system was recalculated by removing the stiffness contribution of the failed yarns. Using a unified approach, this model discussed the possibility of developing a complete CAD/CAM system that could design, analyze, and manufacture complex 3D braided structural composites.

In the analytical model for predicting the elastic moduli and tensile strengths of knitted fabric laminates [2.36], the reinforcement efficiencies of yarns were incorporated into the rule-of-mixtures, and the effect of out-of-plane yarns were neglected. It was reported that the predicted elastic moduli were in reasonable agreement with experimental results while a significant difference existed between the experimental and predicted tensile strengths.

The **fabric geometry model**, based on the unit cell concept and laminate theory, was developed by Ko et al. [2.20] 1986-1990. A uniform state of strain is assumed within the RVE and the effective stiffness matrices are obtained by volume averaging. This model is also proposed for predicting the tensile properties of the warp-knit fabric composites [2.21].

An analytical model was proposed by Vandeurzen et al. [2.45-2.48], for predicting the engineering constants of woven composites. The model is based on micro-cell meshing of a unit cell, and the prediction of the local fiber volume fraction and the yarn orientations. These models were implemented in a custom software application, called TEXCOMP. However, the misorientation of yarns and the nesting of fabric layers were neglected in the unit cell model.

Earlier research was carried out usually relying on the rule of mixtures having fabric volume fraction as the only parameter. On the other hand, those who have looked at yarns as three-dimensional structures have limited their work to simple geometric arrangements of the yarns (postulating quasi-homogeneous material properties), or have used assumptions that were non-geometric in order to simplify the model [2.44, 4.4]. Though the homogenization method is effective in predicting elastic material properties [4.10], omitting the fiber continuity and undulation (crimp) limits its application in simulating complex structures such as textile composites.

More realistic stress-strain distributions can be obtained by using numerical techniques like finite element analysis. The description of the yarn architecture is the most important, but at the same time, the most difficult aspect of the finite element analysis.

Dow et al. [2.10] developed two FEA models to predict properties for their unit cells. The yarns are assumed to be non-circular and change piecewise linearly along the axis of the yarn.

Ma et al. [2.26] treated yarns in a 4-step braid as circular composite rods having bending tensile and compressive rigidities.

In the **modified laminate model**, the RVE for the braid is assumed to consist of two angle-ply laminates, Crane and Camponeschi, [2.7], 1986. The effective Young's moduli are then the same as that of the angle-ply laminates.

A finite element model developed by Dasgupta et al. [2.9] 1996, accounted for the yarn undulation in both directions. The boundary conditions that were prescribed were iso-strain and the elastic properties were calculated by volume averaging the stress and the strain. The inter-yarn gap is taken care of by separating the yarns such that the yarns never touch each other. However, only woven a unit cell was discussed and the mesh was composed of both hexahedral and tetrahedral elements.

Li [2.25] reported an experimental study of the internal structure of braids and identified a unit cell for braided composites, based on the assumptions that yarns were straight rods with circular cross-section and that there were no lateral deformations at the yarn crossover points. They also observed that the structure on the surface of the braid preforms was different from that in the interior.

Cox *et al.* [2.6] presented a three-dimensional FE model, known as the **binary model**, using two types of elements. The fibers were modeled as a two-node line element possessing axial rigidity, while the transverse stiffness, shear stiffness, and Poisson's effect of the composite were represented by an eight-node solid "effective medium" element. This "effective medium" element was considered as homogeneous and isotropic. However, the anisotropy and heterogeneity of this medium, which represents all other properties of the tows, voids, resin pockets, etc., were not considered in this model used to predict failure mechanisms in angle and orthogonal-interlock woven composite.

Another 3D finite element model of the microscale unit cell was developed by Dasgupta et. al. [2.8]. This model was used in a homogenization study to predict the linear thermo-mechanical properties. Numerical results showed a good agreement with the experimental data.

Subsequent studies conducted by Kostar [2.23], and Lei [2.24] revealed that the corners were unique in the preform structure.

Wang [2.49] presented the analysis of the topological structure in three-dimensional braided preforms and defined three distinctive types of unit cells in the preform, namely interior, surface and corner regions.

In order to study the mechanical response of a three-dimensional graphite-epoxy composite material system, Abusafeih et. al. [2.1] created a three-dimensional unit cell FE mesh by using solid elements in an IDEAS software package. Their model took into account the curvilinear geometry of yarn tows in the unit cell and the anisotropy of the elastic response of the fiber with respect to its axis. However, a perfect interface between the fiber and the isotropic epoxy matrix was assumed. Their numerical results showed that the modeling parameters such as fiber geometry, fiber cross-section, boundary conditions, and type of elements used, played an important role in the elastic modulus prediction. Unfortunately, it was not discussed how sensitive the predicted modulus was to these parameters.

Another FE model has been developed by Kalidindi and Franco [2.12, 2.17], to simulate the elastic response of a three-dimensional braided composite. It incorporates the major details of the geometry of the unit cell such as yarn curvature and orientation, and the anisotropic nature of the yarn elastic properties. The study revealed the major

deficiencies of the analytical models and that a suitable weighted average of the isostress and isostrain model predictions is in close agreement with the FE model prediction. Furthermore, the weighting factor was found to be relatively insensitive to braid parameters, yarn volume fraction, and the type of loading, but strongly influenced by the yarn elastic properties. This fairly detailed model had a drawback because RVE-s did not have through the thickness stacking capability, so basically they could not be used for modeling of 3D braided composites.

Han and Pandey [2.13, 2.32-2.34], proposed a micromechanics model to predict thermoelastic properties of plain woven fabric composites. The effective elastic moduli and the thermal expansion coefficients were evaluated under the assumption of uniform strain inside the idealized structure of RVE.

One model for braided composite was reported by Master's et al [2.28]. The geometry of braided samples was digitally mapped and then replicated using a CAD package. The geometry model was then used to create a FE mesh with solid elements. The FE predictions were in reasonable agreement with experimental values for axial stiffness and Poisson's ratio, yet transverse predictions were much worse. The overall results were not much better than analytical models. According to the authors, the primary drawback of this technique as a design tool is that it requires "more skill in application than is usually available in preliminary design".

Finally, Whitcomb and his coworkers analyzed unit cell of a plain weave composite using three-dimensional finite elements to determine the effect of yarn geometry and yarn volume fraction on the composite thermoelastic properties [2.50, 2.51, 2.54]. They proposed an iterative global/local FEA method. The basic idea of this method was

that a coarse global model could be applied to obtain displacement or forces used as appropriate boundary conditions for some local regions. However, there was a potential problem due to the differences in the stiffness of the global and local models.

2.3 Modeling Results of Impact Behavior on Multi-layered Composite Materials

The design of lightweight ceramic/composite armor is a complex task for which three different approaches might be followed: the analytical modeling, empirical method, and numerical simulation.

Over the years, only a few analytic penetration models for impact on ceramic-faced armor were presented in the literature. In 1969, Florence [2.11] developed a model for estimating the ballistic limit of ceramic armors based on the assumption that ceramics only distribute the load over a larger area than that of the impact, whereas the backing plate absorbs all the energy of the impact. This approach was reassessed by Hetherington and Rajagopalan [2.14], 1991.

Ravid *et al.* [2.37], 1989, proposed two analytical models: (a) one for the early stage of high-velocity impact, and (b) two-dimensional, five stage, analytical model for the penetration and perforation of moderate thickness viscoplastic plates by rigid projectile.

Woodward [2.55], 1990, proposed a one-dimensional model for the penetration into ceramic-faced armor, using a lumped mass scheme. This model takes into account both the projectile and ceramic erosion in a fairly simple manner, and allows the consideration of both thin and thick backing plates.

Reijer 1991 [2.38] has proposed a more elaborate model taking into account projectile erosion and mushrooming, different deformation modes for the backup plate, and with references to the constitutive behavior of comminuted ceramics.

Zaera and Sanchez-Galvez [2.59], 1998, proposed a model based on Tate and Alekseevskij's equation for the projectile penetration into the ceramic tile, while the response of the metallic backing is modeled following the ideas of Woodward's and Reijer's models.

While a very large amount of effort has been devoted to the study of the problem of normal penetration of projectiles into homogeneous metal targets (Backman and Goldsmith, 1978 [2.3]; Anderson and Bodner, 1988 [2.2]), only a limited amount of information (at least in open literature) has been published on the behavior of composite materials or their combination with other substances (MDC materials) under impact conditions. It has been established that ceramic-faced targets represent a class of light armor systems that are highly efficient in reducing the penetrability of a given projectile, but only a few publications are available on this subject, most of them dealing with experimental results, with some supplementation by computer analysis based on two-dimensional continuum-mechanics codes (Wilkins et al., 1969 [2.52], Wilkins, 1978 [2.53] and more recently Cortes et al., [2.5]). This type of research was primarily aimed to understand the principal mechanism of response of such targets and to provide a limited database for their application.

The impact process of a projectile into ceramic-faced armor can be simplified by dividing the process on two time regimes. The first part is characterized by the time required for the initial stress waves reflections to go through the armor plate and thus is

on the order of few microseconds. This stage results in shock degradation of the armor and shattering of the projectile. Shocks above the ceramic's Hugoniot elastic limit (HEL) are known to induce damage in ceramics. (The HEL can be defined as stress at which metal deforms plastically. However, for ceramics there still is a considerable debate as to the meaning of HEL). According to Wilkins [2.52], fracture in ceramics at their interface with the backing plate is a result of tension in the ceramic as it follows the motion of the back-up plate after the reflection of the shock wave (spall failure). Hence, a few microseconds after impact, a ceramic fracture conoid has formed in front of the projectile. The angle of this fracture conoid depends on the dynamic loading conditions in the ceramic material, but is usually of the order of 65 degrees [2.38].

Although the energy consumed in the fracture of the ceramic facing is very small compared with the impact energy, the development of a zone of fractured material ahead of the penetrator seems to be of the greatest importance in defeating the projectile. Under high confining pressures, internal friction of a granular assembly of ceramic powder seems to be an important factor in the ballistic efficiency of the armor [2.29].

The second stage includes the resulting structural response period of the armor and is terminated when either the armor is defeated or the projectile is stopped. During this part of the ballistic event, the projectile attempts to penetrate through the comminuted ceramic. Fractured ceramic is pushed away and out through the impact hole while the formed ceramic conoid effectively distributes the concentrated impact load over a large area of the backing plate. That supporting plate has to be able to carry this load and dissipate the energy by plastic deformation. Depending on its mechanical properties, the

plate eventually reaches its limits of energy absorption and fails, either by plug shearing or strain failure.

Experimental results of a recently proposed two layer composite armor consist of an aluminum oxide ceramic sphere layer bonded by epoxy and an angle-ply $[0^\circ/90^\circ]$ Spectra Shield[®] composite backing, showed that a ballistic limit of 3,000ft/sec. (1,000m/sec.), can be achieved, [2.42]. Figure 2.6 shows the predicted (v_{50}) values calculated from the analytical model developed by Florence [2.11], as a function of the areal density of the experimental panels..

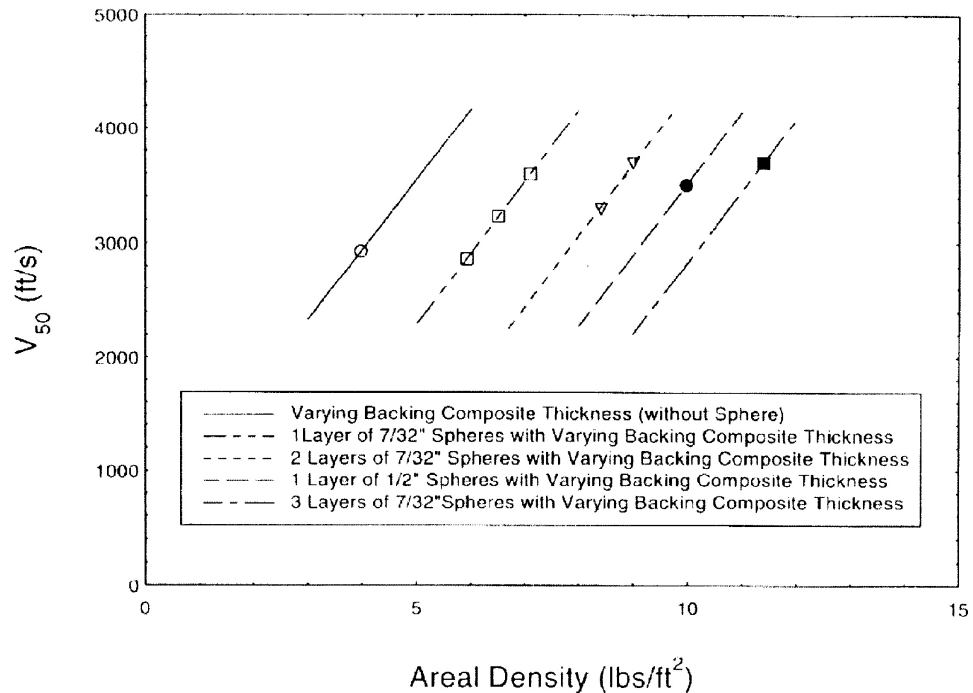


Figure 2.6: Velocity as a Function of Areal Density for Multi-layered Design Composite

In Figure 2.6, the lines are the predicted values when varying the thickness of the backing composite plate and the thickness of sphere face. The data points in the Fig-

ure are the predicted values of actual panels examined in the study [2.42]. The projectile used for the testing was a 7.62mm x 39mm AK-47 type projectile.

Figure 2.7 shows the damaged areas of the front and backing panel [2.42]. Authors also report on the destruction and deformed shape of the projectile and the panel after ballistic testing. Breakage of ceramic spheres was also observed, but the damage was not as severe as it might be observed by shattering of solid tiles to very small pieces, which is usually observed in ballistic impact on ceramic armor.



Figure 2.7: Damaged Areas on the Facing and Backing Layers of Panel After Ballistic Impact

The conclusion from this experimental work was that ceramic sphere facing provides the feasibility for flexible armor manufacturing without sacrificing its ballistic effectiveness.

2.4 Problem Statement

A major objective of impact phenomena studying is to identify those important parameters of both target and projectile that influence penetration. The most important physical and material parameters that affect ballistic penetration are: impact velocity, hardness and shape of the projectile, hardness, density and toughness of the target facing plate, as well as the rigidity and strength of the backing plate, thickness ratio of a plates, etc.

Earlier research was carried out based on a large number of assumptions for simplifying the analysis procedure. These methods provided approximate estimations of mechanical properties, but they cannot be used to analyze variations of mechanical properties with some important architecture parameters due to introduced oversimplified assumptions. On the other hand, due to the immense variety of available composite materials and possible fabric architecture, it is impractical and very time-consuming to obtain material characterizations of various composites by an experimental approach. As a result, there still is a need for comprehensive design modeling tool capable to bridge the gap between textile composite processing parameters and their structural response on variety of loading conditions, addressing in the same time both geometry and material characteristics.

Like any other mechanical property, the energy absorption characteristics of composite materials are sensitive to the fabric architecture (position and crimp of the yarns and inter-yarn gaps). So far no systematic study has been carried out to investigate

this aspect. This may be due to the inherent difficulty to isolate the effect of fiber architecture from the effect of other variables, such as fiber volume fraction.

The design of an armor system to resist projectile perforation requires: armor as thick as possible; high bulk and shear modulus; high yield stress, to maintain the resistance to deformation at high stress levels, resistance to fracture when large tensile stresses occur.

When the total weight must be considered, no one material satisfies all requirements because the total areal density of the target must be minimized. This has led to the development of composite armors in which a ceramic-face plate is backed by a material that can resist failure from tensile stresses. The use of materials of different hardness to produce dual hardness armor, take advantage of the ability of the hard, ceramic layer, to break up or slow down the projectile, whereas the softer backing layer will absorb the remaining impact energy.

Due to their high impact resistance and low density, fabric armors are usually employed for personal protection, and considerable research [7.1, 7.3] has been directed to the study of the ballistic behavior of laminated, woven, and braided fabrics (Figure 2.8 gives a schematic representation of textile reinforced composite).

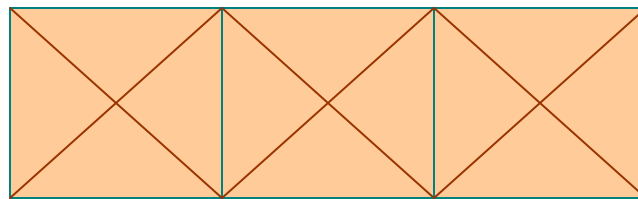


Figure 2.8: Polymer-Reinforced Textile Composite

In order to defeat higher velocity threats and address the need for lighter weight and more complex shape structures, the concept of introducing a hard phase in the spherical form or Gradient Design Composite was developed (Figure 2.9, [2.42]). Using spherical ceramic facing will help contain the ballistic damages within minimum number of spheres and make the armor suitable for repair.

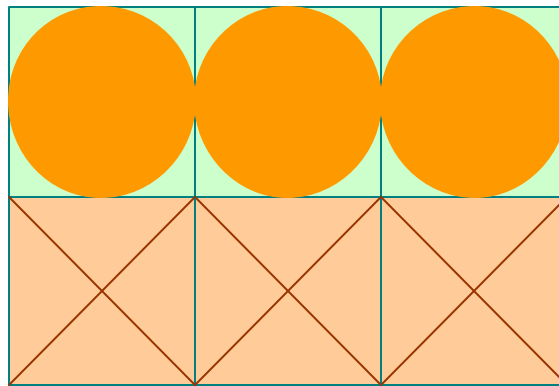


Figure 2.9: Polymer-Reinforced Composite With Ceramic Spheres

The system consists of a hard component with ceramic spheres for destroying the projectile tip and creating a greater surface area to contact between the facing layer and the backing composite plate, which is for maximizing strength and energy absorption.

Besides projectile mass erosion on hard ceramic facing material, a very important mechanism by which armor can reduce the amount of kinetic energy that it has to absorb is changing the projectile direction by deflecting on the spherical ceramic particles.

Dynamic events such as impact phenomena, requires not only knowledge of the propagation of stress waves through the material, but also its constitutive equation. This

equation represents a mathematical description defining the relationship between stress, strain and their time derivatives. Essential to the development of the constitutive equations is information of the dynamic properties of the material system under study. The establishment of these properties for metals is itself a challenging task; for composites this task is further complicated by the directional dependence of the properties due to the anisotropy of the material system. On the other hand, a clear distinction must be made between material and structural response.

In order to understand and quantify dynamic effects, knowledge of stress wave propagation, constitutive equations, and structural dynamic properties have to be integrated (Figure 2.10).

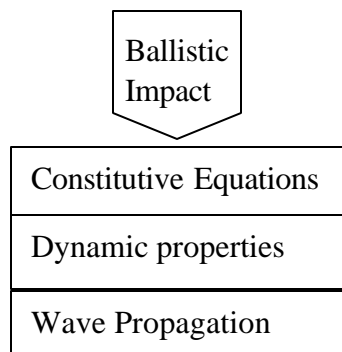


Figure 2.10: Ballistic Impact Modeling Parameters

2.5 Thesis Objective

The main goal of this work is to analyze the static properties of textile composites and impact performance of multi-layered/multiphase composite design material system (MDC) using detailed finite element modeling (Figure 2.11).

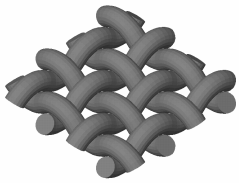
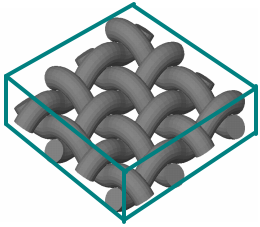
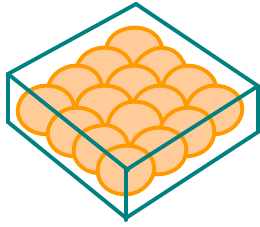
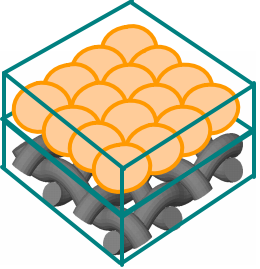
Model type	Solid model (Hexahedral elements)	Velocity range [m/s]	Model description	
			Geometry	Materials
Textile preform		10-100	Full geometry <ul style="list-style-type: none"> • Woven • Braided • Knitted • Angle-ply 	<ul style="list-style-type: none"> • Elastic-plastic • Strain rate effect • Orthotropic
Polymer Matrix Composite		100-300	<ul style="list-style-type: none"> • Full geometry • Hexahedral elements • Volume fraction 	<ul style="list-style-type: none"> • Elastic-plastic • Strain rate effect • Orthotropic preform • Isotropic matrix
Ceramic facing layer		100-500	Monolithic vs. Spherical	<ul style="list-style-type: none"> • Brittle vs. • Elastic-plastic with brittle failure
Multi-layered Design Composite		500-2,000 > 2,000	<ul style="list-style-type: none"> • Full geometry • Hexahedral elements • Monolithic vs. Spherical 	<ul style="list-style-type: none"> • Elastic-plastic with failure • EOS

Figure 2.11: Developed FE Models and Their Characteristics

The geometry of textile reinforcement is one of the most important parameters that influences mechanical behavior of any composite material. In order to address 3D nature of a textile composites structure, it is necessary to develop a model that can generate complex composite architectures using automatic geometry generation.

The characteristic of the present approach is that it considers each material separately. From the computer simulation point of view, the introduction of discrete models for the study of textile composites offers the advantage of using different and more detailed description of material properties for both matrix and fibers, with a more accurate description of the geometry. In this way, more elaborate (and more realistic) failure criteria can be introduced and the effects of fiber architecture on both static, and dynamic properties of these composites can be explored.

It is evident that the complexity of the MDC constructions has increased many folds and so did its structural analysis. The behavior and properties of MDC materials are determined by the composition, form and arrangements, and interaction between the constituents. The intrinsic properties of the materials of which the constituents are composed largely determine the general order or range of properties of the MDC material. Structural and geometrical characteristics - that is, the shape and size of the individual constituents, their structural arrangement and distribution, and the relative amount of each - contribute to overall performance. Of far-reaching importance are the effects produced by the combination and interaction of the components. The basic principle is that by using different components it is possible to obtain combinations of properties and property values that are different from those of the individual constituents.

Thus, the aim of this work is to address the issue of designing the microstructure and material combination of both textile composites and Multi-layered Design Composite materials for optimum performance under the high velocity impact phenomenon and to compare ballistic resistance of spherical ceramic facing, embedded in light epoxy, to that of monolithic ceramic tile backed with textile composite plate.

3. KEY ASPECTS OF NUMERICAL MODELING OF DYNAMIC EVENTS

The high velocity impact of a projectile with a solid target results in an extremely complex mechanical (and not only mechanical) process that has been examined for the past 200 years. A complete description of this problem would involve considerations of all aspects in the theory of continuum mechanics. This includes the compressible fluid flow, dynamics of elasticity and plasticity, but also other behavior such as melting and solidification, vaporization and condensation, and kinetics of phase changes. As a consequence, certain simplifications are needed in order to make the problems feasible. Several models have been proposed for various stages of the impact process [2.2, 2.3].

As discussed in the previous chapter, at the present time, there are three reasonably distinct directions for these investigations:

- ◆ Derivation of empirical formulas based on extensive testing;
- ◆ Development of relatively “simple” models of the perforation process and applying the relevant equations of motion and material behavior, and
- ◆ Full numerical solutions based on solving all the governing equations over a spatial grid at successive time increments.

The general objective of this work is to address the computational modeling of the impact process involving brittle and ductile solids. Thus, current approaches and their characteristics will be briefly reviewed and discussed in the following section.

3.1 Some Considerations in Numerical Modeling

Classical continuum mechanics attempts to describe the dynamics of a continuous media with a set of differential equations established through the application of the principles of conservation of mass, momentum, and energy from a macroscopic point of view. An equation of state relates the density (or volume) and internal energy (or temperature) of the material, with pressure. A constitutive relation describes the particular nature of the material by relating the stress in the material with the amount of distortion (strain) required to produce this stress. The constitutive relation may include work hardening, strain rate effects, thermal softening, etc [3.2].

The differential equations relate material density (ρ), velocity (v_i), specific total energy (e), the stress tensor (σ_{ij}), and external body forces per unit mass (f_i), where subscripts represent standard tensorial notation. Two fundamental descriptions of the kinematic deformation of continuous media exist: the Eulerian (spatial), and Lagrangian (material) description. The conservation equations for the two descriptions are:

Principles of:	Lagrangian	Eulerian
Conservation of Mass	$D\rho/Dt + \rho(\partial v_i/\partial x_i) = 0$	$\partial\rho/\partial t + (\partial/\partial x_i)(\rho v_i) = 0$
Conservation of Momentum	$Dv_i/Dt = f_i + 1/\rho(\partial\sigma_{ij}/\partial x_j)$	$\partial v_i/\partial t + v_j\partial v_i/\partial x_j = f_i + 1/\rho(\partial\sigma_{ij}/\partial x_j)$
Conservation of Energy	$De/Dt = f_i v_i + 1/\rho(\partial/\partial x_j)(\sigma_{ij} v_i)$	$\partial e/\partial t + v_i(\partial e/\partial x_i) = f_i v_i + 1/\rho(\partial/\partial x_j)(\sigma_{ij} v_i)$

The differences in the mathematical description between the two sets of equations are inherent in the definition of the total time derivative D/Dt :

$$\frac{D}{Dt} = \frac{\partial}{\partial t} + v_i \left(\frac{\partial}{\partial x_i} \right) \quad (3.1)$$

The specific total energy is the sum of specific kinetic energy and specific internal energy E :

$$e = \frac{1}{2}(v_i v_i) + E \quad (3.2)$$

Equation that describes Conservation of energy is often rewritten in terms of the specific internal energy:

Lagrangian:
$$\frac{DE}{Dt} = \frac{P}{\rho^2} \left(\frac{D\rho}{Dt} \right) + \frac{1}{\rho} \frac{D\rho}{Dt} \quad (3.3)$$

$$\text{Eulerian: } \frac{\partial E}{\partial t} + v_i \frac{\partial E}{\partial x_i} = \frac{P}{r^2} \left(\frac{\partial \mathbf{r}}{\partial t} + v_i \frac{\partial \mathbf{r}}{\partial x_i} \right) + \frac{1}{r s_{ij}} \mathfrak{E} \quad (3.4)$$

Where (s_{ij}) and (\mathfrak{E}) are the stress deviators and strain rates, respectively, and (P) is the hydrostatic pressure.

Two more expressions are required to complete the set of equations [3.1]. Firstly, an equation of state is necessary to account for the resistance to hydrostatic compression. The increase in internal energy due to thermodynamically non-reversible processes (e.g. plastic work, shock loading), and phase transitions (both solid-solid as well as melting and vaporization) is expressed as:

$$P = P(\mathbf{r}, E) \quad (3.5)$$

Secondly, a constitutive model is required to account for strength effects. In general, it permits the stress to be a function of strain (\mathbf{e}_{ij}) , strain rate (\mathfrak{E}) (both in loading and unloading, i.e. stress relaxation), internal energy (E) (thermal softening), and damage (D) :

$$\mathbf{s}_{ij} = f(\mathbf{e}_{ij}, \mathfrak{E}, E, D) \quad (3.6)$$

Of course, before a solution can be obtained, appropriate boundary and initial conditions must also be prescribed.

Fundamentally, however, there are significant differences between the two numerical approaches. In Lagrangian description, every point in the deforming body is referred to some reference state, and any discretization used in the analysis, deforms with the material. In Eulerian formulation, however, the points are fixed in space and the discretization does not move with the material. Generally Lagrangian formulation is most appropriate for the impact of solid bodies since the surfaces of the bodies in contact will always coincide with the discretization and are therefore well defined. The disadvantage is that large deformations result in severe mesh distortion, which can cause numerical difficulties. Eulerian formulation avoids high distortion of the mesh by definition since discretization is fixed and does not move during the time stepping, but is therefore rather imprecise about boundaries. In order to unite advantages of both approaches a combined formulation of adaptive meshing known as Arbitrary Lagrangian-Eulerian (ALE) is developed [3.2]. In this case boundaries of a material are modeled using Lagrangian formulation whereas the Eulerian description can be used within the body to avoid mesh “piling up” characteristic of the Lagrangian approach.

The processing part of numerical modeling in this work was performed using the ABAQUS-Explicit finite element computer code, dedicated to analyze dynamic problems associated with large deformation, such as high velocity impact, ballistic penetration, material degradation or failure, wave propagation, etc. Some characteristics of computer codes for high velocity impact are presented in Table 3.1:

Table 3.1: Characteristics of Computer Codes for High Velocity Impact

Mesh description	Eulerian and Lagrangian
Spatial discretization	Finite element
Temporal integration	Explicit
Artificial viscosity	Explicit formulation
Material model	Incremental elastic-plastic
Failure criteria	Instantaneous maximal of field variable (principal stress, strain, plastic work, pressure), cumulative damage, micromechanical models
Methods of material characterization	Wave propagation methods -split Hopkinson bar -plate impact -bar-bar impact
Hydrodynamic pressure	High pressure equation of state $p=p(\rho,E)$
Boundary conditions	Reflective and transmittive
Initial conditions	Velocity

As with all dynamic codes, ABAQUS seeks a solution of the momentum equation satisfying the traction and displacement boundary conditions of the exterior and interior boundaries, respectively. The energy equation is integrated in time and is used for a global energy balance. The integration scheme is based on the central difference method and displacements and velocities are updated accordingly. The principal limitation during integration is the size of the time step, which should be small enough so that a second wave cannot travel across the smallest element during one integration step.

It is important to note that developed code generates textile composite models composed of only 3D solid continuum brick elements. Solid elements in general, satisfy equilibrium and compatibility conditions in all directions (in a numerical sense) throughout the unit cell, and therefore allow for a better representation of the stresses, displacements, and strains in the unit cell. In particular, using brick solid elements is essential in applications where large deformations, plasticity and material failure are involved.

Accordingly, both monolithic ceramic plate and facing layers of ceramic spheres embedded in epoxy were modeled using continuum brick elements.

There are several inherent problems in transforming a physical space to a discrete model and solving it on computers with limited precision using a finite element method. Several important issues can influence the accuracy of the solution and lead to disagreement between computation and experiment. Some of these issues are briefly listed and discussed.

Each finite element can be characterized by considering the following:

- Family (depends on type of problem intended to solve: continuum, solid, shell, beam, truss...);
- Number of nodes (interpolation), determines how the nodal degrees of freedom will be interpolated over the domain of the element (first order elements with nodes in element corners, and second order elements having additional nodes in the mid point of each element's side);
- Degrees of freedom (the primary variables existing at the nodes);
- Integration (full, represents the minimum integration order required for exact integration of the strain energy for an undistorted element with linear material properties; reduced, offers the integration rule of one order less than full integration).

The stiffness and mass of an element are calculated numerically at sampling points called “integration points” (Gauss points) within the element. Depending on the number of integration points, elements could be divided to those with full and reduced integration.

First order fully integrated elements are prone to “shear locking” (an overly stiff behavior resulting from shear strains present solely because of the numerical formulation used to model bending of the structure). This can be overcome by using first order reduced-integration elements that evaluate the constitutive equations at one point (usually the element centroid).

However, another spurious deformation mode is of concern when using these elements, known as hourglassing. Since there is only one integration point in a centroid, the axial strain measured at the centroid is zero because the length of the isoparametric line through the centroid is unchanged even as the element is bent. To avoid this potential numerical problem, several elements through the thickness have to be used.

This essentially brings another important issue in numerical modeling; the size and shape of elements used in simulation.

The main factors concerning finite element meshing are the size of elements, their number and shape (aspect ratio). Theoretically, the ideal mesh is uniform in all coordinate directions and converges to the critical variable for the problem.

Convergence of the solution can be determined by several ways [3.3]. Here, the unit cell is meshed with an increasing level of refinement and the percent difference between the maximum values of strain energy density, computed for each model, was used as a convergence criterion. A comparison of the results for the woven unit cell models with 3,000 elements and more (Figure 3.1), proved to be unaffected by the mesh density (having the strain energy difference of 2%), so a model with 16x12x12 3D eight-noded elements is chosen for the further analysis.

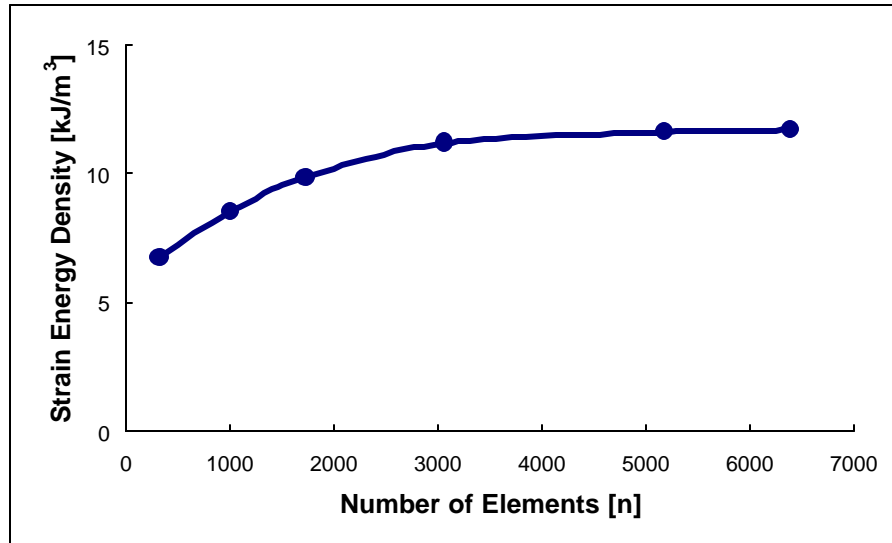


Figure 3.1: Convergence of the Solution Study

4. STRUCTURE-PERFORMANCE MODELING OF 3D TEXTILE COMPOSITES

Based on previous work, summarized in Chapter 2, the Finite Element method proved to be superior to other methods and theoretical analysis modeling techniques developed for predicting mechanical properties of textile composites because:

- It addresses the architectural design of the composite with the least number of assumptions. The only compromise is that typically attention is focused on a single unit cell, and special cells (edges, corners) are ignored.
- It allows introducing more complex and more realistic models for each constituent, which in turn should allow addressing properties more difficult to predict such as strength, failure and ballistic performance. A single limitation imposed by the need to keep the problem numerically feasible is that the behavior of individual fibers is only considered through a homogenized but anisotropic model at the yarn level.

A downside in using FEM is that the task of generating the finite element mesh is laborious. Automatic mesh generation should be helpful but there are two issues that need to be addressed: (a) the need for an all-hexahedral mesh, and (b) the requirement for the fiber and matrix meshes to match at the interface.

Meshing is a process of spatial decomposition. A physical 3D space is decomposed into small elements with required topology and geometry constraints. Different algorithms differ in the way that they decompose the 3D space.

Automatic mesh generation for tetrahedral elements exist [4.9]. A hexahedral mesh is preferred over a tetrahedral or a mixed mesh because it is computationally advantageous for large deformations, plasticity and material failure problems [4.1, 4.9]. Attempts for hexahedral mesh generators are based on the so-called “structured mesh” [4.4, 4.5, 4.8]. Strictly speaking, a structured mesh is one in which all interior nodes of the mesh have an equal number of adjacent elements. Some hexahedral mesh generators are successful for moderately complicated geometries. For example, in the review paper [4.9], the mapping/sub-mapping algorithm, the sweeping algorithm, the whisker weaving algorithm, and the grid-based method are referenced. Even if such algorithms can address fibers and matrix individually, matching the two meshes at the interface is difficult if not impossible.

In this study, an alternative approach is proposed. In summary, the developed algorithm starts with a regular structured mesh in a parallelepiped; elements are assigned to fiber or matrix on the basis of a mathematical model for the fibers, and then the elements near the fiber-matrix boundary are adjusted to match the interface as good as possible. Finally, a mesh smoothing operation eliminates distorted elements.

This algorithm was implemented in MAPLE-symbolic computation system (Waterloo Maple, Inc, Waterloo Ontario, Canada) and currently produces ABAQUS input files (Hibbitt Inc., Rhode Island, 2001), but can be adapted for any finite element code. The advantage of this approach is the generation of an all hexahedral mesh. Details of the algorithm are given in a section below.

Consequently, the main goal of the work presented in this chapter is to develop the engineering modeling tool for the structural design of textile reinforced composite

materials. As it is shown in Figure 4.1, based on the modeling hierarchy of a textile preforms, using both architecture based modeling and material based modeling, a library of different yarn architectures has been developed. They can be used as an engineering design tool in simulation and structural optimization of various applications.

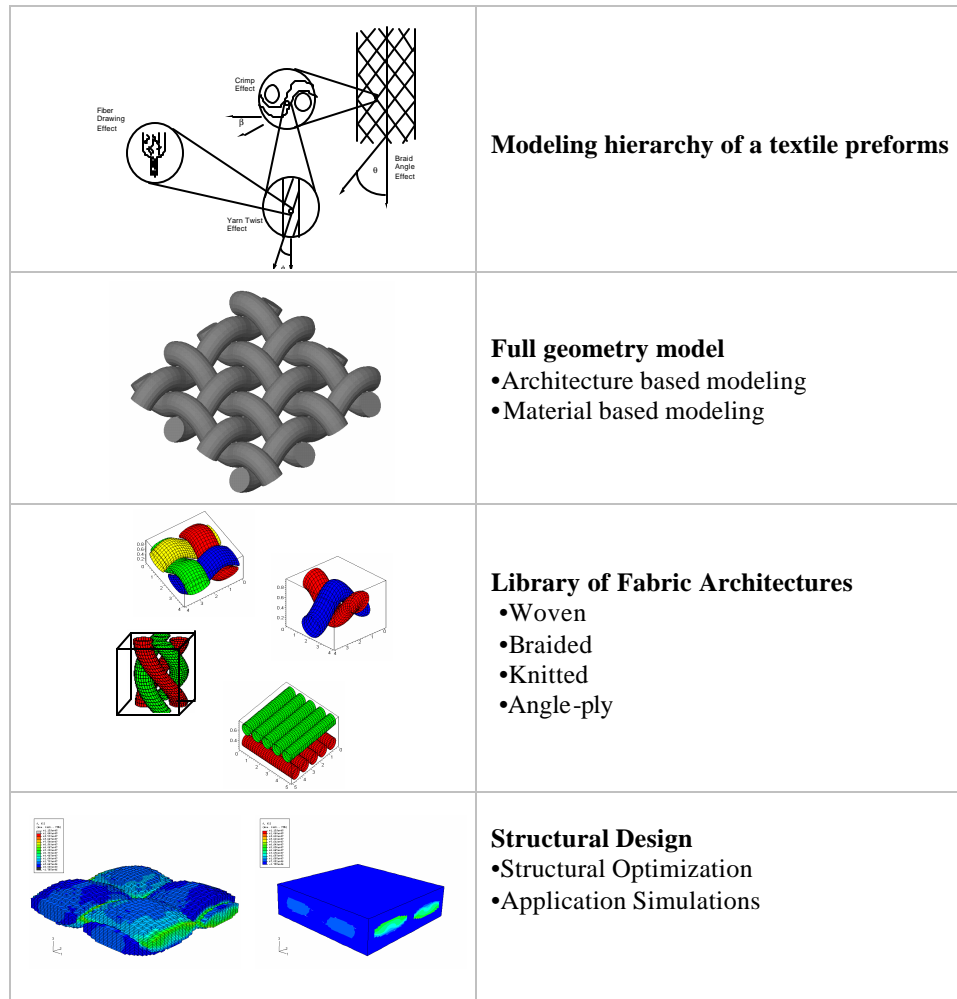


Figure 4.1: Engineering Modeling Tool

Developed models assume that yarns, separated by matrix, do not touch each other. The elastic properties of yarns are taken to be identical to those of fibers. The warp and weft yarns are packed perfectly. The voids of resin and nesting resin on the

interlacing areas of preform are ignored. Further, it is postulated that matrix is not infiltrating into the preform and consequently, fabric mechanical properties resume initial yarn material characteristics.

The main advantage of presented approach is that the developed algorithm generates all-hexahedral-element meshes for arbitrary solids embedded in the parallelepiped. Mesh density, boundary and load conditions of a textile and its RVE-s are functions of only few parameters that can be easily controlled and changed.

Numerical models of composite plates for any structural application can be built by multiplication of unit cells, or simple by extension of a RVE to specific plate size.

4.1 A New Efficient Algorithm for Structured Finite Element Mesh Generation of Fabric Geometry Models (FE-FGM)

This section presents in detail an algorithm that generates a structured FE mesh in a rectangular unit cell that contains a matrix and number of fibers whose location is mathematically prescribed. The algorithm (a listing of the basic program is given in the Appendix) is shown schematically in Figure 4.2.

Yarn Representation

The yarn is defined as a volume along a parametrically defined 3D curve. For example, if (x_0, y_0, z_0) , is the center of the yarn, at that point the orientation of the ellipse is defined with two angles:

(φ) —angle between the normal (\vec{n}) on the ellipse plane and the global (y) axis;

(θ) —angle between the long semiaxis (a) and the global (x)-axis.

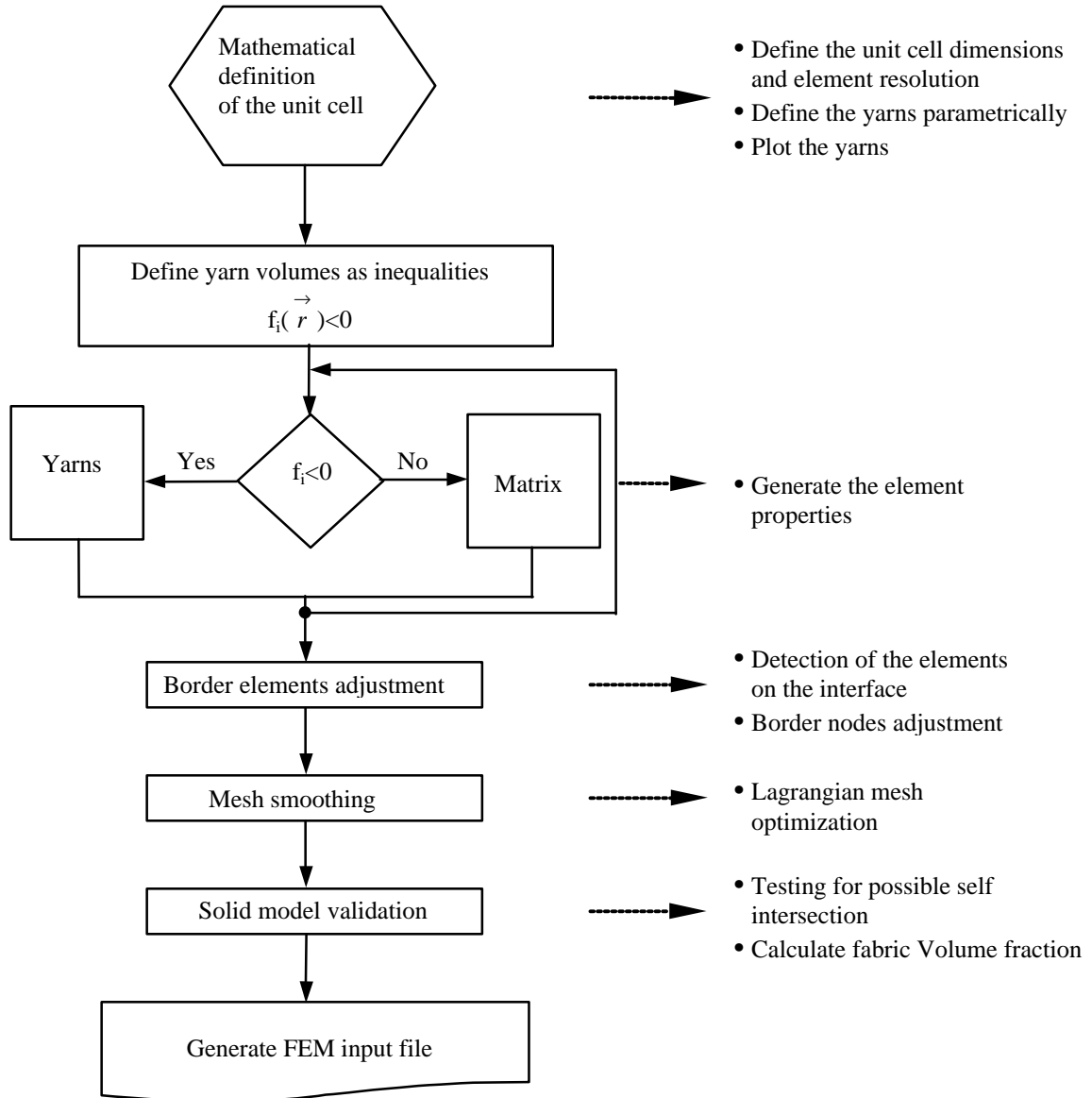


Figure 4.2: Algorithm of a MAPLE Code

Although many general situations can be addressed, here we consider mainly yarns of ellipsoidal cross section that are constant across the length with axes parallel to the cell sides, Figure 4.3.

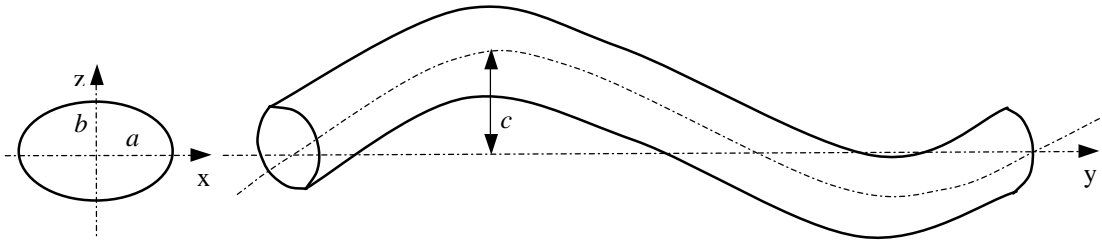


Figure 4.3: Yarn Architecture and Cross-section

The flattening factor of the yarn is the ratio of the two semi-axes of the ellipse (a , and b). The crimp factor, (c) is given as the length of warp yarn between two adjacent filing yarns over filing spacing, according to Peirce's model [4.11]. In this case, for a given center (x_0, y_0, z_0) , the yarn is defined as an inequality

$$\left(\frac{x-x_0}{a}\right)^2 + \left(\frac{z-z_0}{b}\right)^2 - 1 < 0 \quad (4.1)$$

Although, curves can be adequately represented as a collection of points, an analytical representation has several advantages [4.12]: (a) precision, (b) compact storage and (c) ease of calculation of intermediate points. Mathematically, either a parametric or a nonparametric form can be used to represent a curve. A nonparametric

form is either explicit or implicit. For a 2D curve, an explicit, nonparametric form is given by

$$y = f(x) \quad (4.2)$$

In this form, for each (x)-value only one (y)-value is obtained. Consequently, closed or multiple-value curves, e.g., a circle, cannot be represented explicitly. An implicit representation of the form:

$$f(x, y) = 0 \quad (4.3)$$

does not have this limitation. Both explicit and implicit nonparametric curve representation are dependent on the selected coordinate system. Moreover, when points on an axis-dependent nonparametric curve are calculated at equal increments in (x) or (y), they are not evenly distributed along the curve length. This unequal distribution of points affects the quality and accuracy of the created model. Limitation lead to an interest in parametric curve representations.

In parametric form each coordinate of a point on a curve is represented as a function of a single parameter. For a two-dimensional curve with (t) as a parameter, the Cartesian coordinates of a point on the curve are:

$$x = x(t), y = y(t), z = z(t) \quad (4.4)$$

The parametric form is suitable for representing closed and multiple valued curves.

Element Identification

The developed method starts covering the domain of interest with a finite set of parallelepipeds termed voxels (three-dimensional volume elements). Their size is arbitrary, but their number is directly related to the precision of calculation. Each element in the volume under consideration is identified as either yarn or matrix by an element identification method. If the domain of interest (unit cell) is rectangular parallelepiped of dimensions (LxWxH), then an element can be defined according to its center point:

$$\vec{x}_{ijk} = \left(\left(i - \frac{1}{2}\right) * \frac{L}{N_L}, \left(j - \frac{1}{2}\right) * \frac{W}{N_W}, \left(k - \frac{1}{2}\right) * \frac{H}{N_H} \right) \quad (4.5)$$

where $(i=0...N_L, j=0...N_W, k=0...N_H)$, and N_L, N_W , and N_H are number of elements per side.

If at the location $x=x_e$ the center of the yarn is at (x_e, y_e, z_e) then if:

$$\left(\frac{y_e - y_0}{a} \right)^2 + \left(\frac{z_e - z_0}{b} \right)^2 < -1 + \mathbf{d} \quad (4.6)$$

where (δ) is a tolerance, then the element belongs to the yarn otherwise it belongs to the matrix.

Smoothing of the Boundary

The fiber-matrix interface at this point is inaccurate and jagged. This can be partially corrected by projecting all the nodes that are within a tolerance (ϵ) from the interface onto the interface. This operation improves significantly the accuracy of the representation of the fiber-matrix interface, but may generate some distorted elements. For this reason if the projection of a node to the interface creates a heavily distorted element the node is not moved. As a result, a small number of elements will remain intersected with the interface.

The accuracy of the geometric representation of the fabric can be improved by: (a) global reduction of the element size, which unfortunately leads to fine resolution in relatively featureless areas; (b) usage of more complex but more efficient element creation techniques. For example, a “quad-three” decomposition on a planar object, introduced by Baehmann [4.9], would divide any partially filled element into four sub-elements. This would continue until a predefined accuracy limit is reached. A similar three-dimensional approach (octree) would divide each hexahedral element into eight sub-elements.

At the present time, however, for the textile architectures discussed here (woven unit cell with $16 \times 16 \times 12$ elements, and $\delta=0.0635$, $\epsilon=0.00635$, 24 elements intersect the interface), performed convergence studies show a good degree of accuracy of the current models (see Chapter 3).

The algorithm then confirms that the textile preforms are not touching each other at any point, and calculates fabric volume fraction, as well as resulting number of elements and nodes in generated finite element mesh.

Subsequently mesh smoothing is applied at each node for both matrix and fabric at the location of the node based on the locations of the surrounding nodes and elements. In this case, Laplacian smoothing is used, which relocates a node by calculating the average of the positions of each of the adjacent nodes connected by an element edge to the node in question [4.9].

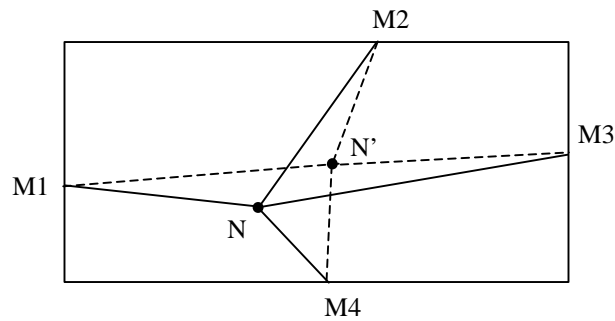


Figure 4.4: Relocation of a Node During a Mesh Sweep

In Figure 4.4, the new position of node (N) is determined by averaging the position of the four nodes, (M), connected to (N) by element edges. The locations of nodes (M2) and (M3), in this case, will pull node (N) up and to the right to reduce element distortion.

Finally an output file is generated to commercial FE software. In this work, an ABAQUS input file is created.

Depending on the density of mesh generated, the pre-processing step, of modeling a 3D FE textile composite unit cell, is of the order of seconds to minutes on modern PC Pentium IV 1.6MHz machine with 512MB of RAM memory.

4.2 Numerical Models of Textile Composite Unit Cells

Three-dimensional finite element analysis was carried out to evaluate the stiffness constants for a developed textile composite unit cells. Figure 4.5 shows numerical models of the unidirectional (0°), angle-ply ($0^\circ/90^\circ$), plain woven, 3D braided and knitted textile composite unit cells considered in this part of the work. The unit cell dimension is 6.35mmx15mmx15mm.

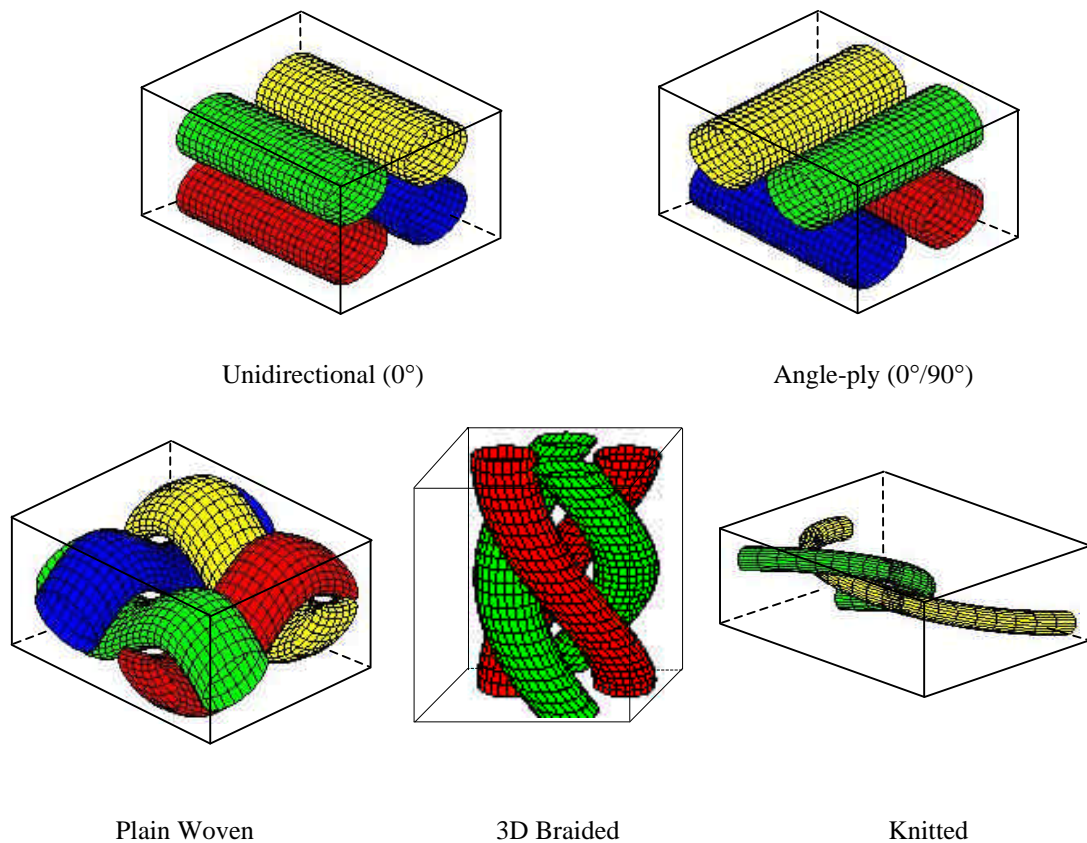


Figure 4.5: Representative Unit Cell Models of Different Textile Composites

While plain woven fabric unit cell is modeled assuming sinusoidal yarn shape (Peirce's model [4.11]), knitted geometry of a fabric structure is represented using an

analytical model developed by Leaf and Glaskin [4.7]. For a 3D braided composite unit cell, as a first approximation, the “helix fiber cell” model proposed in [2.17], is used (Figure 4.5 “3D Braid”).

Each mesh has 3,072 solid elements (8 noded bricks) and 3,757 nodes. A convergence study was performed prior to the finite element analysis to ensure adequate mesh density for each model, as it is indicated in Chapter 3.

Table 4.1: Boundary Conditions

Case	Strain vector	Boundary conditions
A	$\epsilon_x=0.001$	$\partial x _{x=lx}=0.0011_x; \partial x _{x=0}=0; \partial y _{x=0}=0;$ $\partial y _{x=ly}=0; \partial z _{z=0}=0; \partial z _{z=1}=0;$
B	$\epsilon_y=0.001$	$\partial x _{x=lx}=0; \partial x _{x=0}=0; \partial y _{x=0}=0;$ $\partial y _{x=ly}=0.0011_y; \partial z _{z=0}=0; \partial z _{z=1}=0;$
C	$\epsilon_z=0.001$	$\partial x _{x=lx}=0; \partial x _{x=0}=0; \partial y _{x=0}=0;$ $\partial y _{x=ly}=0; \partial z _{z=0}=0; \partial z _{z=1}=0.0011_z ;$
D	$\gamma_{xy}=0.001$	$\partial x _{y=ly}=0.00051_y ; \partial x _{x=0}=0; \partial y _{x=0}=0;$ $\partial y _{x=lx}=0.0005 1_x ; \partial z _{z=0}=0; \partial z _{z=1}=0;$
E	$\gamma_{yz}=0.001$	$\partial x _{x=lx}=0 ; \partial x _{x=0}=0; \partial y _{x=0}=0;$ $\partial z _{z=0}=0; \partial y _{z=lz}=0.00051_z ;$ $\partial z _{y=ly}=0.0005 1_y;$
F	$\gamma_{xz}=0.001$	$\partial x _{z=lz}=0.00051_z ; \partial x _{x=0}=0; \partial y _{x=0}=0;$ $\partial y _{x=ly}=0; \partial z _{z=0}=0; \partial z _{x=lx}=0.0005 1_x;$

In order to obtain the stiffness matrix coefficients, both normal and shear loading were considered for computing normal and shear moduli. Six FE cases were run (Table 4.1) for the same model of a unit cell, corresponding to the six individual strain

vectors $(\epsilon_x, \epsilon_y, \epsilon_z, \gamma_{xy}, \gamma_{yz}, \gamma_{xz})$. The relevant boundary conditions for each case correspond to the displacement of a homogeneous strain field.

The average stresses are computed by dividing the resultant nodal forces with the corresponding cross-sectional area. Effective modulus is computed by dividing this average stress by the applied strain. Computing the average strain in the transverse direction and dividing it by the applied strain also compute the Poisson's ratios.

One of the representative textile composite unit cell models is presented in Figure 4.6.

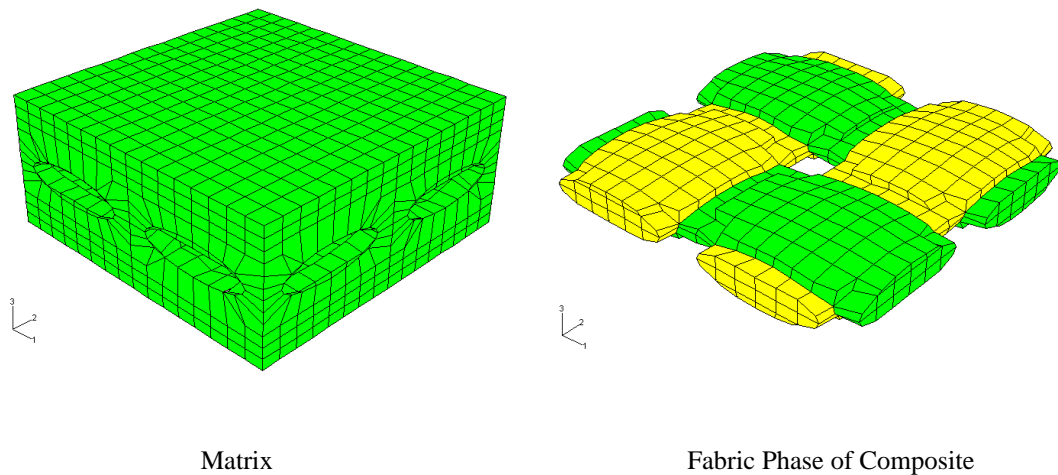


Figure 4.6: FE Model of a Woven Composite Unit Cell

To validate the present numerical model, a comparison is carried out using experimental data available in the literature. The constituent material properties and the unit cell geometries for the woven textile composite examples are listed in Table 4.2.

Table 4.2: Properties of Constituent Materials

Dasgupta <i>et al.</i> [2.9] Woven Unit cell size: 1.68x1.68x0.228mm Volume fraction: $V_f=0.26$	Glass fiber	$E_1=58.61\text{GPa}$, $E_2= E_3=14.49\text{GPa}$, $G_{12}=5.38\text{GPa}$, $\nu_{12}=0.25$, $\nu_{23}=\nu_{13}=0.247$ $G_{13}= G_{13}=2.14\text{GPa}$
	Epoxy matrix	$E=3.45\text{GPa}$, $\nu=0.37$
Naik [2.31] Woven Unit cell size: 2.82x2.82x0.255mm Volume fraction: $V_f=0.64$	Graphite fiber	$E_1=144.8\text{GPa}$, $E_2= E_3=11.73\text{GPa}$, $G_{12}=5.52\text{GPa}$, $\nu_{12}=0.23$, $\nu_{23}=\nu_{13}=0.3$ $G_{13}= G_{13}=2.65\text{GPa}$
	Epoxy matrix	$E=3.45\text{GPa}$, $\nu=0.35$

Table 4.3 compares the developed FE model of the unit cell (for the elliptic cross-section with the a/b ratio of 3:1), with available literature results. In both cases, the engineering constants obtained from the presented numerical model were in good agreement with available results.

Table 4.3: Comparison of Continuum Properties

Source	E_1, E_2 [GPa]	E_3 [GPa]	G_{13}, G_{23} [GPa]	G_{12} [GPa]	ν_{13}, ν_{23}	ν_{12}
Experiment (Dasgupta <i>et al.</i> [2.9])	14.38	6.25	1.94	3.94	0.463	0.167
Predicted by FE-FGM	13.78	6.19	1.88	3.55	0.452	0.182
Experiment (Naik [2.31])	64.38	11.49	5.64	4.87	0.396	0.027
Predicted by FE-FGM	63.51	10.88	4.91	4.93	0.385	0.039

4.3 The Influence of Fabric Architecture on Textile Composite Mechanical Properties

To explore the effect of fabric architecture on textile composite mechanical properties, a set of simulations was performed on the woven textile composite unit cell. The input engineering elastic constants of the composite material composed of a Spectra® fabric/epoxy matrix, are given in Chapter 4.

The influence of yarn shape, yarn orientation and fabric volume fraction on the elastic properties is considered (Figure 4.7 and Figure 4.8). It was found that in-plane Young's moduli (E_{11} , E_{22}) are strong functions of fabric volume fraction, while (E_{33}) is not (Figure 4.7), which shows tailoring capabilities of this class of composites. Simulations have predicted that shear moduli also are dependent on fabric volume fraction (Figure 4.8).

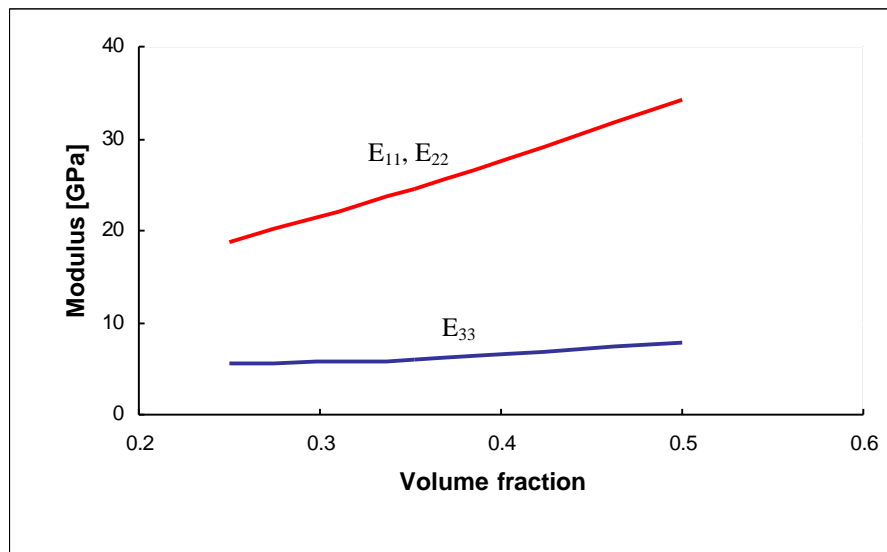


Figure 4.7: Influence of Fabric Volume Fraction on Composite Elastic Properties

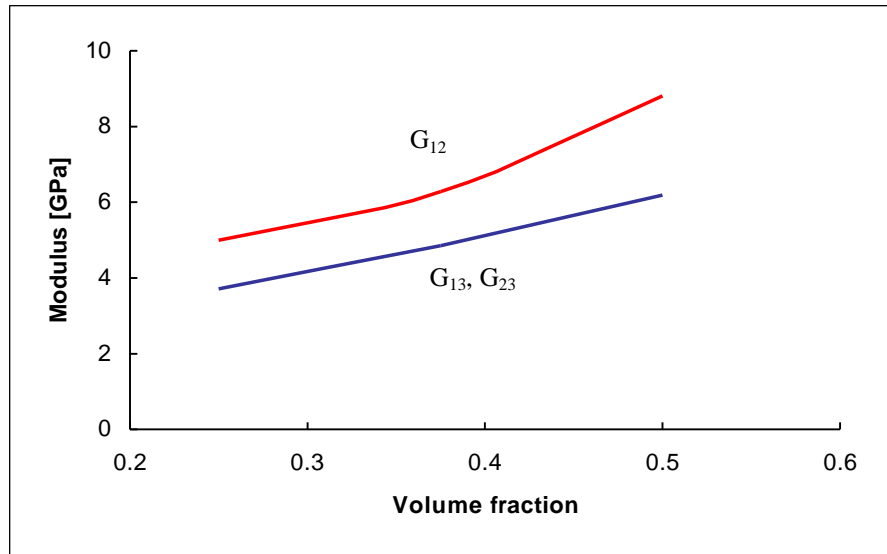


Figure 4.8: Shear Moduli as a Function of Volume Fraction

As it is shown in Chapter 2, considerable effort has been devoted to predicting textile composites mechanical properties and effectiveness of various reinforcement concepts. However, it seems that the analysis and experiments performed on advanced composites are usually (with a few exceptions, like [2.4]) reported for individual systems. The modeling tool established here allows the development of structure-property maps for different textile composite systems.

A parametric study is performed in order to compare engineering elastic constants for different textile composite architectures, unidirectional (0°), angle-ply ($\pm 45^\circ$, $0^\circ/90^\circ$), plain woven, 3D braided and knitted. The geometric parameters considered include fiber volume fraction (which is varied from 20%-60%, except for knitted unit cell, which was 20%-40%), and different yarn arrangements. The material parameters are matrix and fabric elastic properties for a Spectra[®]/epoxy composite system.

The longitudinal Young's modulus of an angle-ply ($0^\circ/90^\circ$) laminate showed to be lower than that of a unidirectional lamina (UD in Figure 4.9), but better transverse elastic properties and in-plane shear resistance (Figure 4.10) can be achieved through the stacking of the unidirectional laminae with different fiber orientations.

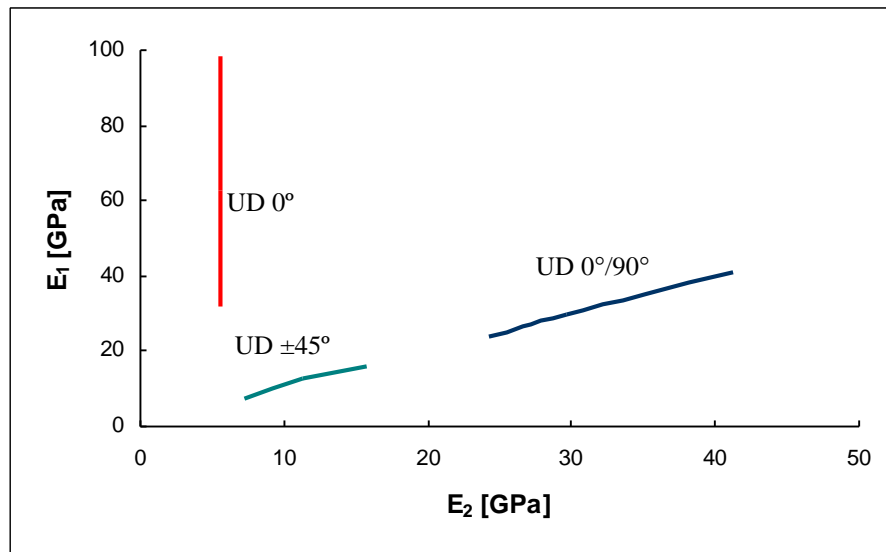


Figure 4.9: Young's Modulus as a Function of Laminae Stacking Sequence

Figure 4.10 demonstrate that for ($\pm 45^\circ$) angle-ply, the in-plane stiffness drops to a minimum, while the shear modulus reaches its maximum.

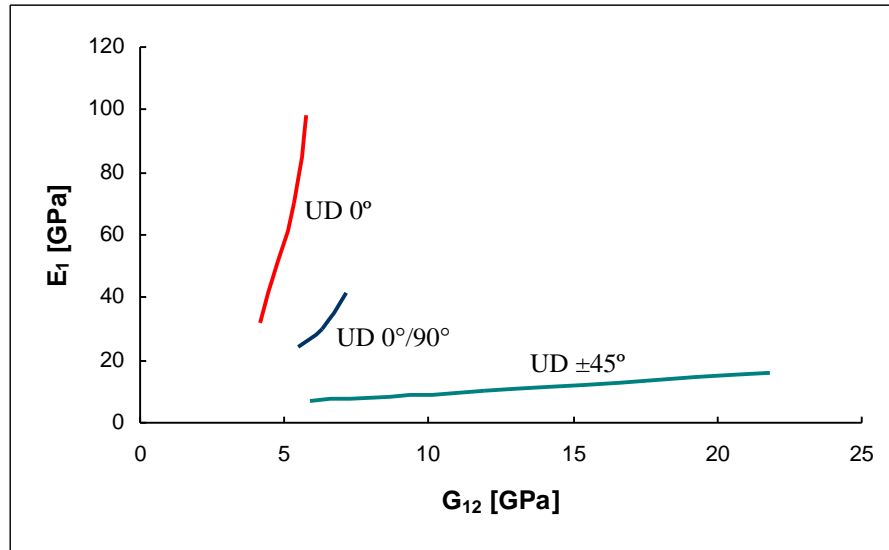


Figure 4.10: In-plane Elastic Properties for Angle-ply Laminated Composites

Numerical analysis showed that resulting stiffness for all considered architectures lays within the lower and upper bounds of the corresponding unidirectional unit cell, for the given material properties of a Spectra[®]/epoxy composite. The longitudinal Young's modulus of a 3D braided composite, with braiding angle of (15°), is predicted to be higher than that of two-dimensional woven textile composites (Figure 4.11).

Knitted fabric composites, on the other hand, generally have lower stiffness and strength [4.3], due to relatively low fabric volume fractions and more opened, looped yarn architecture.

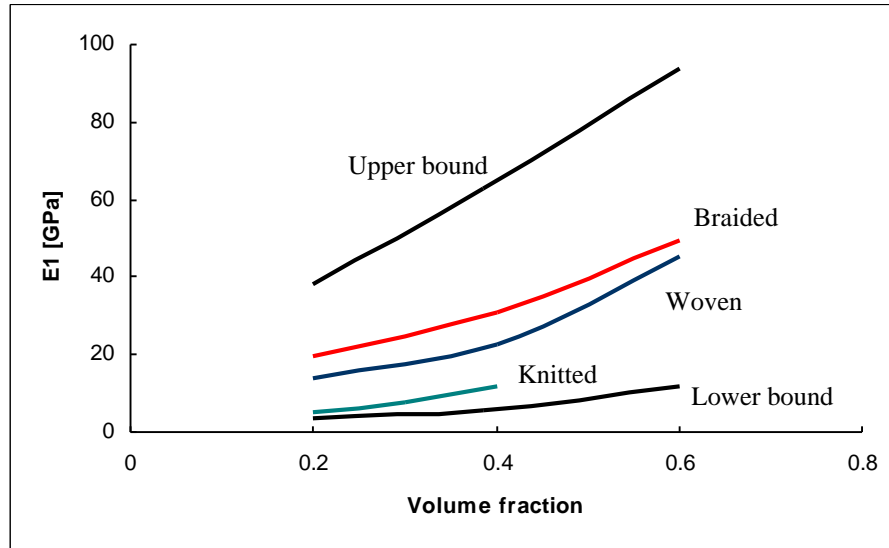


Figure 4.11: Stiffness as a Function of Volume Fraction for Different Textile Composite Architectures

However, woven composites provide more balanced properties in the fabric plane than other composites, behaving similar to angle-ply ($0^\circ/90^\circ$) cross-ply, although the fiber waviness tends to reduce the in-plane efficiency of the reinforcements, as it is shown in Figure 4.12.

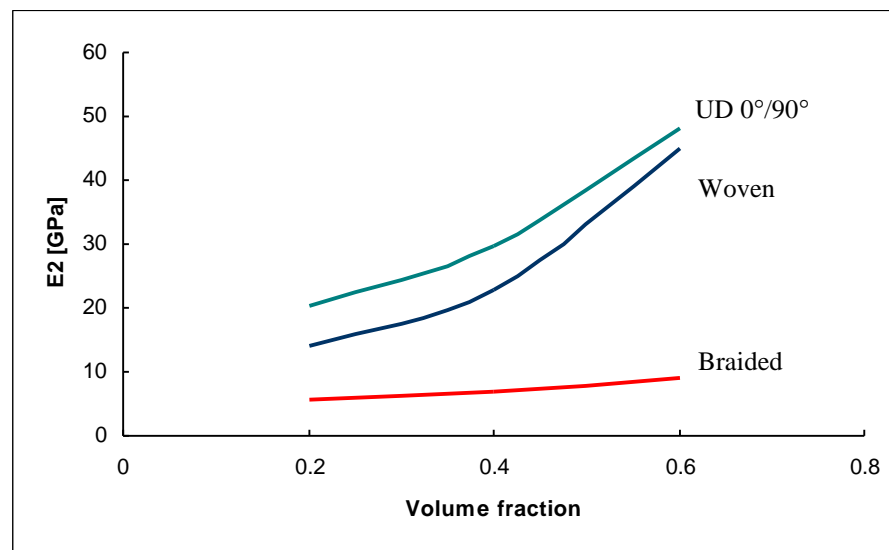


Figure 4.12: The Effect of Unit Cell Architecture on In-plane Mechanical Properties

Out of plane mechanical properties for all tested unit cell textile composites are predicted to be much lower than those in the fabric plane (Figure 4.13), as expected.

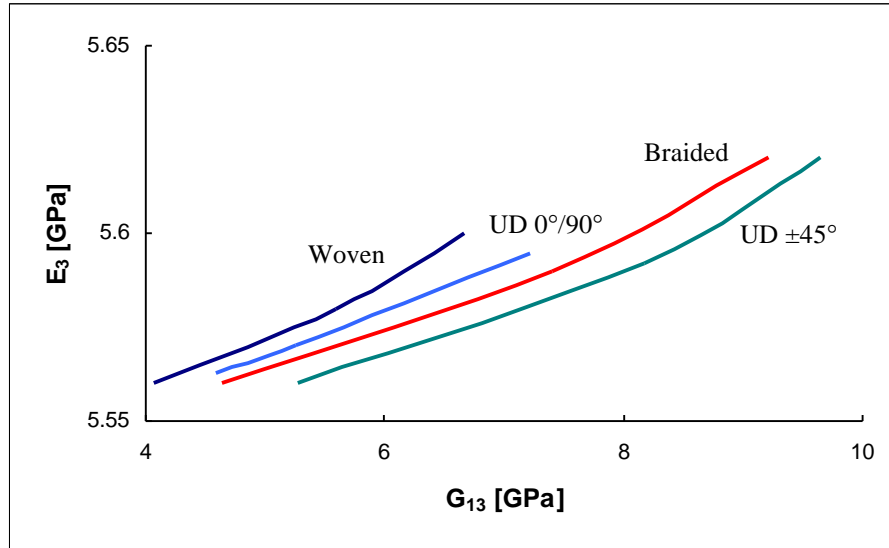


Figure 4.13: Out of Plane Elastic Properties as a Function of Textile Architecture

The elastic properties of braided composites also show strong dependence on fiber orientation, as illustrated in Figure 4.14, which is in a good agreement with experimental findings [4.6].

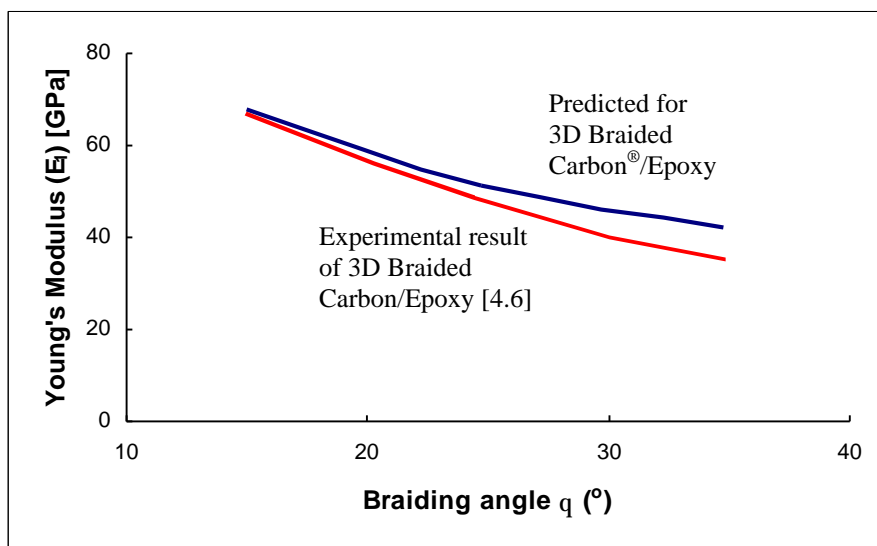


Figure 4.14: Stiffness of a Braided Textile Composite as a Function of Braiding Angle

The Effect of Fiber Shape on Elastic Mechanical Properties

The advantage of this model is that it can isolate the effect of specific geometry factors. For example, the Young's modulus for different yarn shapes was evaluated, keeping the same crimp value of 10%, and a woven composite volume fraction of 40%. It was found that the flatter the yarn cross-section the higher the stiffness of the composite in the reinforced plane (Figure 4.15). It is noteworthy that the modulus in the reinforcement direction increases by more than 50% when the flattening factor goes from 1 to 4.

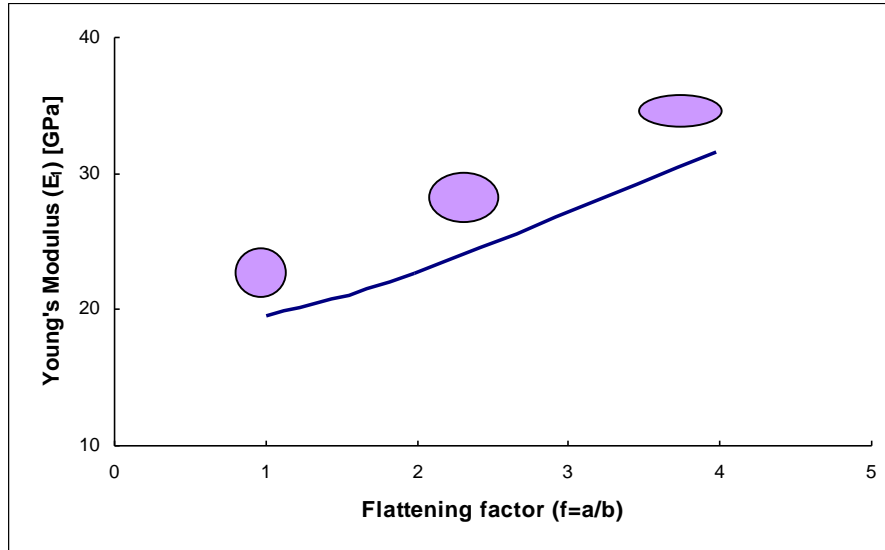


Figure 4.15: The Influence of Yarn Cross-section on Woven Composite Mechanical Properties

Fabric undulation and yarn cross-sectional shape are actually correlated, because flattening the yarns decreases the distance between warp and weft yarns, which reduces fabric undulation, lowering the directional cosines along the fiber's axis and thus improving fabric stiffness. At the same time, with low crimp, the reinforcement is better aligned along the loading axis. This is also predicted elsewhere [4.10].

Therefore, fabric crimp should affect in-plane stiffness. This is confirmed numerically in Figure 4.16. The Young's modulus decreases by increasing fabric crimp, for the constant cross-section of ($a/b=3.5$), and volume fraction of 30%, since textile waviness reduces yarn to fabric tensile translation efficiency.

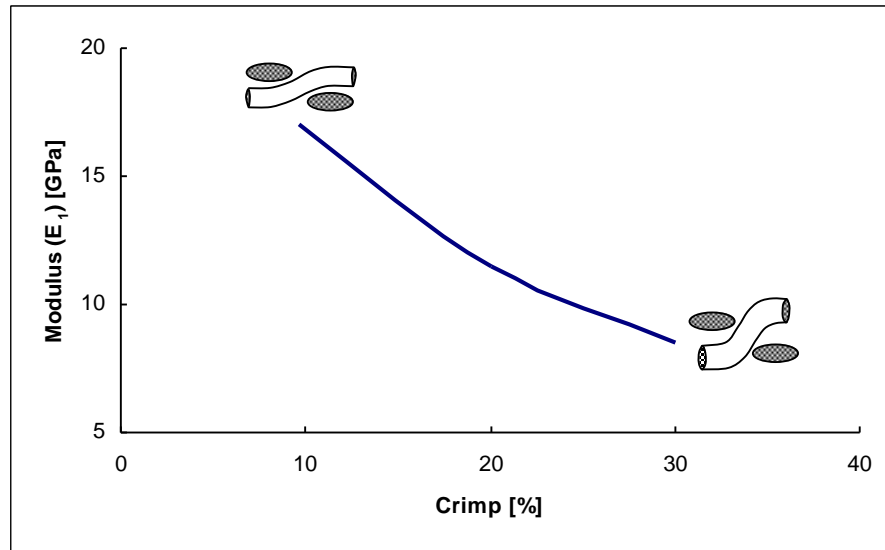


Figure 4.16: Elastic Properties as a Function of Fabric Architecture

Nonlinear Behavior of Textile Composites

Due to its architecture, and interactions between their elementary components, textile composites exhibit a complex mechanical behavior and nonlinear response even in elastic region of deformations. In order to capture those nonlinearities, the presented model includes large displacements and finite strains. When the woven composite unit cell ($V_f=35\%$) is submitted to axial tensile and compressive deformations it exhibits considerable differences between extensive and compressive stiffnesses, see Figure

4.17. Under tensile loading, as yarns are straightened, the composite stiffness increases. During compression, yarns “buckle” and bend, which results in a loss of axial stiffness.

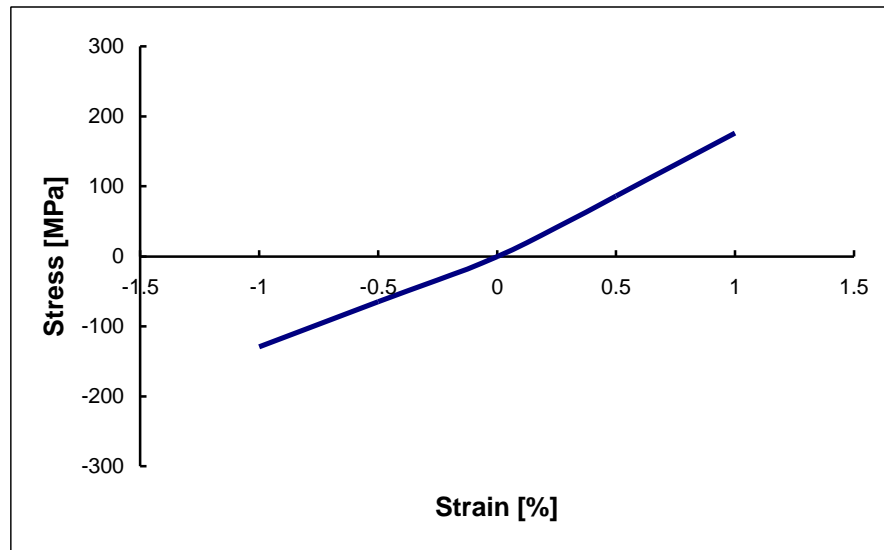


Figure 4.17: Variations of the Stress as a Function of Axial Strain

Another aspect of non-linearity is coming from the effect of the yarn crimp (fabric undulation) on the stress/strain curve. Figure 4.18 shows the predicted stress/strain behavior for three different interlacing densities of a woven unit cell (for volume fractions of 20%, 35% and 50%).

The model predicts stronger non-linearity for a more undulated fabric (more dense packing of the woven unit cell). This essentially bilinear behavior of more undulated yarns, results from the tendency of the yarn to straighten itself which in turn increases the stiffness of the composite.

These results are in line with similar observations (prediction) by Paumelle et al [4.10].

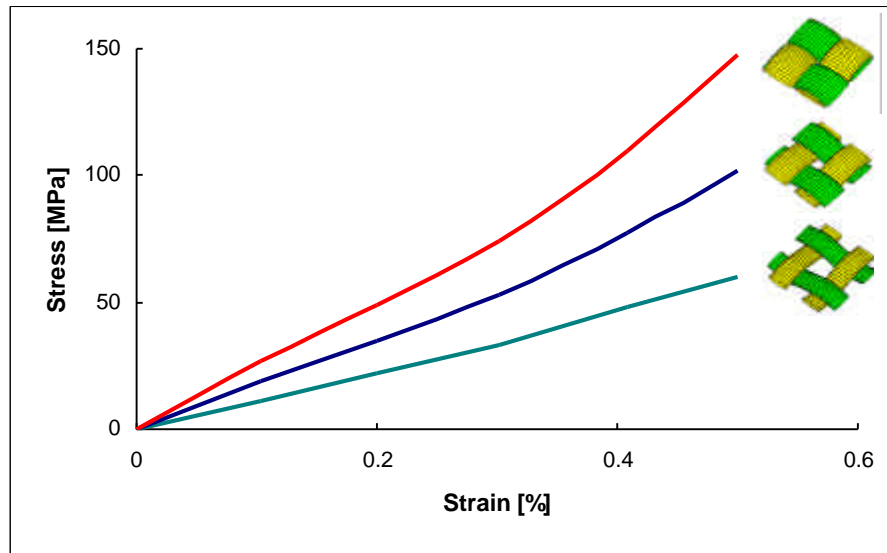


Figure 4.18: Fabric Crimp Effect on Textile Composite Mechanical Properties

It could be concluded that the structure-property maps can represent the basis for material selection and composite component design. These results can be extended to generate a wider range of information that would make available the structural optimization of textile composite systems through various reinforcement architectures and different material combinations.

5. MATERIAL MODELS

Contrary to similar analysis of materials such as steel or aluminum, the simulation of high velocity impact and penetration processes for non-isotropic fiber reinforced material is a more difficult research task [2.3, 7.1, 7.2]. Such analysis is needed to understand the complex dynamic interactions between structural components undergoing large multidimensional deformations and nonlinear material behavior including failure, de-lamination, erosion, etc.

In order to simulate the dynamic behavior of composite materials, the constitutive equations must cover the elastic regime, the material failure, and the behavior of the partially or completely failed material.

From the computer simulation point of view, the introduction of simple discrete models for the study of textile composites offers the advantage of an introduction of different material properties for both matrix and fibers, and possibility of more accurate description of the geometry. Further, more elaborate (and more realistic) failure criteria can be introduced.

The goal of this work is providing the guidelines for the evaluation of polymer-ceramic composites as substitutes of monolithic ceramic facings backed by textile composites. The main advantages of such armor structures are low weight and the ability to manufacture complex and flexible shapes.

In the modeling of the polymer/ceramic facing system, geometric effects are of particular interest, such as the uniformity of penetration resistance, the optimization of packing geometry (in terms of fraction, arrangement, size distribution etc.), baseline comparisons with monolithic ceramic facing, and later on the optimization of multiple layers. To this end, separate models are required for the individual phases.

Before making a detailed description of material models used in simulations, in the next two paragraphs, mechanical and physical characteristics of both ceramic and polymer materials are briefly reviewed.

Ceramics

Ceramics can be defined as inorganic, nonmetallic materials processed or consolidated at high temperature and/or pressure. This definition includes a wide range of materials known as advanced ceramics and is much broader than the common dictionary definition, which includes only pottery, tile, porcelain, and so forth. The classes of materials generally considered being ceramics are oxides, nitrides, borides, carbides, silicides, and sulfides. Intermetallic compounds such as aluminides and beryllides are also considered ceramics, as are phosphides, antimonides, and arsenides [5.1].

Ceramic materials can be subdivided into traditional and advanced ceramics. Advanced ceramics can be subdivided into structural and electronic ceramics based on their primary function or application. Structural applications include engine components, cutting tools, bearings, valves, wear and corrosion-resistant parts, heat exchangers, fibers and whiskers, biological implants, and lightweight armor. The general advantages of advanced structural ceramics over metals and polymers are high-temperature

strength, wear and impact resistance, and chemical stability, in addition to the enabling functions the ceramics can perform.

Important requirement for applications of materials in protective systems is resistance to failure under impact loading or wear resistance. While metals generally exhibit ductile behavior, ceramic materials generally exhibit brittle failure; they are much more susceptible to failure due to high local stresses from impact loading. Ceramic whisker and fiber-reinforced ceramics possessing high toughness have also been developed. These advances have opened additional engineering applications for advanced ceramics.

In general, ceramic materials have a much higher hardness than metals, a property that leads to high wear resistance.

The shock response of ceramics is result of their high hardness and brittleness. They have a high Hugoniot elastic limit (HEL~20GPa). Dislocation activity occurs at very high stress levels, which is associated with micro cracking, since plastic deformation generates residual stresses that give rise to large tensile stresses once the shock pressure is removed.

Polymers

The terms polymer, are used to designate high-molecular-weight materials of either synthetic or natural origin. Plastics are relatively stiff at room temperature, rubbers or elastomers are flexible and retract quickly after stretching, and fibers are especially strong filamentary materials. As properties have been improved, plastics have been developed which can be readily and economically fabricated, and which can be used for previously inappropriate engineering purposes such as gears, bearings, and

structural members. Such engineering plastics may frequently be used advantageously to replace metals or other materials.

The physical behavior of a semicrystalline polymer is very dependent on the percentage of crystallinity, on the size of the crystalline units, on the number and nature of intercrystalline links, and on the amount and nature of uncrystallized impurities. The crystalline melting point is also important, and is itself dependent on the degree of perfection in the crystalline units and on the presence of impurities. Good mechanical behavior requires a balance of properties.

When a polymer is stressed, and then the stress released, some or all of the deformation may be recoverable. The term elastic memory applies to cases in which a polymer is deformed at an elevated temperature, as in the shaping of a sheet into a dome, and then is cooled before the tangled chains have reached an equilibrium condition in the new shape. Strains are said to be frozen in, and at a later time, especially if the product is warmed, these strains cause the product to assume a distorted shape.

In engineering applications, the toughness or the ability to resist fracture assumes considerable importance for plastics. Much research has been directed to the understanding of fracture processes, on one hand, and to the improvement of toughness, on the other. In general, toughness appears to require some combination of high modulus with the ability to dissipate applied energy by relaxation of molecular segments or of added materials.

5.1 Introduction of Failure Models

It is well known that the absorption of energy in ballistic situations depends strongly on the evolution of damage in the target and the resulting progressive degradation of its properties during its interaction with the projectile. For this reason, any computational simulation of impact phenomena must integrate in a rational way the dominant damage mechanisms in the target (and occasionally in the projectile). There are three ways that damage can be integrated in a finite element simulation:

- Ductile/Brittle Interfaces [5.2]: In this case the connectivity of the elements is allowed to change during impact, via a force-displacement law for element boundaries that includes a separation criterion based on maximum force, displacement or other criteria that combine both forces and displacements. Such models are useful in modeling fragmentation, and usually allow no interactions between elements after they have been separated. Such models preserve kinetic energy, and special formulations are required to give consistent, mesh-independent fracture behavior. The best applications suitable for these models are the studies of fragmentation and post-impact debris.
- Element Elimination [2.57, 5.2]: In these models, failure is considered to occur at the element level, on the basis of strain, stress or combined stress-strain criteria. After the failure condition is satisfied in a particular element, the element is “eliminated” from the model. In other words, the element no longer participates in the subsequent analysis. This is a key disadvantage of this approach occurs when failed material is contained in the impact area and participates in the damage resistance even after the initial failure (comminution).

- Distributed Damage [5.3 5.4]: In order to represent quantitatively the effects of the intermediate stages of damage development, models with distributed damage are used. The variables assigned to damage may have a physical or phenomenological interpretation. An evolution equation for damage is necessary to complete the model and must be integrated together with the equilibrium equations. The representation of non-monotonic damage evolution can represent cases where the external loading – e.g., large compressive hydrostatic pressure etc. can result in damage healing (partial closure of a previously open crack). Distributed damage models provide great flexibility in the description of the physical phenomena associated with damage. They tend, however, to be relatively complex. As a result their validation is not straightforward, particularly because the evaluation of the material parameters can be at best, not straightforward.

For simplicity, we have selected an element failure model for the polymeric constituent. The role of the polymer backing plate is to transmit load before local failure. After failure, it is postulated that its contribution to impact resistance is negligible. On the other hand, two different material models for ceramic facing were explored: a distributed damage model, and a brittle tensile failure model.

5.1.1 A Cracking Model for Ceramic Facing

This section describes the cracking constitutive model for brittle materials used for a ceramic facing. This is a “smeared” model in the sense that damage is considered to be homogeneous within an element - even if the length of individual cracks is much

smaller than the element size. It is a “fixed orthogonal crack model”, because it considers damage to be described by micro-cracks oriented along mutually perpendicular planes. These cracks are considered to develop in the undamaged material when a maximum principal stress criterion is satisfied. The direction of the maximum principal stress at that time defines the normal to the plane, along which the micro-cracks appear. Subsequent cracks may develop along the same plane or two other planes normal to the initial crack plane. The coordinate system defined by the cracks may rotate due to rigid rotation of the elements. Cracks are considered to be irreversible, in the sense that once generated, they will always be there. There is the possibility, however, of partial closure of a previously open crack due to compressive forces normal to its plane. The basis of the model is the work of Crisfield and Hilleborg [5.2, 5.4], and its “plasticity-like” theory which is briefly described below.

Strain Rate Decomposition

The total macroscopic strain is partitioned into an elastic part and a crack-induced part:

$$d\mathbf{e} = d\mathbf{e}^{el} + d\mathbf{e}^{cr} \quad (5.1)$$

The elastic part of the model requires the description of elastic response to be dependent on damage.

Given a system of cracks, a geometric relation between the stress with respect to the global coordinates and the stress in local coordinates can be written as:

$$t = T^T \mathbf{s} \quad (5.2)?$$

Where (\mathbf{T}) is the rotation matrix between the global coordinates system and the crack directions. The global stress-strain relation is given by:

$$d\mathbf{s} = E(d\mathbf{e} - \mathbf{T} d\mathbf{e}^{cr}) \quad (5.3)$$

A consistency condition is employed for the development of crack-induced strains based on the local stresses with respect to the crack system.

$$C = C(t, \mathbf{s}^{III}) = 0 \quad (5.4)$$

(t)-is a stress tensor expressed in the local crack system,

($\sigma^{I,II}$)- represents a tension softening model (Mode I fracture) in the case of the direct components of stress and shear softening/retention model (Mode II fracture) in the case of the shear components of stress (material properties).

The consistency condition can be written for a plane of cracks for open and closed cracks as follows:

$$\text{Open crack:} \quad C_{nn} = t_{nn} - \mathbf{s}_t^I(\mathbf{e}_{nn}^{cr}) = 0 \quad (5.5)$$

Where $\mathbf{s}_t^I(\mathbf{e}_{nn}^{cr})$ is the tension softening evolution, and

$$\text{Closed crack:} \quad C_{nn} = t_{nn} - \mathbf{s}_c^I(\max \mathbf{e}_{nn}^{cr}) = 0 \quad (5.6)$$

Where $\mathbf{s}_c^I(\max \mathbf{e}_{nn}^{cr})$ is the crack closing/reopening evolution, which depends on the maximum crack opening strain. Simply stated, for an open crack system, the maximum stress that can be carried in the direction normal to the crack depends of the current crack induced strain (which implicitly represents a crack size). For a crack that is temporarily closed (e.g., due to the application of compressive stress normal to it), the maximum allowed tensile stress depends on the maximum tensile strain attained over the time history of the crack.

Mode I Behavior

The model describes the post-cracking behavior of the material on the basis of the brittle fracture concept of Hilleborg [5.4]. The fracture energy required to form a unit area of a crack is considered to be a material property and can be computed from measuring the tensile stress (σ_t^I) as a function of the crack opening displacement:

$$G_f^I = \int \mathbf{s}_t^I du_n \quad (5.7)$$

Here, (u_n^{cr}) is the displacement across the crack; and (u_n^{el}) is the elastic part of the displacement. In other words, the fracture energy is the total area under the curve in Figure 5.1. The material behavior is defined by the maximum stress under tension (s_{max}) and the maximum displacement under tension, as well as by the shape of the curve.

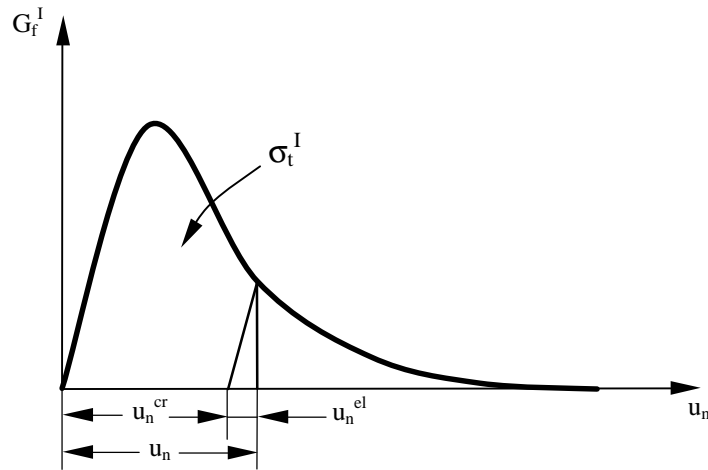


Figure 5.1: Mode I Fracture Energy Based Cracking Behavior

In addition, a length scale is introduced by assuming that the strain induced by cracking is given by:

$$du_n^{cr} = h d\epsilon_{nn}^{cr}$$

It is important to note that the length (h) must be defined appropriately. In ABAQUS implementation, (h) is computed from the dimensions of the elements. This introduces a mesh- sensitivity in the results. Further ideas on the elimination of this mesh sensitivity are being considered.

Mode II Behavior

Mode II behavior, i.e., crack extension due to non-normal stresses with respect to the crack, is only considered in this model in the post-cracking regime. In other words, crack initiation can only be caused by the tensile principle stresses while normal, and shear stresses with respect to the crack can cause crack extension. This model de-

defines the total shear stress as a function of the total shear strain (shear direction (nt) is used as an example):

$$t_{nt} = D_{nt}^{II}(\mathbf{e}_{nn}^{cr}, \mathbf{e}_{tt}^{cr})g_{nt}^{cr} \quad (5.8)$$

$D_{nt}^{II}(\epsilon_{nn}^{cr}, \epsilon_{tt}^{cr})$ is a stiffness which depends on crack opening and may be expressed as:

$$D_{nt}^{II} = \mathbf{a}(\mathbf{e}_{nn}^{cr}, \mathbf{e}_{tt}^{cr})G \quad (5.9)$$

where (G) is the undamaged shear modulus; and $\alpha(\epsilon_{nn}^{cr}, \epsilon_{tt}^{cr})$ is the damage function. A commonly used mathematical form for this dependence, when there is only one crack associated with direction n , is the power law:

$$\mathbf{a} = \frac{\left(1 - \frac{\mathbf{e}_{nn}^{cr}}{\mathbf{e}_{max}^{cr}}\right)^p}{1 - \left(1 - \frac{\mathbf{e}_{nn}^{cr}}{\mathbf{e}_{max}^{cr}}\right)^p} \quad (5.10)$$

which is determined by the damage state via (ϵ_{nn}^{cr}). Here (p) and (ϵ_{max}^{cr}) are material parameters.

This total stress-strain shear retention model differs from the traditional shear retention models in which the stress-strain relations are written in incremental form:

$$\Delta t_{nt} = D_{nt}^{II}(\mathbf{e}_m^{cr}, \mathbf{e}_t^{cr}) \Delta g_{nt}^{cr} \quad (5.11)$$

where $D_{nt}^{II}(\boldsymbol{\varepsilon}_{nn}^{cr}, \boldsymbol{\varepsilon}_{tt}^{cr})$ is an incremental stiffness which depends on crack opening.

The difference between the total and incremental formulations is best illustrated by considering the shear response of the two models in the case when a crack is simultaneously opening and shearing (see Figure 5.2 for the total, and Figure 5.3 for incremental model). In the total approach, it is obvious that the shear stress tends to zero as the cracks opens and shears, while, in the incremental model, the shear stress tends to be a finite value. This may explain rather stiff responses that are usually obtained with the conventional shear retention models.

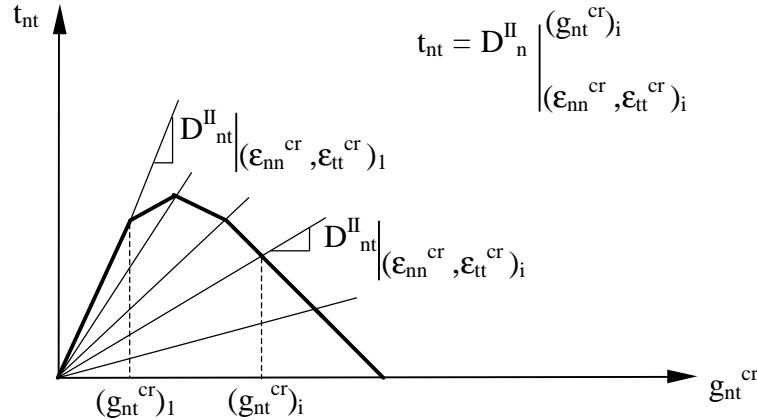


Figure 5.2: Crack Opening Dependent Shear Retention (Total) Model

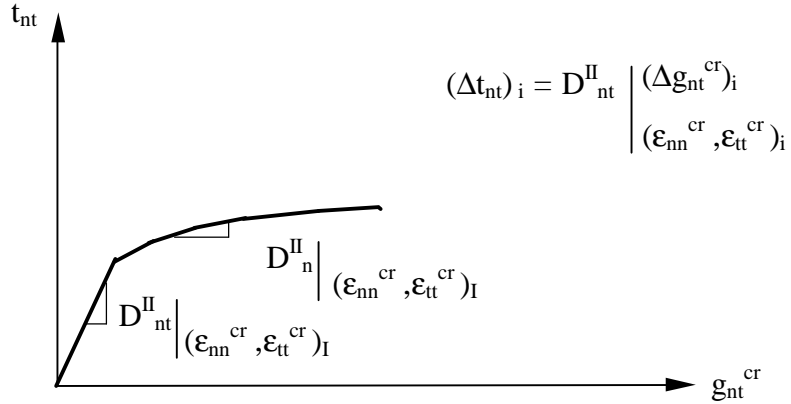


Figure 5.3: Crack Opening Dependent Shear Retention (Incremental) Model

5.1.2 A Brittle Tensile Failure Model

This model uses the hydrostatic pressure stress as a failure measure to model dynamic spall or a pressure cutoff. Ceramic facing was assumed to fail when the hydrostatic pressure (p), exceeds the specified hydrostatic cutoff stress, (σ_c). At this value of stress, at an element integration point, the material point fails. When the tensile failure criterion is met it is assumed that the material underwent brittle failure. Brittle tensile failure was modeled by setting the deviatoric stress components to zero, and the pressure stress is required to be compressive (Figure 5.4). This failure choice corresponds to point (1). Elastic perfectly plastic behavior was assumed for compressive behavior of the ceramics. The Von Mises yield criterion and the Rankine failure criterion were used to model facing material in this case.

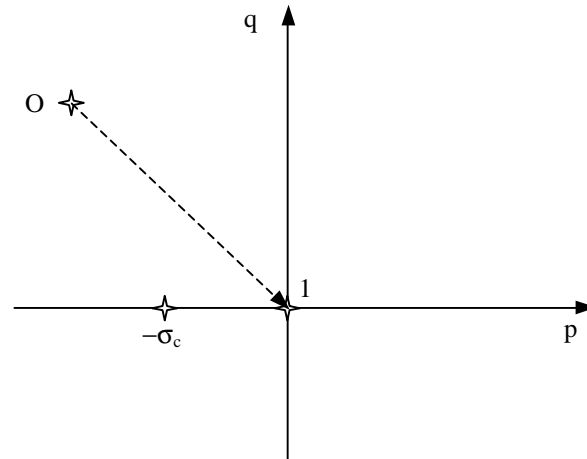


Figure 5.4: A Brittle Tensile Failure Model

5.2 Element Failure Model for Polymer Matrix Composite

The ductile failure model, used for both the fabric and matrix phase of the polymer matrix composite, provides a simple failure criteria, which are designed to allow the stable removal of elements from the mesh as a result of tearing or opening of the structure. The failure model is based upon the value of the equivalent plastic strain. When the equivalent plastic strain, at a material point, reaches the value defined as the plastic failure strain, (ϵ_f^{pl}), the material point is failed. If all of the material points in the element fail, the element loses its ability to resist any further load and, hence, it is removed from the mesh.

In the study of the conditions that lead to fracture, the calculated results should correctly describe the plasticity behavior of both fiber reinforcement and the matrix material prior to fracture. In this case, it was assumed that fracture occurred when the mate-

material is in the plastic state, i.e. ductile fracture. Brittle fracture, can be considered a limiting case of ductile fracture, if fracture occurs after very little plastic flow.

The ductile failure model is based on a damage-Von Mises plasticity theory with isotropic hardening. The damage manifests itself in two forms: degradation of the yield stress with damage and damaged elasticity.

Figure 5.5 illustrates the deviatoric stress/strain behavior of the material model. The solid curve represents the actual stress while the dashed curve represents undamaged behavior, that is, when only elasto-plasticity is considered.

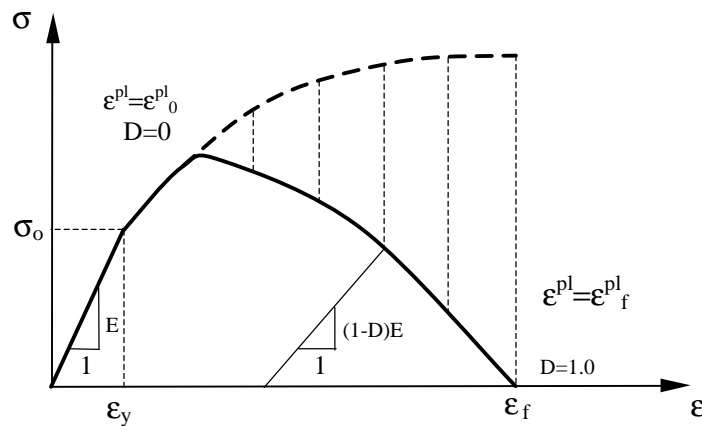


Figure 5.5: Stress-Strain Curve Using the Ductile Mode

Until the initial yield stress, (σ_0), is reached, the material behaves as anelastic. Plastic strain then occurs following the conventional Von Mises plasticity theory. If the strain continues to increase, damage will increase from zero. When the plastic strain is less than or equal to the offset plastic strain, (ϵ_0^{pl}), to a value of one, when the plastic strain reaches the plastic failure strain, (ϵ_f^{pl}). At that time the corresponding total strain is (ϵ_f).

The damage (D), is calculated from the equivalent plastic strain as:

$$D = \frac{\mathbf{e}^{pl} - \mathbf{e}_0^{pl}}{\mathbf{e}_f^{pl} - \mathbf{e}_0^{pl}} \quad (5.12)$$

where \mathbf{e}^{pl} is the current equivalent plastic strain experienced by the material. The equivalent plastic strain is defined as:

$$\mathbf{e}^{pl} = \int_0^t \sqrt{\frac{2}{3} \mathbf{\dot{e}}^{pl} : \mathbf{\dot{e}}^{pl}} dt \quad (5.13)$$

where $\mathbf{\dot{e}}^{pl}$ is the plastic strain rate tensor.

The material's elastic response is based on damaged elasticity. The damaged elastic moduli are given as:

$$G_D = (1 - D)G \quad (5.14)$$

$$K_D = (1 - D)K \quad (5.15)$$

where (G_D) is the damaged shear modulus and (K_D) is the damaged bulk modulus. The unloading path along the damaged modulus is shown in Figure 5.5.

The damaged plastic yield surface is defined as

$$\mathbf{s}_y = (1 - D)\mathbf{s}_y(\mathbf{e}^{pl}) \quad (5.16)$$

Yield surface shrinks to a single point in stress space when the damage reaches a value of one. Due to the damaged elasticity, the model becomes nonlinear in terms of the equivalent plastic strain. Therefore, the decomposition of a strain into its elastic and plastic parts is history dependent.

Low density, high strength polymeric fibers, such as aramid (Kevlar[®]) and ultra high molecular weight polyethylene (UHMWPE) (Spectra[®]) fibers, have been extensively used in composites for high velocity impact applications such as body armors, vehicles, and other structural and mechanical elements. In this work, the projectile is modeled as an elastic-plastic steel material, ceramic facing is assumed to be made of alumina, and the polymer matrix composite, consisted of a Spectra[®] fabric embedded in an epoxy matrix. The epoxy matrix is modeled as a homogeneous isotropic elastic material, while the Spectra[®] fabric is assumed to be elastic orthotropic.

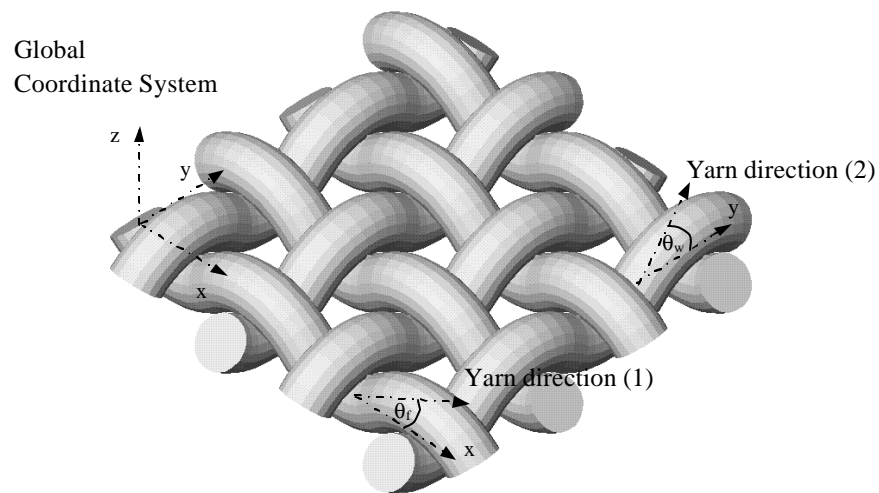


Figure 5.6: Material Orientation Systems

Since the longitudinal (in fiber direction) and transversal yarn mechanical properties are different, elastic characteristics are given in material directions in the local material coordinate systems shown in Figure 5.6.

The existence of the fabric undulation leads to the reduction of the effective elastic moduli in both “x” (fill) and “y” (warp) directions. Hence, the input mechanical properties for the crimped yarns are determined according to Lekhnitskii’s equations [5.5], in which the properties vary with their locations and degrees of undulation. The relevant equations for the fill direction are:

$$E(\mathbf{q}_f)_x = \left[\frac{1}{E_1} \cos^4(\mathbf{q}_f) + \left(\frac{1}{G_{13}} - 2 \frac{\mathbf{n}_{13}}{E_1} \right) \sin^2(\mathbf{q}_f) \cos^2(\mathbf{q}_f) + \frac{1}{E_3} \sin^4(\mathbf{q}_f) \right]^{-1}$$

$$E(\mathbf{q}_f)_y = E_2$$

(5.17)

$$\mathbf{n}(\mathbf{q}_f)_{xy} = E(\mathbf{q}_f)_x \left[\cos^2(\mathbf{q}_f) \frac{\mathbf{n}_{12}}{E_1} + \sin^2(\mathbf{q}_f) \frac{\mathbf{n}_{23}}{E_2} \right]$$

$$G(\mathbf{q}_f)_{xy} = \left[\sin^2(\mathbf{q}_f) \frac{1}{G_{23}} + \cos^2(\mathbf{q}_f) \frac{1}{G_{12}} \right]^{-1}$$

For the warp direction:

$$E(\mathbf{q}_w)_x = E_2$$

$$E(\mathbf{q}_w)_y = \left[\frac{1}{E_1} \cos^4(\mathbf{q}_w) + \left(\frac{1}{G_{13}} - 2 \frac{\mathbf{n}_{13}}{E_1} \right) \sin^2(\mathbf{q}_w) \cos^2(\mathbf{q}_w) + \frac{1}{E_3} \sin^4(\mathbf{q}_w) \right]^{-1}$$

(5.18)

$$\mathbf{n}(\mathbf{q}_w)_{xy} = E(\mathbf{q}_w)_x \left[\cos^2(\mathbf{q}_w) \frac{\mathbf{n}_{12}}{E_1} + \sin^2(\mathbf{q}_w) \frac{\mathbf{n}_{23}}{E_2} \right]$$

$$G(\mathbf{q}_w)_{xy} = \left[\sin^2(\mathbf{q}_w) \frac{1}{G_{23}} + \cos^2(\mathbf{q}_w) \frac{1}{G_{12}} \right]^{-1}$$

The input engineering elastic constants of the composite material composed of Spectra[®] fabric/epoxy matrix used in static analysis, are given in Table 5.1

Table 5.1: Engineering Elastic Constants of Composite Material Constituents

Property	ρ	E_1	E_2	E_3	ν_{12}	ν_{23}	ν_{13}	G_{12}	G_{23}	G_{13}
Material	[kg/m ³]	[GPa]	[GPa]	[GPa]				[GPa]	[GPa]	[GPa]
Epoxy	1,200	3.45	3.45	3.45	0.35	0.35	0.35	1.3	1.3	1.3
Spectra	970	172	4.72	4.72	0.4	0.4	0.4	36	3.4	3.4

Material properties used in impact simulations for both the projectile and the target, are listed in Table 5.2.

Table 5.2: Material Properties Used in Impact Models

Property	Steel	Alumina	Epoxy	Spectra [®]
Density (kg/m ³)	7,800	3,900	1,200	970
Modulus (GPa)	210	350	3.45	268
Poisson's ratio	0.3	0.22	0.35	0.4
Plasticity σ (MPa), ϵ_{pl}	1,240; 0.00 1,550; 0.10	2,400; 0.00	50	3,000; 0.00
Tensile strength (MPa)	/	360	/	/
Strain to failure	0.025	/	0.05	0.03

As already mentioned, two different constitutive models suitable for brittle materials, offered in ABAQUS finite element package, were explored: a brittle cracking model, and a brittle tensile failure model. Both of them were tested in impact analysis of a cylindrical steel projectile on Multi-layered/Multiphase Composite plate consisting of a monolithic ceramic facing backed by an angle-ply ($0^\circ/90^\circ$) composite, presented in Figure 5.7.

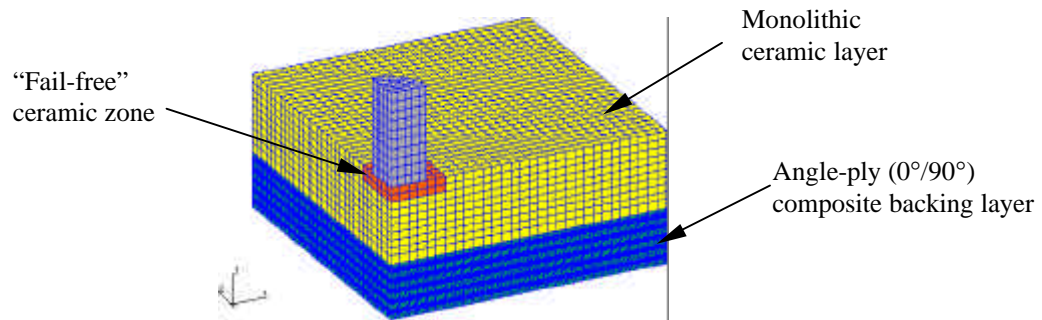


Figure 5.7: Fail-free Zone in Ceramic Layer Under the Projectile

The displacement of the projectile tip as a measure of the penetration depth and projectile velocity were tracked throughout the solution as it is shown in Figures 5.8 and 5.9.

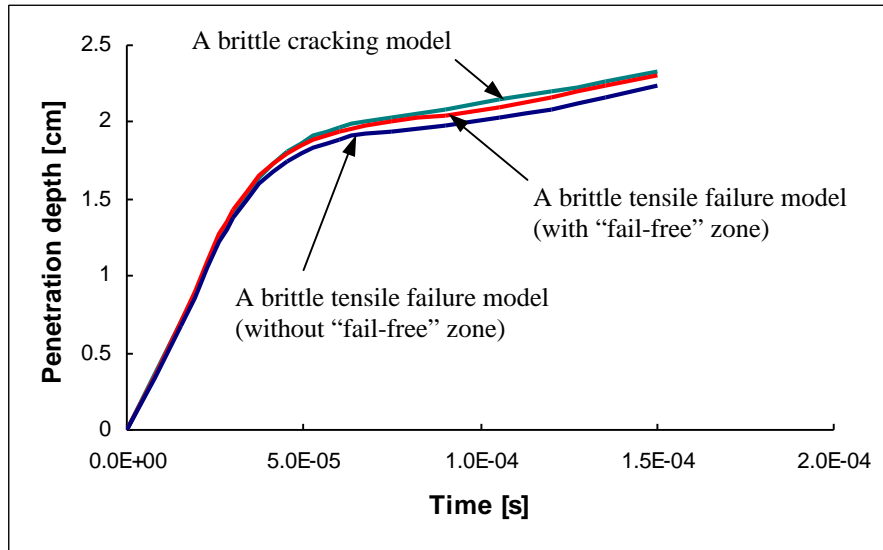


Figure 5.8: Depth of Penetration as a Function of Ceramic Material Model

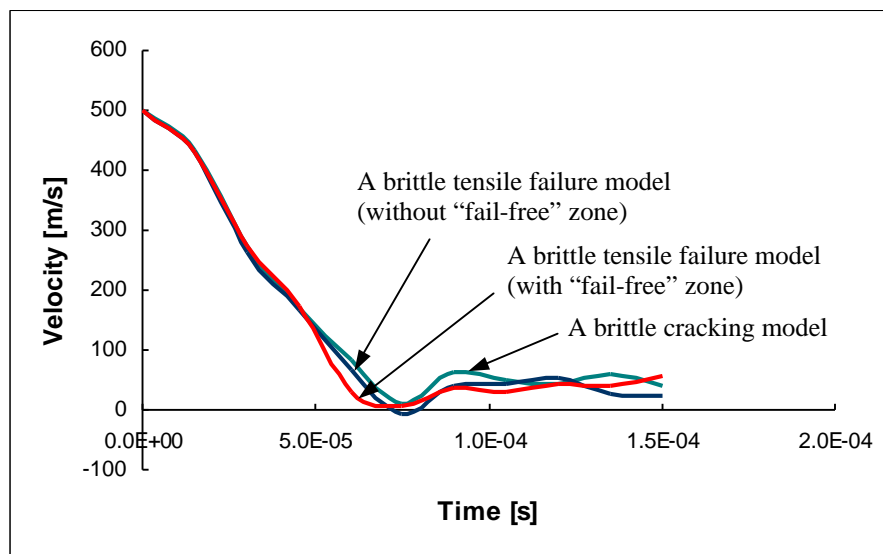


Figure 5.9: Effect of Ceramic Material Model on Velocity Time History

Based on some experimental results [5.7, 5.8], alumina below the projectile crushed and consolidates during the impact. To model this behavior, as it is suggested in [5.7], a limited number of alumina elements directly below the projectile were not allowed to fail in tension. The addition of this “fail-free” zone greatly improved the stability of the solution and has solved convergence problems due to mesh distortion. At the same time, results showed to be unaffected by the chosen ceramic constitutive model. A brittle tensile failure model was used in impact simulations.

Due to the very limited experimental results available in (at least, open) literature, for these simulations, the viscoelasticity of a Spectra[®] polymer fabric is introduced in a stepwise manner. Static Young’s moduli are used, but elevated, according to a specific strain rate. Table 5.3 shows Spectra[®] modulus for different rates of strain [5.6].

Table 5.3: Spectra[®] Fiber Modulus Strain Rate Dependency

Strain rate (min^{-1})	10	500	1,000	5,000	10,000
E [GPa]	101	130	145	221	268

6. PROJECTILE MODELS AND CHARACTERISTICS

One of the factors affecting the penetration resistance of armor systems is the characteristics of the projectile: its geometry (shape and caliber), material, initial velocity, and incident angle [6.1].

Projectile geometries may be broadly divided into three major groups:

- 1) Armor-piercing bullets;
- 2) Rods, and
- 3) Fragment-simulating projectiles.

In order to explore the role of the projectile shape on armor ballistic resistance, high velocity impact of three different kinds of projectiles were modeled. All modeled projectiles have a caliber of 7.62mm, and mass of 125 grains, which corresponds to 8g of a 7.62 NATO projectile. They were further modeled as a deformable, elastic plastic steel material.

In Figure 6.1, finite element models for a different kind of projectiles are presented.

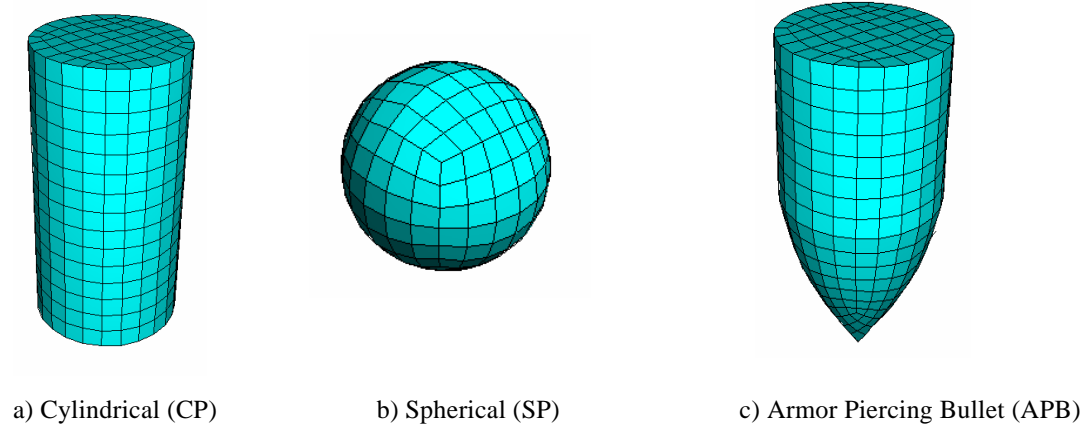


Figure 6.1: Projectile Models Used in Simulations

In order to obtain the targeted projectile mass, due to different volume, the density for different shapes had to be adjusted as it is shown in Figure 6.2.

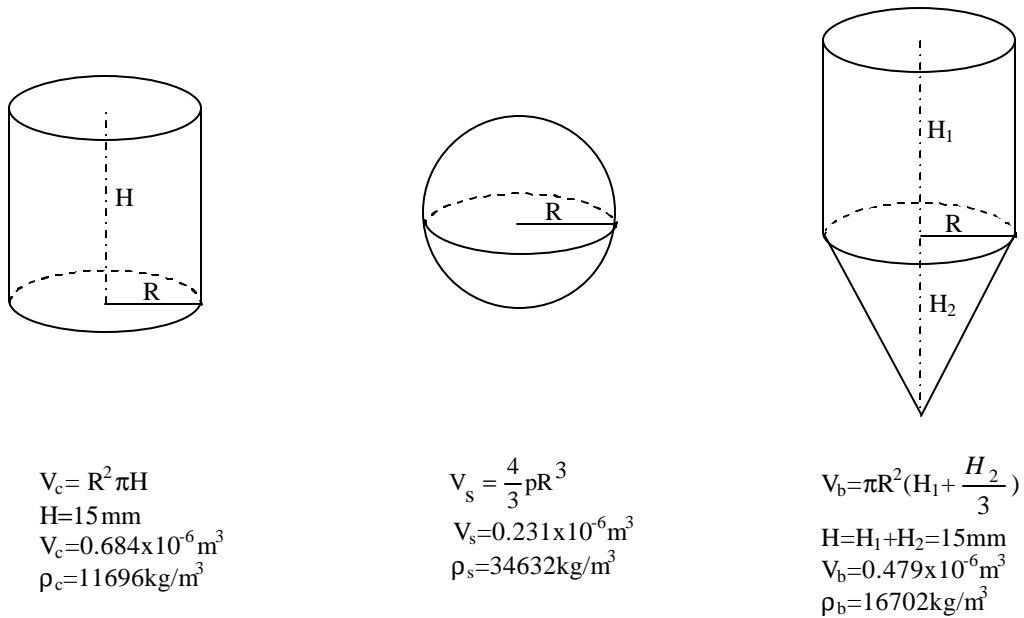


Figure 6.2: Geometric Characteristics of Different Projectile Shapes

The rotational speed, or spin, of a projectile was also taken in consideration. Assuming that the projectile makes one turn for each ten of its lengths path, for a given projectile geometry (H- is its length and R diameter), the rotational speed is given as [2.3]:

$$v_{rot} = \frac{R^2 \mathbf{p}}{10H} v$$

Table 6.1 gives rotational speed for a range of simulated impact velocities.

Table 6.1: Calculated Projectile Rotational Speed

v [m/s]	Turns/s	Rad/s
100	666.67	11.635
250	1,666.67	29.1
500	3,333.35	58.175
750	5,000	87.26
1,000	6,666.7	116.35

However, simulations showed a better ballistic resistance by the target in the case when the projectile had added rotational speed, as it is presented in Figure 6.3. Due to friction and additional contact, further projectile deformation is predicted which affected its penetration speed and contributed to the faster projectile slowing down (steeper curve in the case of APB with rotation).

In order to simplify the number of runs, in further impact simulations, the cylindrical projectile was used without self-rotating.

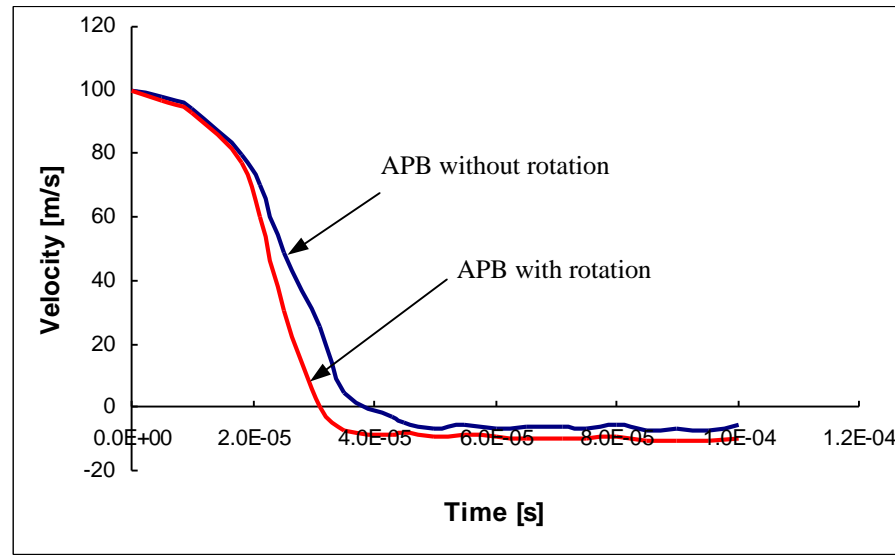


Figure 6.3: Effect of Projectile Rotational Speed on Velocity Time History for Impact on 6.35mm Monolithic Ceramic Plate

Based on experimental findings [8.7], it is noted that sharpened impactors are less effective in perforating the ceramic target. There are two principle penetration mechanisms by which the perforation is effected, namely “plugging” or “shearing”, that is dominant for blunt projectiles, and piercing, characterized by lateral displacement of target material, which is the prevailing mode of penetration in the case of armor piercing bullets. The harder the material, the more resistant it is to lateral displacement. Thus, when the pushing-aside mechanism of penetration occurs, involving APB, the resistance to penetration increases with increasing hardness of the armor. On the other hand, the plugging mechanism involves the shearing out from the armor of a cylindrical disk under the blunted projectile, causing relatively little deformation and no lateral compression of the armor. Harder materials tend to plug more readily and completely, and thus, the resistance to penetration decreases. Figure 6.4 shows the simulated ballistic resistance of a monolithic ceramic plate for different projectile shapes, showing good agreement with

experimental findings, because the sharpen APB was stopped while the blunt cylindrical projectile was able to penetrate the target.

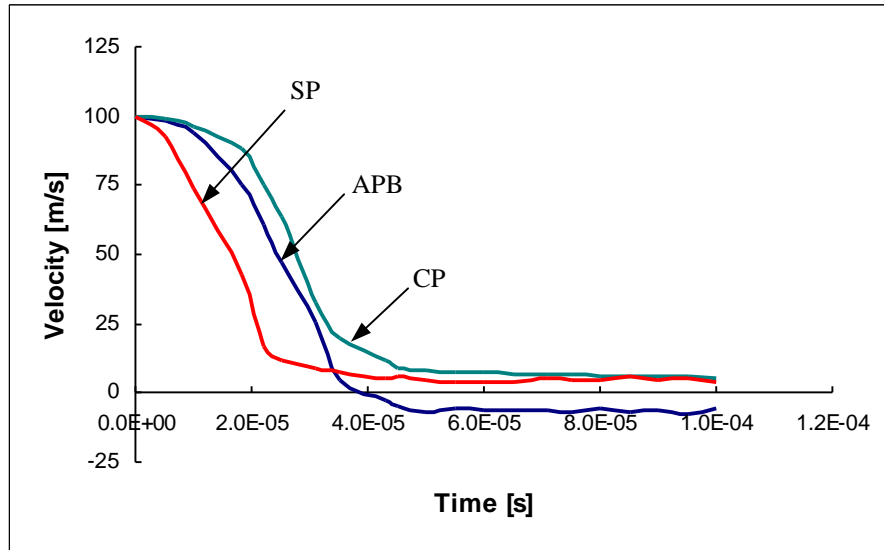


Figure 6.4: Effect of the Projectile Shape on Velocity Time History for Impact on 6.35mm Monolithic Ceramic Model

During the penetration process, the tip of the projectile is significantly eroded (Figure 6.5), because of the high amplitude stress wave generated as the result of the relatively large acoustic impedance of the ceramic and its much higher elastic compressive limit compared to hard steel. The impedance, a property that governs wave propagation in a material, is defined as a product of the sonic velocity and the material's density.

The impact simulation of a cylindrical projectile on a monolithic ceramic plate (Figure 6.5) showed the tensile failure (given in red) that occurs due to interaction of stress waves with the geometric boundary-spall effect on the plate's outer face, which is confirmed in experiments [2.29, 2.38, 2.39].

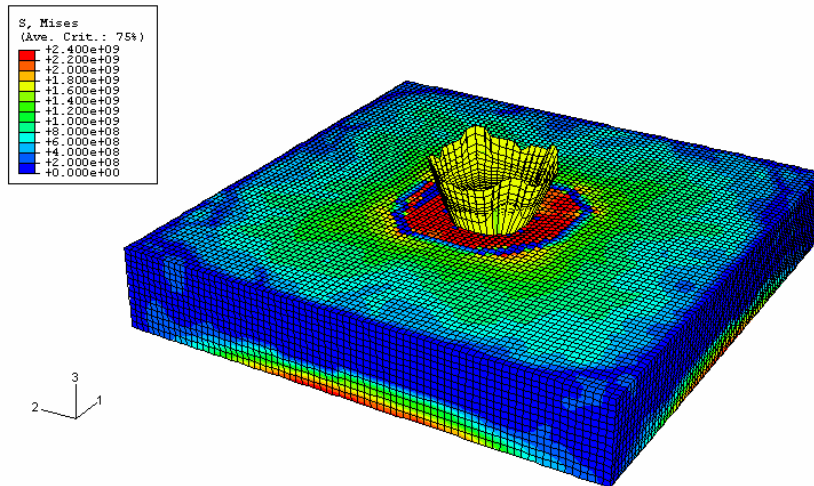


Figure 6.5: FE Simulation of Ballistic Impact on Monolithic Ceramic Plate

The numerical simulations have predicted a high deformation of a projectile during and after the impact, which was in good correlation with the experimental findings, as it is shown in Figure 6.6 [8.8].

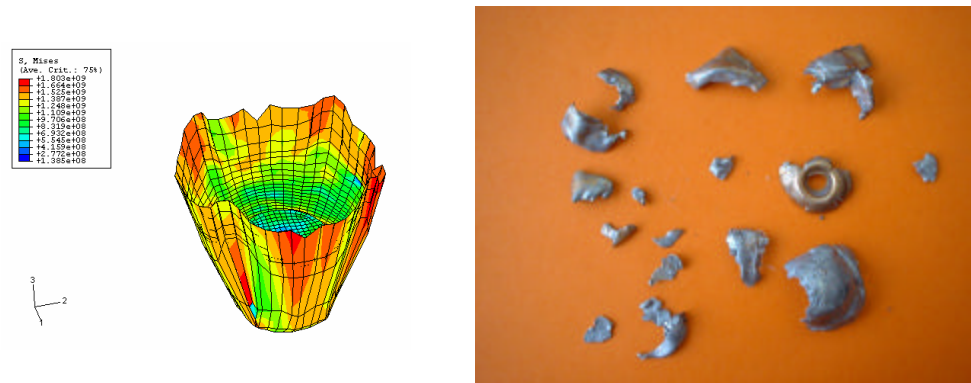


Figure 6.6: Comparison Between FE Model of a Deformed Projectile and the Projectile Fragmentation After Ballistic Test

7. NUMERICAL MODELING OF IMPACT BEHAVIOR OF TEXTILE COMPOSITES

Textile composites, because of their lightweight and high specific strength, have been extensively used for high velocity impact resistance in applications such as armor vehicles, body armors, and in various structural elements [7.1, 7.5, 7.6].

The most important characteristics of the textile composite structural component in any application are the type of the fibers and resins used, the way fibers are arranged, and the fiber/matrix interface bond strength [7.1]. Angle-plyed unidirectional, and woven fabrics are the most commonly used textile architectures in composites for ballistic applications.

In order to explore the role of textile reinforcement in armor impact performance, 25,000 3D eight-nodded finite elements with 28,611 nodes was generated using both, a newly developed FE-FGM algorithm, and an ABAQUS computer code.

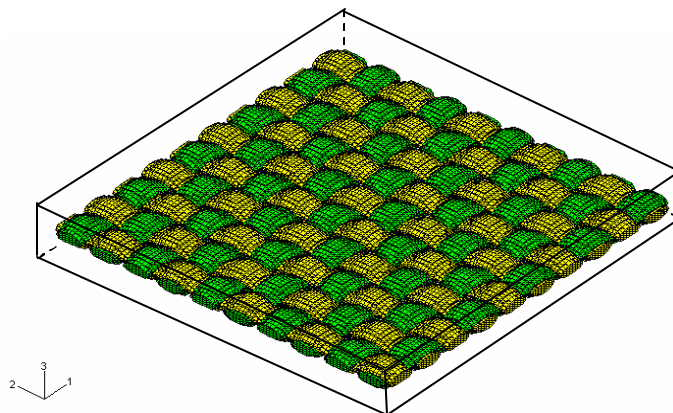


Figure 7.1: FE Model of a Fabric Phase of Woven Composite Plate

The simulation focused on plain woven and angle-ply ($0^\circ/90^\circ$) Spectra[®]/epoxy polymer matrix composite models (Figure 7.1 and 7.2). The dimension of a plate model is 75mm x 75mm with a thickness of 6.35mm, and the volume fraction was varied from 35% to 50%.

A cylindrical projectile with a diameter of 7.62mm was modeled as a deformable, elastic plastic steel material, with a velocity range of 10m/s-1,000m/s.

Angle-ply laminates are usually made of multi-layered sheets placed under different angles. In this work, for computational efficiency, a two-layer angle-ply laminate was considered.

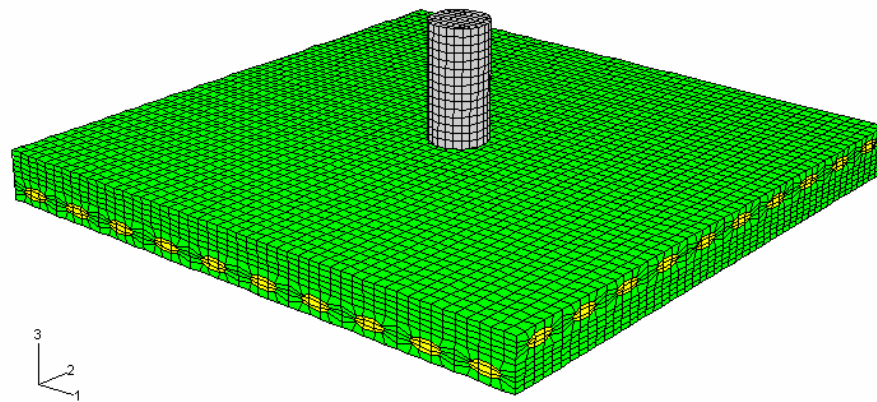


Figure 7.2: FE Model of Angle-ply ($0^\circ/90^\circ$) Plate Under the Impact of Cylindrical Projectile

The effect of boundary conditions was investigated for both moderate and high impact velocities. Generally, the boundary conditions depend on projectile size, its initial velocity, and target geometry and thickness. In this case, where the cylindrical steel projectile impacts at a velocity of 100 m/s, the impact resistance of a target depends on boundary conditions as it is shown in Figure 7.3. In the first case, the model is firmly

gripped on all four edges. In the second case the plate is gripped firmly along two edges and in the third case no edges are gripped. It can be seen that even for the case with no edges gripped, the fabric still provides a significant amount of resistance due to inertia, while the best ballistic resistance was experienced with the model with all edges gripped.

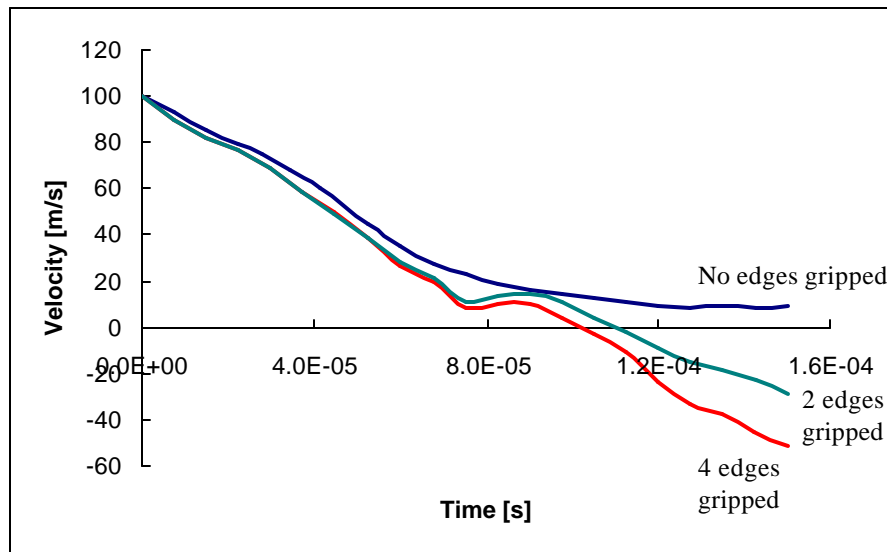


Figure 7.3: Boundary Condition Influence on the Target Ballistic Resistance

However, the higher-velocity impact response is dominated by stress wave propagation through the material, in which the structure does not have time to respond, which leads to very localized damage. In that case, the boundary condition effects can be ignored because the impact event is over before the stress waves have reached the edge of the structure. Based on these results, all further simulations were performed with unclamped ends.

Results

The role of strong anisotropic fibers, which carry most of the applied load in the composite structure, is presented in Figure 7.4, where the impact resistance is compared for a neat epoxy plate versus the textile reinforced plate of the same thickness with different fabric volume fractions.

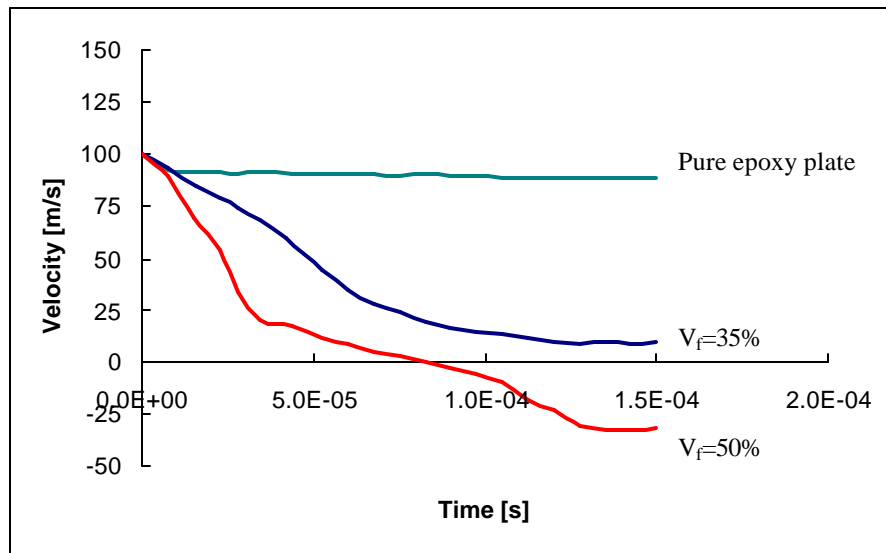


Figure 7.4: The Role of Textile Reinforcement in Composite Ballistic Resistance

A much lower residual velocity, and better ballistic resistance are predicted for textile composite systems, showing the importance of fabric reinforcement for composite structural integrity.

In addition, the effect of the fiber volume fraction is also an important parameter in textile composite structural performance. While a woven reinforced plate with a 50% volume fraction was capable of stopping the projectile, a target with 35% fabric content was penetrated.

The developed engineering design tool was capable of evaluating the influence of different material and loading conditions on the textile composite ballistic resistance. One of design parameters of interest is impact velocity. In a range of incident velocities, from 10m/s up to 1,000m/s, each of them is related to a different dynamic event in the engineering practice [7.6]. For instance, a bird strike on an airplane structure occurs at velocity of 10m/s. Small-arm projectiles have velocities in the range of hundred meters per second, while velocities of an armor piercing bullets are in the range of 1,000m/s (Figure 7.5).

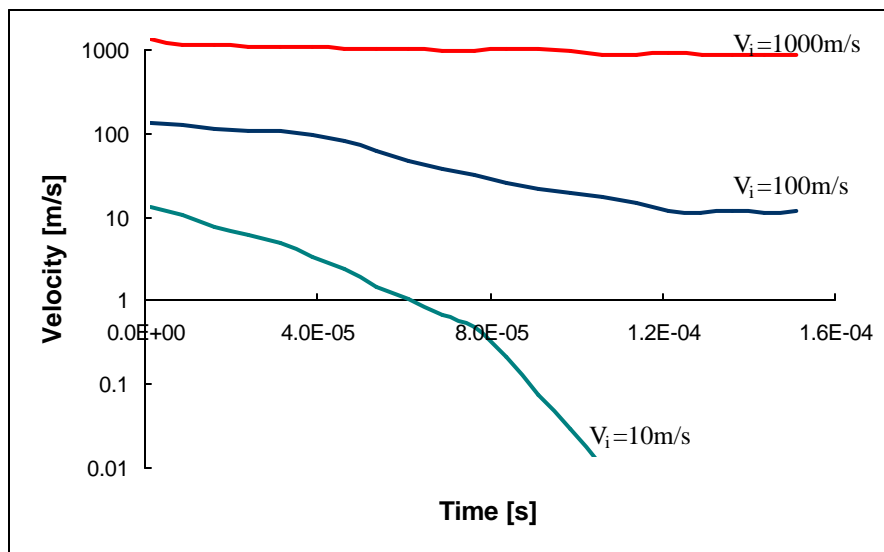


Figure 7.5: Effect of Impact Velocity on Velocity Time History

Thus, simulations have shown that a 35% volume fraction woven composite plate would be easily perforated by a 1,000m/s projectile. However, the same value of volume fraction performed well against a 100m/s projectile and completely stopped one moving at 10m/s.

Woven vs. angle-ply

The most important characteristic of a protective ballistic system is its ability to slow down and stop the projectile. The best way to estimate armor penetration resistance is to measure the residual velocity of a projectile. From Figure 7.6, that shows the velocity time history for different textile architectures, it is clear that the fabric geometry plays an important role in the textile composite impact resistance. While a woven composite model is completely perforated for a given impact velocity, the projectile was stopped by the angle-ply, composite.

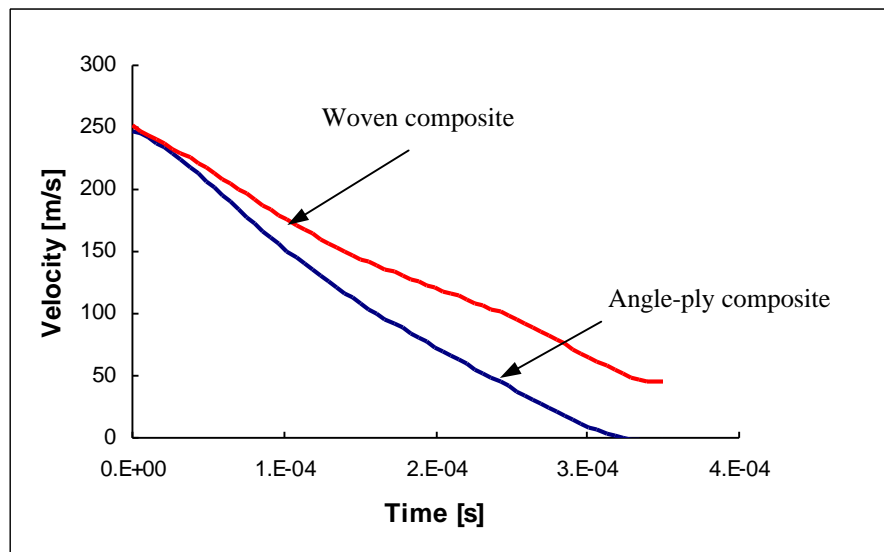


Figure 7.6: Effect of Composite Fabric Architecture on Velocity Time History

Woven composites provide more balanced mechanical properties in the fabric plane than other composite systems [2.20]. Zikry et al [7.3], have presented experimental results that show the better impact resistance of an angle-ply composite plate. These simulations showed the same trend with experiments.

Keeping in mind the differences between the two textile architectures, two main reasons may contribute to the relative composite ballistic performance. First,

woven fabric undulation leads to the reduction of the effective elastic moduli in both the fill and warp directions, resulting in an overall decrease in ballistic resistance.

Although woven architecture absorbs a large amount of strain energy, the associated deflections are very large (Figure 7.7) and the longitudinal strain wave velocity is small, suggesting that energy is transferred slowly through the material system. This shows the potential of using this kind of composites in applications where structural flexibility is important, perhaps in the lower velocity range.

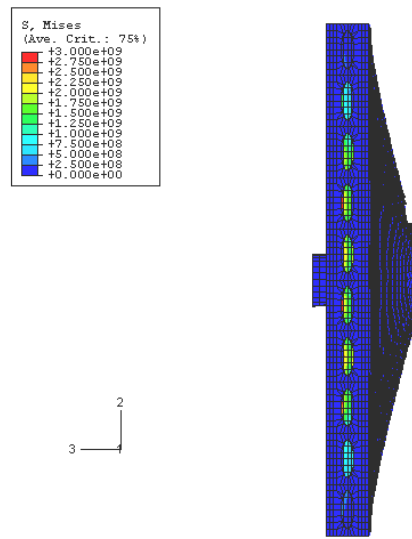


Figure 7.7: Conical Deformation and Rupture of the Plain Woven Composite Plate at an Impact Velocity of 250m/s

In order to understand this behavior, the stress distribution in one-quarter of both the angle-ply and plain woven fabric phase of the composites for the 250m/s impact is compared (Figure 7.8). A higher in-plane modulus gives a higher stiffness in the initial structural response of the straight preform than that of the crimped one, while the crossover points and the undulation of a woven reinforcement lead to a reduction of the

effective elastic moduli in both the fill and warp directions resulting in an overall decrease in ballistic resistance.

Thus, the models have predicted faster energy dissipation for the angle-ply ($0^\circ/90^\circ$) structure in the initial stage of penetration.

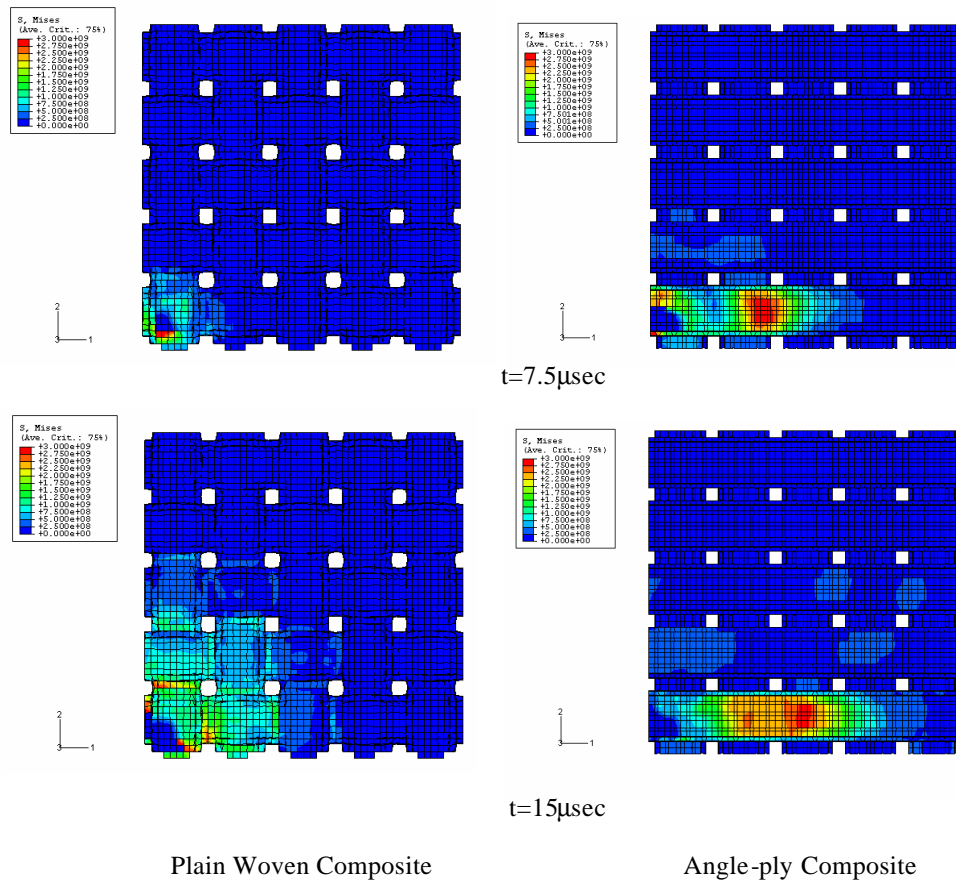


Figure 7.8: Effect of Reinforcing Architecture on Impact Energy Transfer in Composite Structure

In addition, the failure mode and the extent of damage is an important parameter that differentiates the structural behavior of individual reinforcement geometries.

Since the target is composed of various material systems, stress pulses incident to an interface will have components transmitted and reflected waves depending on the mechanical impedance, areal density and the speed of the wave [7.1]. At the moment of

impact (within 10 μ sec), a very high stress develops at the impact point (Figure 7.9). As a result, fiber breakage is expected. As time passes, the highest stress moves away from the impact site.

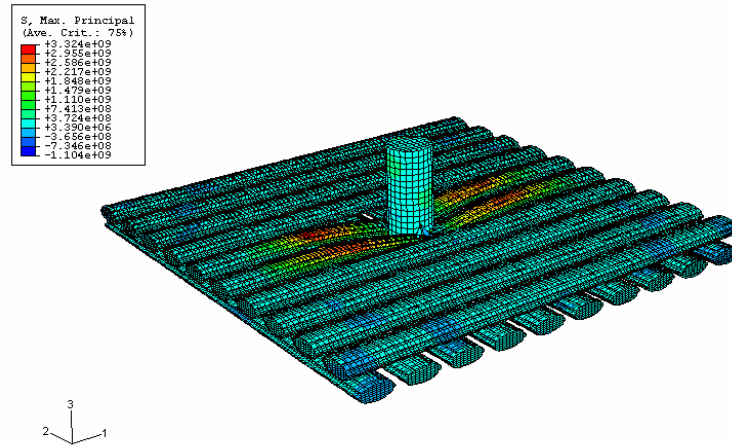


Figure 7.9: Maximal Principal Stress Distribution in Fabric Phase of Composite During the Initial Stage of Impact

In the case of the angle-ply laminated plate, our model predicts damage growth along the principal directions of fiber alignment and the resulting tearing of the matrix phase. Figure 7.10, shows equivalent plastic strain, where material in red has already failed. Consequently, damage is distributed over a larger area, and the impact energy dissipation is higher.

Indeed, experiments [7.3] identify de-lamination as the major failure mode in the case of the angle-ply composite target.

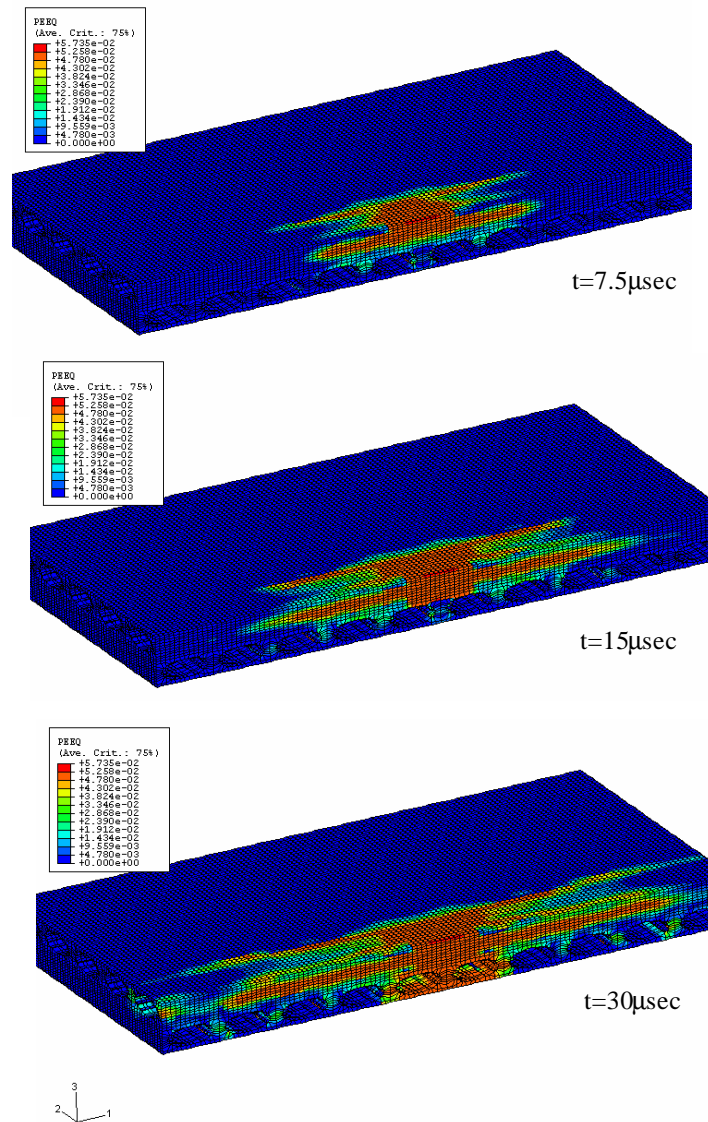


Figure 7.10: Equivalent Plastic Strain Contours in Matrix Phase of Angle-ply Textile Composite ($v=250\text{m/s}$), Plotted on Undeformed Mesh

On the other hand, simulations of the impact on woven composite have predicted that stress concentrations and fiber breakage (material in red has already failed) will occur not only under the projectile penetrating the target material (Figure 7.11

shows half of a model during the impact), but also at the fiber crossover points, exceeding the strength of material, as shown in Figure 7.12.

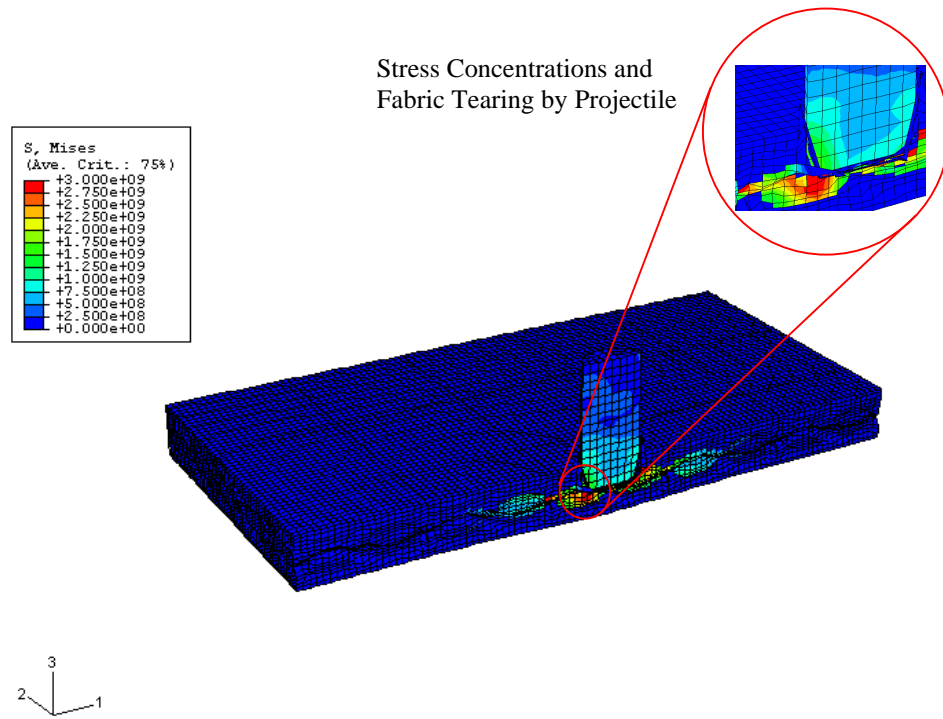


Figure 7.11: Stress Concentrations in the Woven Fabric During Projectile Penetration

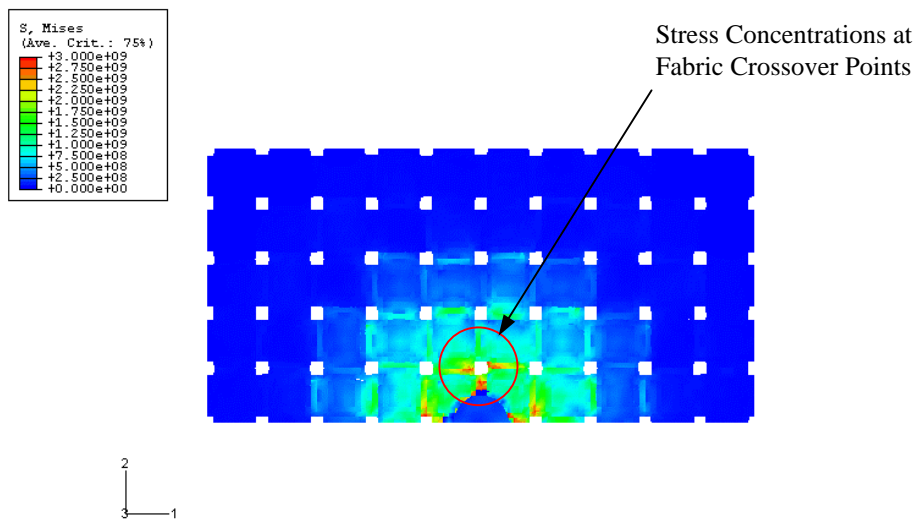


Figure 7.12: Stress Concentrations at Fabric Crossover Points During the 250m/s Impact on Woven Composite

Thus, the penetration results from fiber breakage along the weave directions (material in red has already failed) and the penetration area in the case of moderate impact velocities has a square shape (Figure 7.13, epoxy phase is removed in order to visualize reinforcement during ballistic impact).

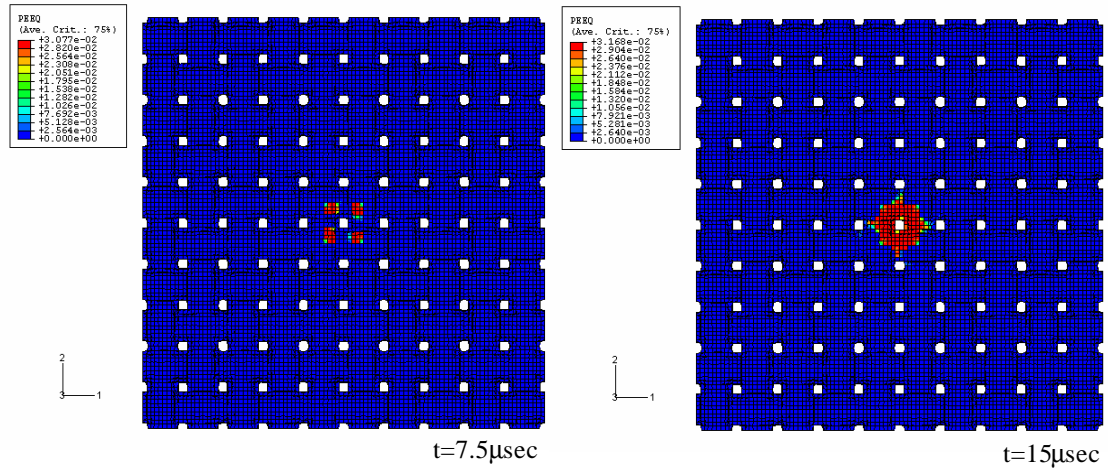


Figure 7.13: Equivalent Plastic Strain Contours at Front Side of Woven Phase of Textile Composite ($v=250\text{m/s}$)

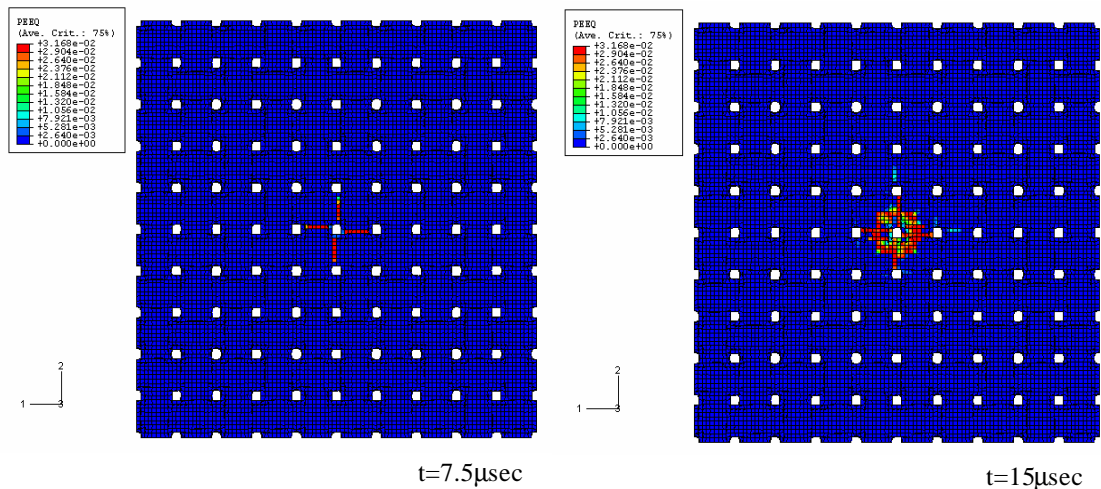


Figure 7.14: Equivalent Plastic Strain Contours at Back Side of Woven Phase of Textile Composite ($v=250\text{m/s}$)

As a result, the projectile penetrates the target, leaving a square shape hole (Figure 7.15), which is confirmed by experiments [7.3].

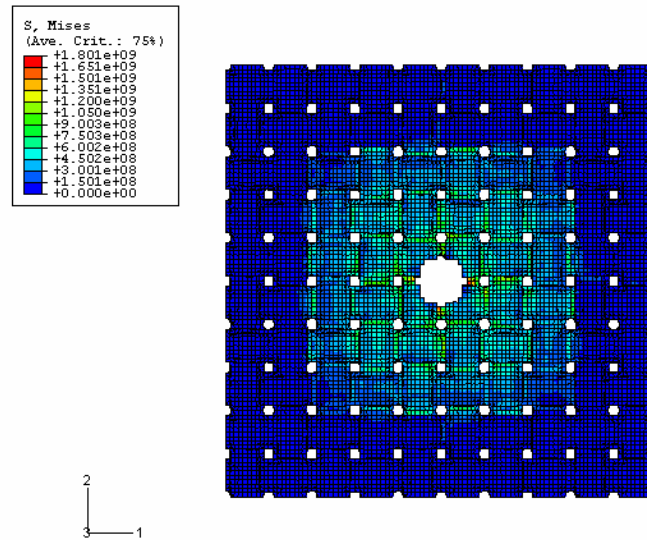


Figure 7.15: Square Shape of a Hole in Fabric Phase of Woven Composite After Impact of 250m/s

Accordingly, Figure 7.16 gives equivalent plastic strain contours for a matrix phase of woven textile composite, during the impact of 250m/s.

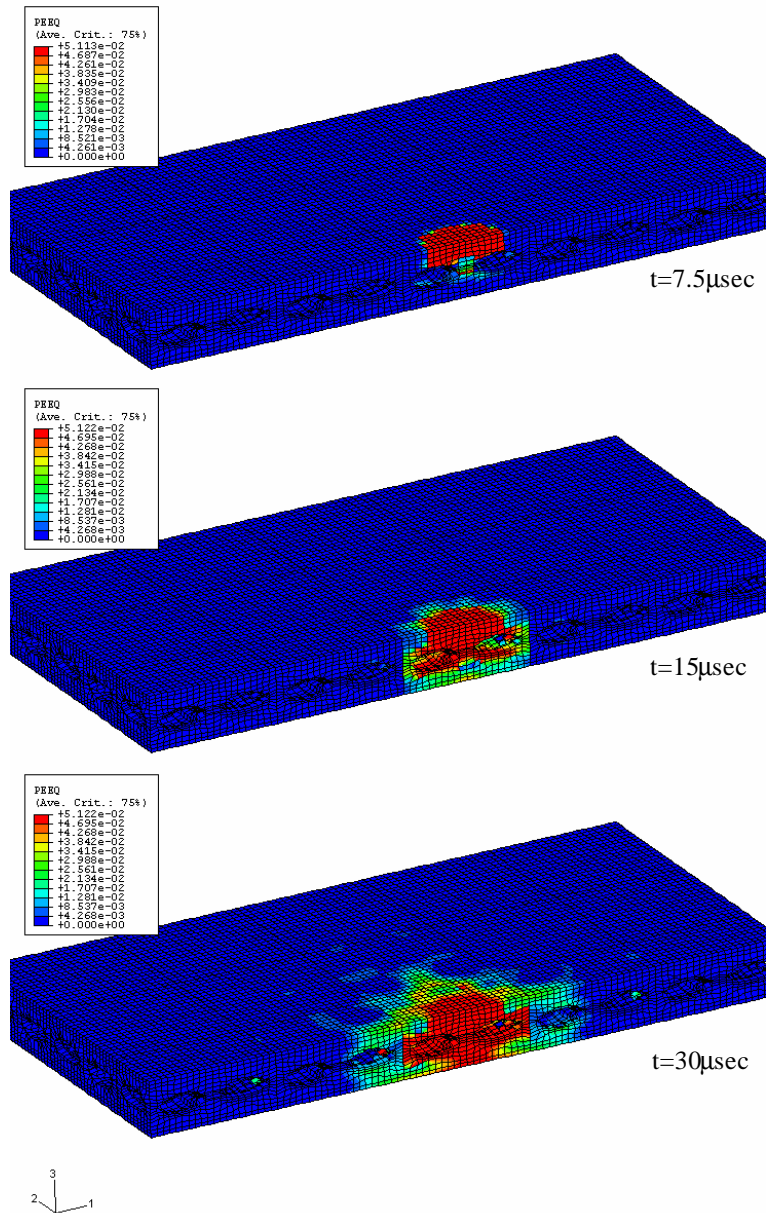


Figure 7.16: Equivalent Plastic Strain Contours in the Matrix Phase of Woven Composite Target

The formation of a square-shaped area during the penetration of a projectile indicates the local character of failure which results in a lower amount of energy absorption compared to that of the angle-ply laminated composite target.

Thus, it could be concluded that for moderate impact velocities, as a result of projectile compression, after extensive yarn stretching, the reinforcement exhibits tensile failure.

However, in the case of high velocity, the hole becomes circular (Figure 7.17), assuming the shape of the penetrating projectile. In other words, the projectile plugs through material causing shear failure. This is also in good agreement with experimental findings by Flanagan, et al [7.3], where, as a result of ballistic tests, the dynamic failure evolution of textile composites was performed, and failure modes for different textile architectures were identified.

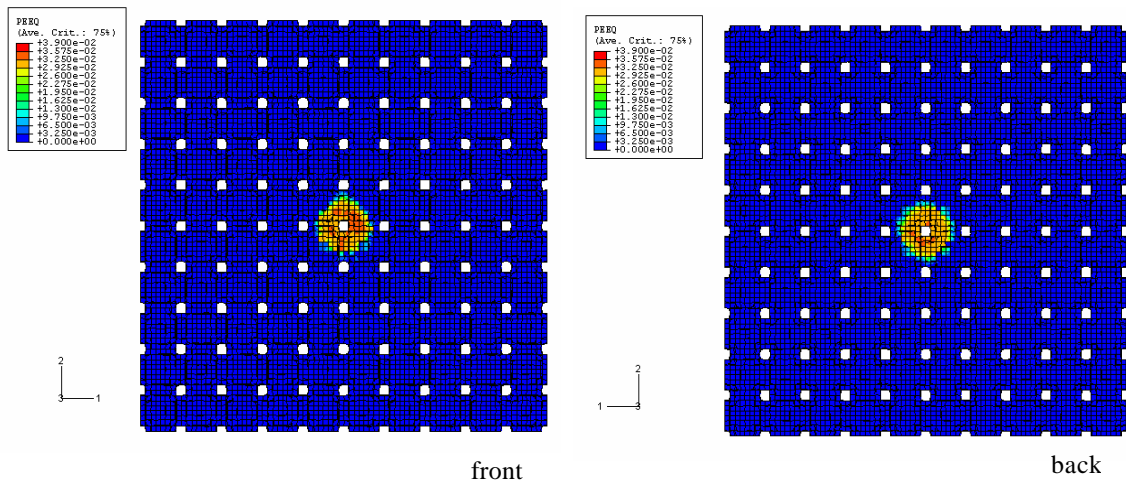


Figure 7.17: Equivalent Plastic Strain Contours in Woven Phase of Textile Composite ($t=7.5 \mu\text{sec}$, $v=1000\text{m/s}$)

Consequently, Figure 7.18 represents equivalent plastic strain contours in the matrix phase of the composite, showing material failure of a circular shape.

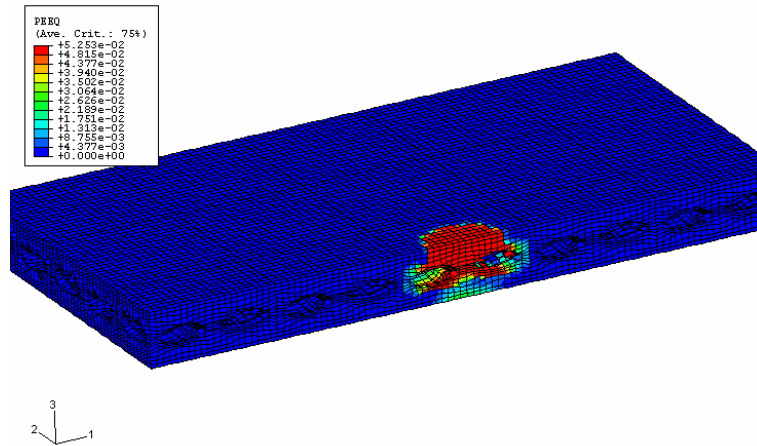


Figure 7.18: Equivalent Plastic Strain Contours in the Matrix Phase of Woven Composite ($v=1000\text{m/s}$)

As a result, the projectile penetrates the target forming a circular hole (Figure 7.19).

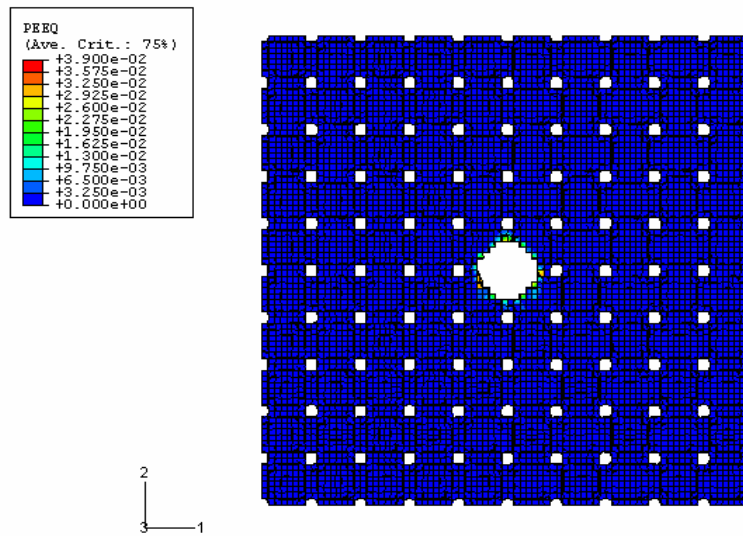


Figure 7.19: Circular Shape of a Penetration Area in Fabric Phase of Woven Composite After Impact of 1000m/s

It could be concluded that the impact simulations have shown higher impact resistance of layered, angle-ply fabric structures compared to woven textile composites with the same areal density.

Further, presented approach was able to address particular failure modes using detailed finite element modeling of textile reinforcing structures. Thus, the transition from tensile to shear mode is predicted for woven textile composite as the impact velocity increases, which is in good agreement with experimental results available in literature.

8. NUMERICAL MODELING OF IMPACT BEHAVIOR OF INTEGRATED MULTI-LAYERED/MULTIPHASE COMPOSITE MATERIAL

Main objectives in modeling of Multi-layered/Multiphase Composites are to:

(a) simulate such a complex material system; (b) address the significance of the various design parameters such as material property, textile and overall composite architecture; (c) evaluate the difference in performance between a full ceramic facing versus a set of ceramic spheres embedded in light epoxy; (d) address the role of spherical size, and their packing arrangement in armor ballistic resistance; and (e) compare the performance of the spherical facing system with respect to the position of impact in anticipation of a non uniform response due to non-alignment of the projectile and spheres. This type of analyses also provides information regarding the extent of the damage zone in the neighborhood of the projectile in both the facing and backing material.

All previous studies of the interaction between projectiles and ceramic targets have highlighted aspects of modeling, energy, ceramic fracture, and ballistic performance assessment. Ceramic fragmentation is important because a large proportion of projectile kinetic energy is redistributed as a kinetic energy of ejected ceramic particles, however, toughness itself is not found to be an indicator of performance [8.3, 8.4].

Ceramic-based armors are typically available in plate form. Manufacturing of more complex shapes is quite challenging especially in the facing/backing plate configuration. To address this issue a new concept a Multi-layered Design Composite-MDC (Figure 8.1) has been proposed [2.42], which consists of: (a) facing made of ceramic

spheres embedded in epoxy, and (b) a fiber reinforced spectra/epoxy composite. In addition to complex shape formability, the proposed design is lighter and provides a natural interface with the backing. . At the same time, localized damage may be at least to a certain extent, repairable. In return, substitution of a monolithic ceramic plate with particulate ceramics may reduce the ballistic capability of this system.

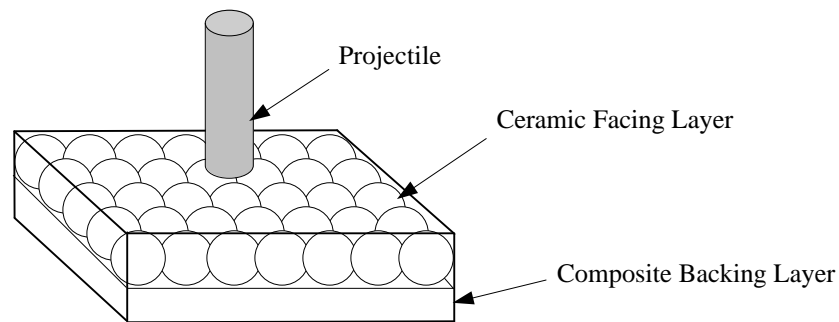


Figure 8.1: MDC Material Concept

This system offers a level of inhomogeneity that may induce rotation of the projectile; a mechanism widely recognized for reduction of penetration capability [2.52]. To avoid weak spots in the areas between the spheres, a second layer can be used with the sphere centers placed on top of the interstices of the first layer.

Several sets of simulations were performed in order to evaluate effects of ceramic facing (monolithic vs. spherical), size of spheres (6.35mm, 9mm, and 12.7mm), impact site (Figure 8.2), as listed in Table 8.1, and architecture of a textile composite backing plate (woven vs. angle-ply), on armor ballistic performance.

Table 8.1: Varying Parameters in Ballistic Impact Simulations

Spherical size	Projectile shape	Impact site (Figure 8.2)
-6.35mm (1/4")	-Armor Piercing Bullet	-Central impact (Site 1)
-7.62mm	-Cylinder	-Oblique impact
-9mm	-Sphere	-Side impact (Site 2)
-12.7mm (1/2")		-Middle impact (Site 3)

The termination time for the numerical simulations was set at 150 μ s. This particular value was arrived at after several iterations and after analyzing the maximum displacement and kinetic energy distributions of the projectile with respect to time.

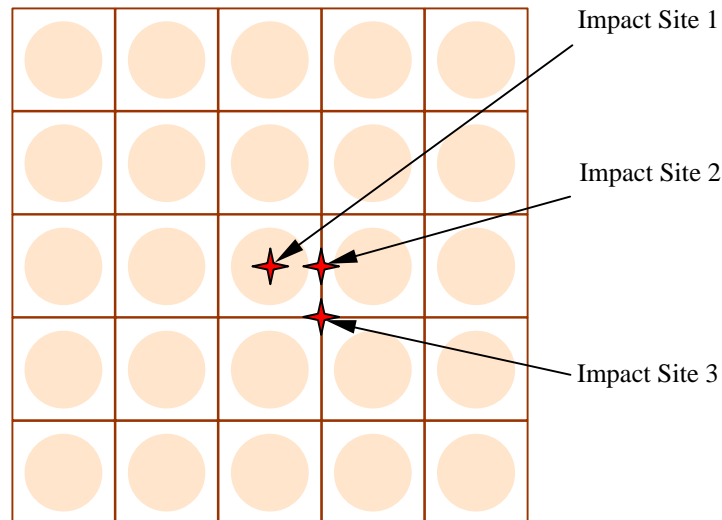


Figure 8.2: Schematic Representation of Simulated Impact Sites

An important consideration for system integration is the deformation of the back face, or the deflection of the armor material on the back surface. Even though the armor may defeat a threat projectile, the back face deformation can cause other damage, for example, blunt force trauma to a person wearing an armored vest or a helmet. When body armor defeats an impacting penetrator by expanding and deforming, there is a

transfer of kinetic energy to the body. The damage to tissue caused by this energy is called blunt trauma.

The displacement of the projectile tip and center point of both the ceramic and back plate surface, as a measure of the penetration depth and blunt trauma effect, respectively, were tracked throughout the solution. The velocity of the projectile, as well as the time history of the energy, for the model constituents, is also recorded.

Similarly to the case of impact on textile composite models (Chapter 7), the effect of boundary conditions was investigated for both moderate and high impact velocities. However, for the velocity range under our consideration, the simulations showed no effect of boundary conditions on the target ballistic performance. It is apparent during the ballistic event that the localized material response in the vicinity of the applied load becomes primarily important whereas the overall geometric configuration of the structure becomes secondary. Again, it can be concluded, that boundary conditions for high velocity impact, in this case, can be ignored because the impact event is over before the stress waves have reached the edge of the structure [2.29]. Typical FE model of an integrated MDC, consisted of 276,340 8-noded brick elements, and 328,907 nodes is presented in Figure 8.3.

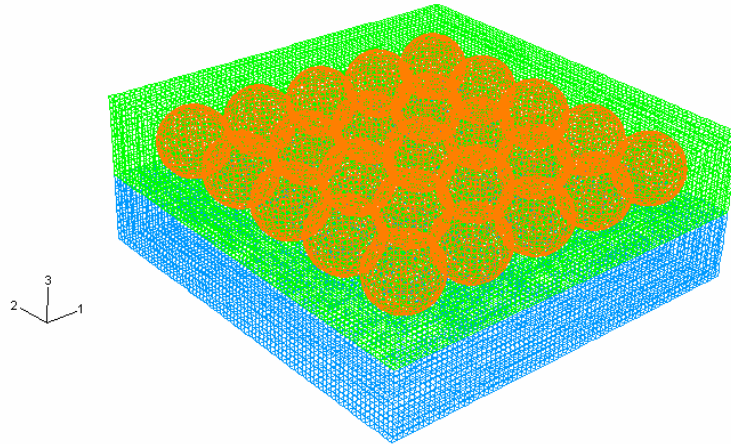


Figure 8.3: FE Mesh of Integrated Design Composite Model

Impact Performance of Ceramic Facing Plate

In this section, the ballistic resistance of monolithic ceramic tile is compared with that of spherical ceramic facing. Three different, commercially available sizes of the spheres are considered: 6.35mm, 9mm and 12.7mm (Table 8.3). In order to address the role of packing factor, the performance of 12.7mm spheres is compared with two layers of 6.35mm spheres, as shown in Figure 8.4, where the spheres are arranged so that top layer is located at the interstitial position of the bottom layer.

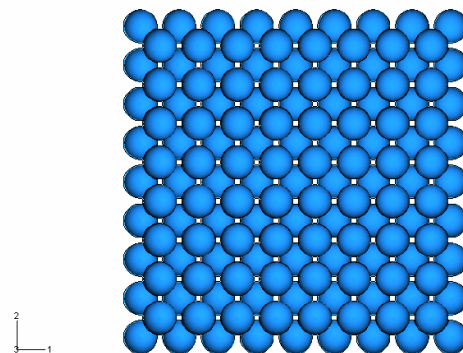


Figure 8.4: Ceramic Facing Model Composed of Two Layers of 6.35mm Spheres

First the ballistic performance against a 300m/s cylindrical projectile was simulated for 3 facing plates of a total thickness of 12.7mm for (a) monolithic ceramic, (b) 30% volume fraction of a single layer ϕ 12.7mm ceramic spheres embedded in epoxy, and (c) a double layer of ϕ 6.35mm spheres embedded in epoxy. The history of the projectile velocity (for a node at its top) during impact is shown in Figure 8.5.

As expected the simulations predicted that the monolithic ceramic plate would stop the projectile, while the both sphere/epoxy systems were penetrated.

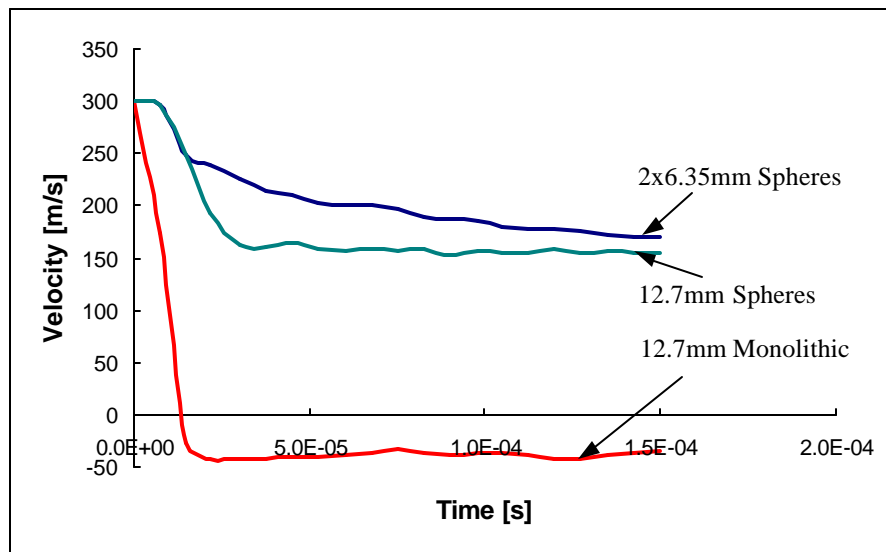


Figure 8.5: Velocity Time History for Different Ceramic Models

A comparison on the basis of equal areal density (A_p) was also considered (Table 8.2). In this case ballistic resistance of a 6.5mm monolithic ceramic plate is compared with the ϕ 12.7mm and 2x ϕ 6.35mm systems.

Table 8.2: Characteristics of Different Ceramic Facing Models

Ceramic Model		6.35mm	2x6.35mm	9mm	12.7mm
Ceramic spheres embedded in epoxy	m [kg]	0.0725	0.145	0.11	0.145
	A_p [kg/m ²]	12.675	25.35	21	25.35
	V_f [%]	30	30	30	30
Monolithic tile	m [kg]	0.14	0.28	0.2	0.28
	A_p [kg/m ²]	24.75	49.5	35	49.5
Equivalent monolithic ceramic plate with equal areal density	t [mm]	3.25	6.5	5.35	6.5

An alternative way to compare ballistic performance of different targets is to evaluate absorbed impact energy for each system (Figure 8.6). Simulations have predicted that the projectile would penetrate all 3 systems. It can be seen that the absorbed energies for all systems are comparable, with the monolithic ceramic offering approximately 20% higher absorbed energy than spherical ceramic systems.

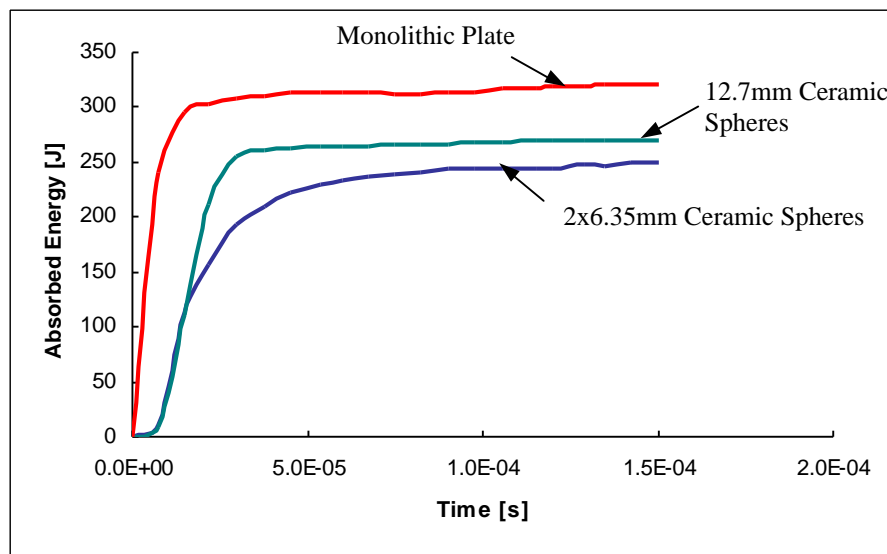


Figure 8.6: Absorbed Energy of Different Ceramic Plate Models

An implicit conclusion from this comparison is that an increased volume fraction of alumina will improve ballistic resistance and it depends on the designer to optimize ceramic contents for maximum ballistic limits that preserve the manufacturing advantages of the sphere system with respect to complex shapes. It is to believe that this limit should be close to 50% for a single layer of spheres.

As shown in Figure 8.6, simulations have predicted that, one layer of larger ceramic spheres (12.7mm) would perform slightly better than two layers of 6.35mm spheres. Because of a different stacking sequence, even for same overall areal density of targets, the mass of the spheres below the projectile is not the same. Thus, besides greater inertia, larger deformation of the projectile during the impact on bigger spheres (see Figure 8.7) contributes to slower penetration through the target material.

Figure 8.7 presents Von-Mises stress distribution (all stresses are given in N/m^2), during simulated impact on ceramic plates with 12.7mm particles (epoxy phase is removed, so the performance of ceramic spheres could be visualized).

Enlarged detail shows projectile erosion due to shearing and formation of a mushroom head, while the ceramic spheres are penetrated, as it is reported in ballistic experiments [2.38, 2.41].

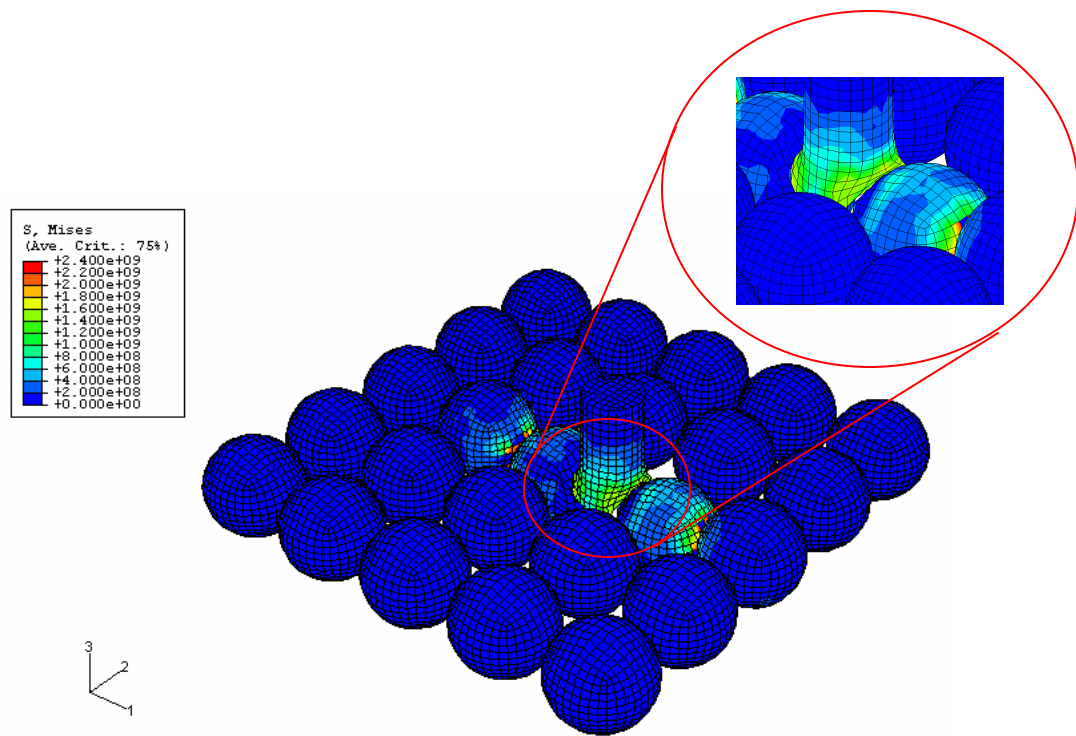


Figure 8.7: Contours of Von Mises Stress During the Simulated Impact Between Two 12.7mm Spheres

An important consideration in the ballistic performance of the sphere-system is that when the projectile diameter is the same, or smaller than the diameter of the spheres, a significant level of non-uniformity may be presenting the impact response of the material. This can be manifested in two ways: (a) the response of the material may depend on the location of the impact and (b) the asymmetry in the response may induce projectile rotation, which is considered to be an important energy absorption mechanism. To explore these ideas, projectile impact is simulated at 3 locations shown in Figure 8.8, which shows the projectile velocity history hitting 9mm spheres embedded in epoxy ($V_f=30\%$).

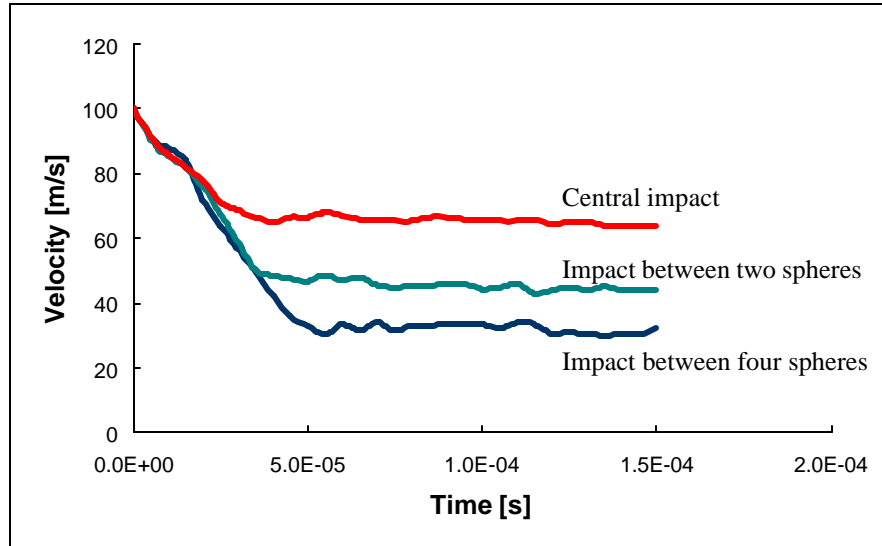


Figure 8.8: Effect of Impact Site on Velocity Time History for a 9mm Thick Facing with Ceramic Spheres

Figure 8.8 shows that residual velocity of the projectile varies by almost 50% depending on the impact location. Maximum energy absorption occurs when the projectile hits at the interstitial between four spheres. An explanation of this behavior can be seen in Figure 8.7 where an impact between two spheres “engages” both of them. Accordingly, minimum energy absorption is observed when the impact occurred directly on the center of one sphere because the surrounding spheres do not contribute substantially in resistance to projectile penetration.

In addition, simulations of 300m/s impact (Figure 8.9), show that packing factor of proposed multi-layered spherical ceramics embedded in light epoxy plays an important role in optimization of armor ballistic resistance.

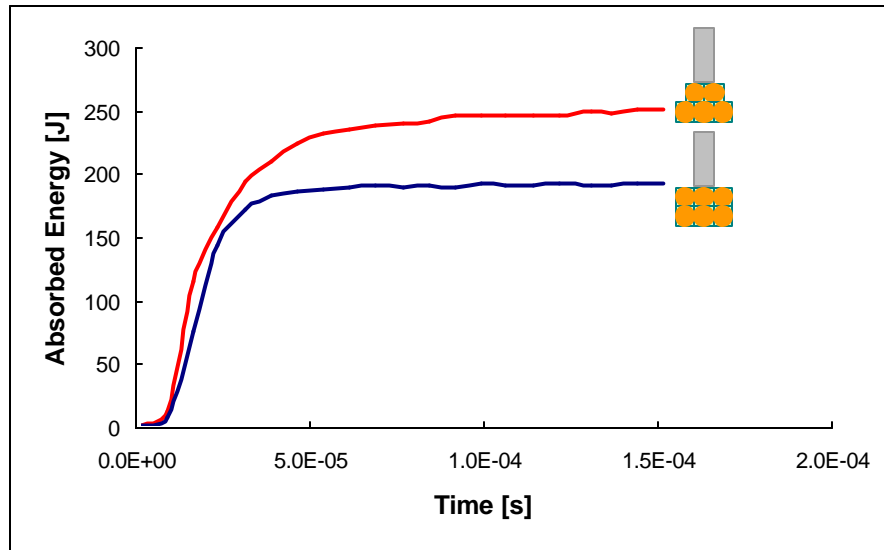


Figure 8.9: Absorbed Energy of Two Layers of 6.35mm Spheres with Different Stacking Sequence

Absorbed impact energy is greater in the case when layers of ceramic spheres are shifted compared to the model where they are simply placed one on the top of the other because larger number of spheres participate in the impact, as it is shown in Figure 8.10. It is possible that other arrangements such as a close packed configuration may lead to a higher energy absorption.

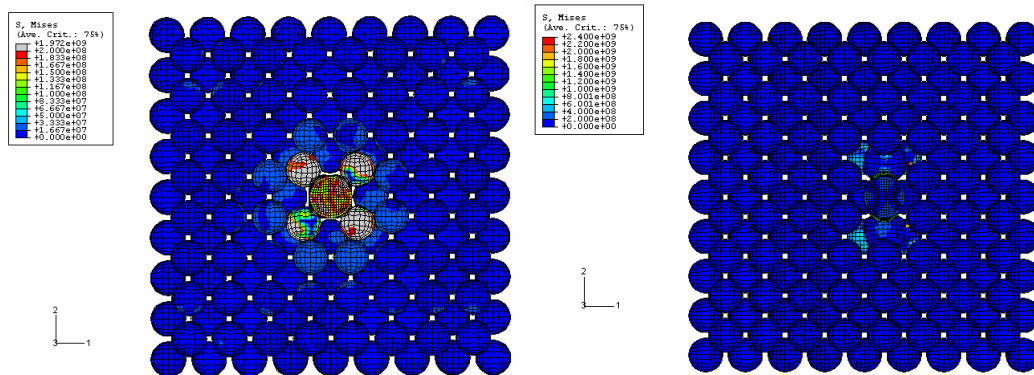


Figure 8.10: Von Mises Stress Distribution During the Impact on Two Layers of 6.35mm Spheres Plate, Between Four and two Spheres ($t=30\mu\text{sec}$)

A second implication of the inhomogeneity in the material response is the possible induced projectile rotation. Indeed, simulations have shown (Figure 8.11 where epoxy phase of a facing plate is removed, so that penetration and projectile yawing could be visualized), that even for a slightly asymmetric course of impact (0.5mm off the point between two spheres), the projectile changes direction by deflecting on the particulate ceramic facing, considerably losing its initial velocity (see graph in Figure 8.14). This is a very important characteristic of spherical ceramic facing, since the probability of hitting in between the spheres is much higher than a central hit. In that sense, the central impact under the normal angle, although much less likely, could be considered as a worst-case scenario of ballistic event.

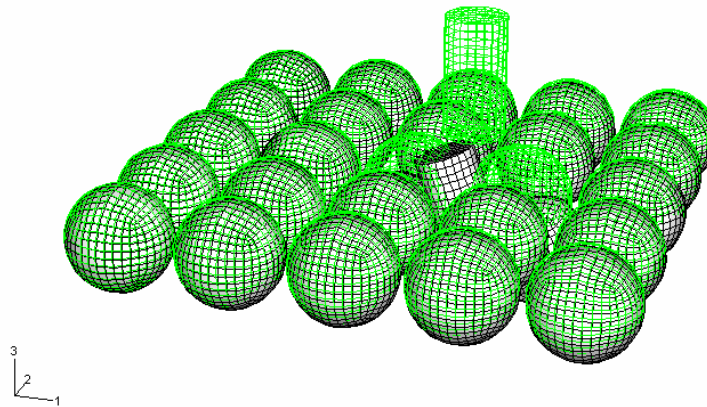


Figure 8.11: Superimposed Un-deformed (Green) and Deformed Model (in White)
Simulation Showing Considerable Projectile Re-direction During Impact

Figure 8.12 represents absorbed energy distribution with respect to the point of impact for a model with 12.7mm ceramic spheres after 300m/s impact. In this case, in contrast to the model with 9mm spheres, because of larger distance between the parti-

cles, a hit in-between both two and four spheres showed to have lower ballistic resistance. However, a non-symmetric impact, due to projectile re-direction, would have the highest energy absorption.

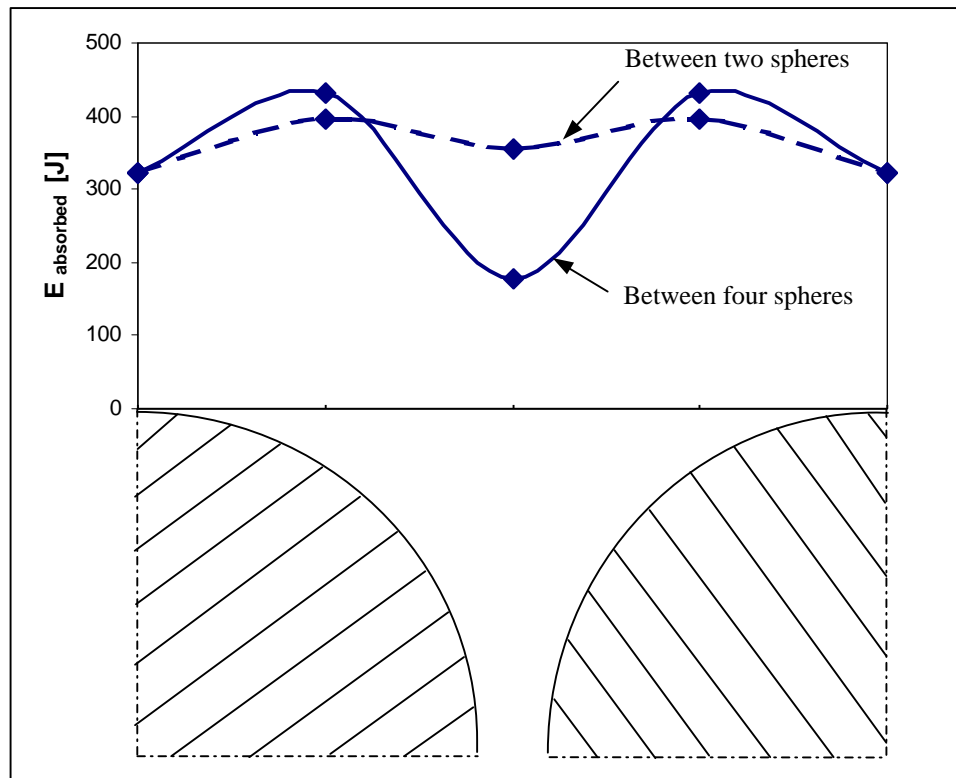


Figure 8.12: Absorbed Energy With Respect to Projectile Impact Position

The results of numerical analysis predict good ballistic resistance of spherical ceramic systems compared to that of corresponding monolithic plates, for moderate impact velocities. It is shown that for the same areal density, more layers of ceramic spheres could be placed in the armor facing plate, introducing shield flexibility without sacrificing its ballistic resistance significantly.

Modeling of Multi-layered/Multiphase Design Composite Armor

Multi-layered Design Composite material, where ceramic facing is backed by textile composite plates with different fabric architectures (woven and angle-ply unidirectional), for volume fractions of 35% and 50%, where also considered.

As already mentioned in Chapter 2, and confirmed by numerous experiments [2.3, 2.11, 2.27, 2.38], the ballistic resistance of the ceramic plate is improved by adding a more ductile backing plate, usually made of aluminum, steel or a light, textile composite material.

Simulations (Figure 8.13) show a considerably lower residual velocity and better ballistic resistance of MDC armor, composed of 12.7mm ceramic spheres embedded in epoxy and 35% woven backing plate, compared to a single spherical ceramic plate.

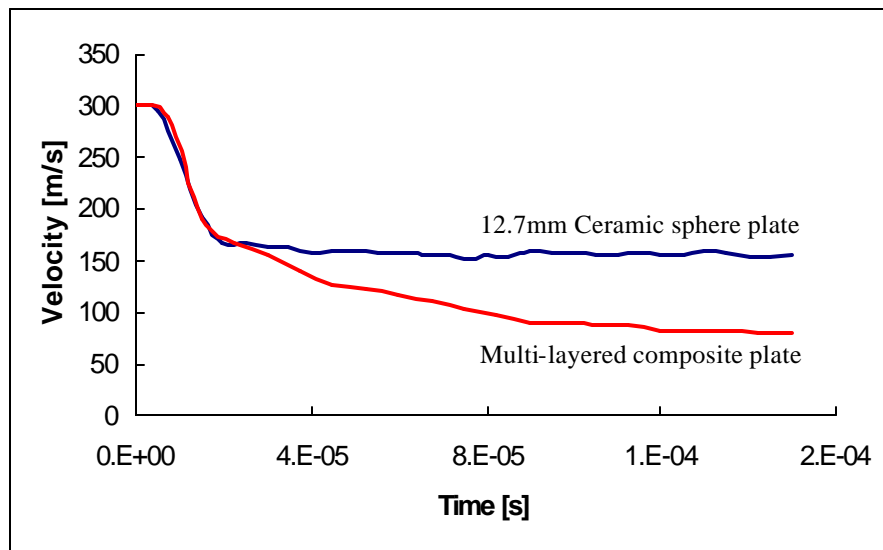


Figure 8.13: Backing Composite Plate Role in Armor Ballistic Resistance

Ballistic resistance of MDC with spherical ceramic facing backed with an angle-ply composite plate was compared with that of an armor system composed of monolithic ceramic tile with the same areal density, (Figure 8.14). With an impact velocity of 300m/s, both plates were perforated, and residual velocity, and impact resistance showed to be similar.

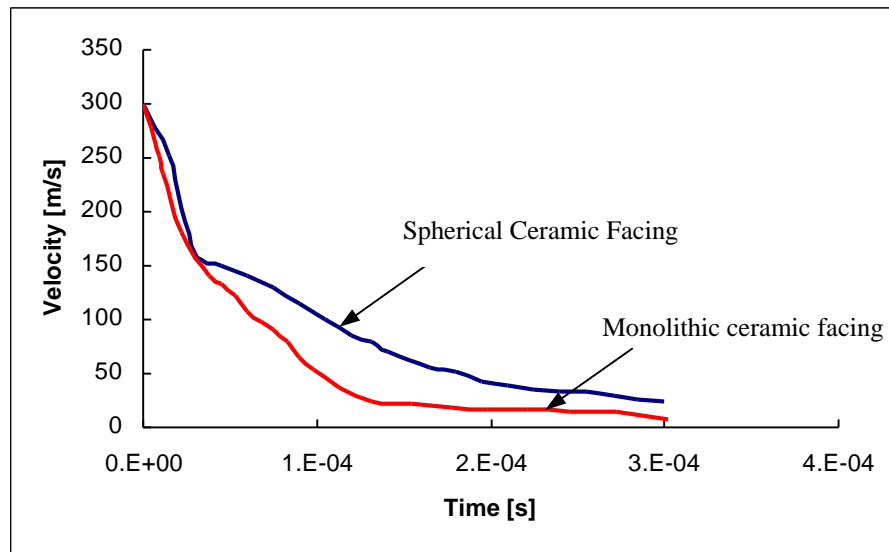


Figure 8.14: Effect of Ceramic Facing on Ballistic Resistance of Multiphase Models

Figure 8.15 compares the velocity time history for a projectile hitting one facing ceramic sphere directly, and in-between them, with the tumbling effect shown in Figure 8.11.

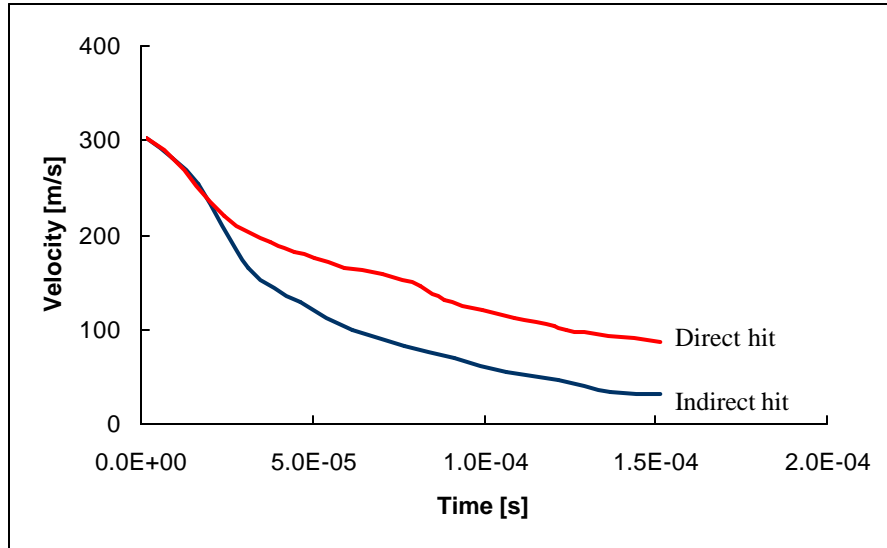


Figure 8.15: Projectile's Yawing Results in Better Armor Penetration Resistance

Simulations have predicted that by changing the projectile direction, spherical particles embedded in epoxy would be able to considerably lower residual velocity and enhance the ballistic resistance of a target.

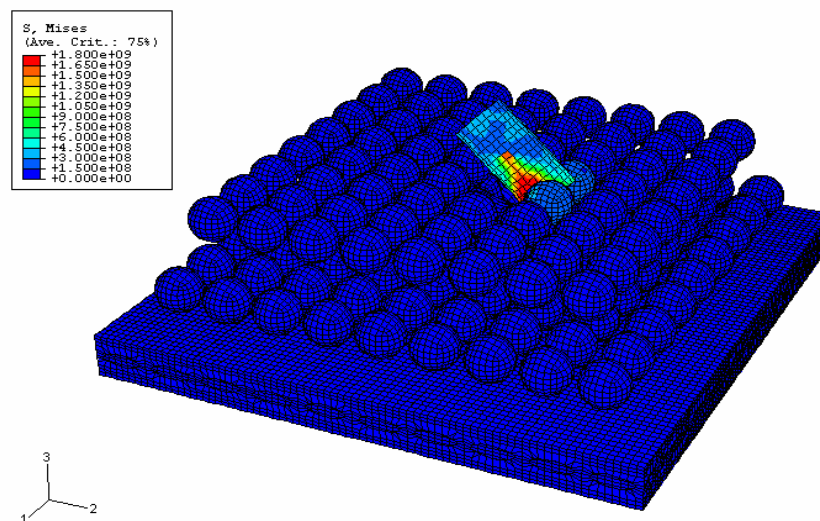


Figure 8.16: Simulation of an Oblique Impact on Integrated Material System

Oblique (angle) impact (Figure 8.16, where epoxy matrix is removed from the facing plate for clarity reasons) gives an even better ballistic resistance when compared to direct (central one), and for that reason, is not studied further.

An important issue in modeling armor ballistic resistance is to find the optimal combination of both backing and facing layer thicknesses for maximum impact energy absorption. In Figure 8.17, for the same areal density, absorbed ballistic energy is plotted for three different models. Two of them were composed of only a ceramic and textile composite, and the third one was an armor model containing equal thickness layers of both ceramic facing and textile composite backing.

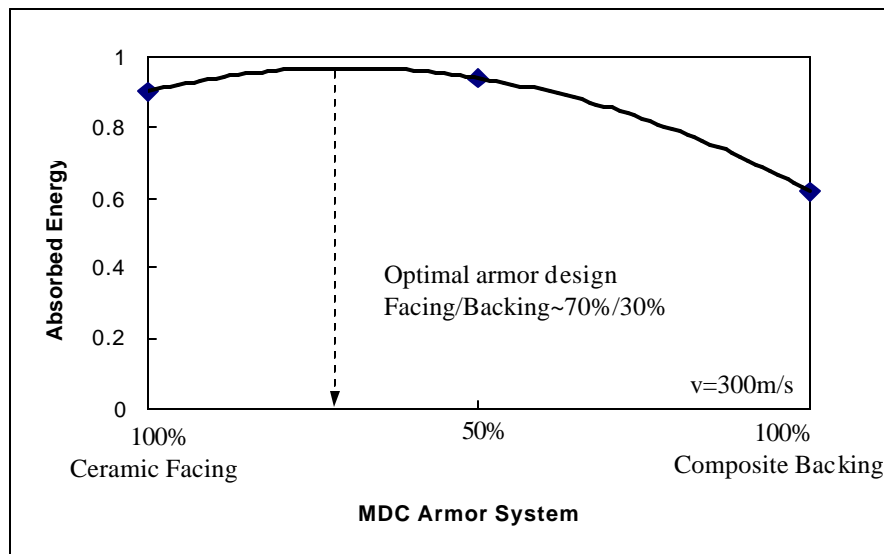


Figure 8.17: Optimal Combination of Multiphase Composite Armor

Although more simulations are needed for a better prediction, initial results show a trend for optimal armor design with maximum energy absorption, when a multi-layered/multiphase design composite model composed of ceramic facing and textile composite backing with the thickness ratio of approximately 70%/30% is used. This cor-

relates very well with some experimental findings [8.9] where that ratio was found to be 72%/28%.

After impact, the kinetic energy of the projectile is imparted to the armor, and as the projectile penetrates the target, the kinetic energy will be reduced while the internal energy of the system will increase. Evolution of these energies for different parts of a system (normalized by the projectile impact energy), with respect to time, is shown in Figure 8.18. Kinetic energy dissipation is an indication that the velocity of the projectile is being reduced as it penetrates the armor.

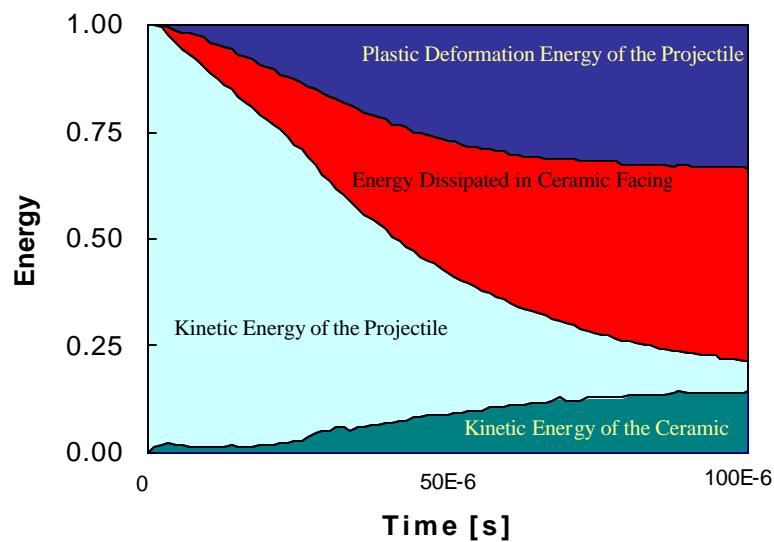


Figure 8.18: Energy Time History for Angle-ply Textile Composite with Monolithic Ceramic Facing

Both experimental results and numerical findings [Chapter 7] have showed that a unidirectional angle-ply composite laminate has better ballistic resistance when compared to that of a woven textile composite. It is postulated that an un-crimped reinforcement, due to better translation efficiency (higher stiffness), is capable of transferring

energy faster from the impact site. Further, during projectile penetration, different textile architectures exhibit different failure modes, which influences their ballistic resistance.

Absorbed projectile impact energy is mainly transformed into kinetic and plastic energy dissipated in the target and deformation of the projectile.

An energy time history for MDC models with monolithic ceramic facing and two different backing plate reinforcing architectures (woven and angle-ply) is given in Figure 8.19.

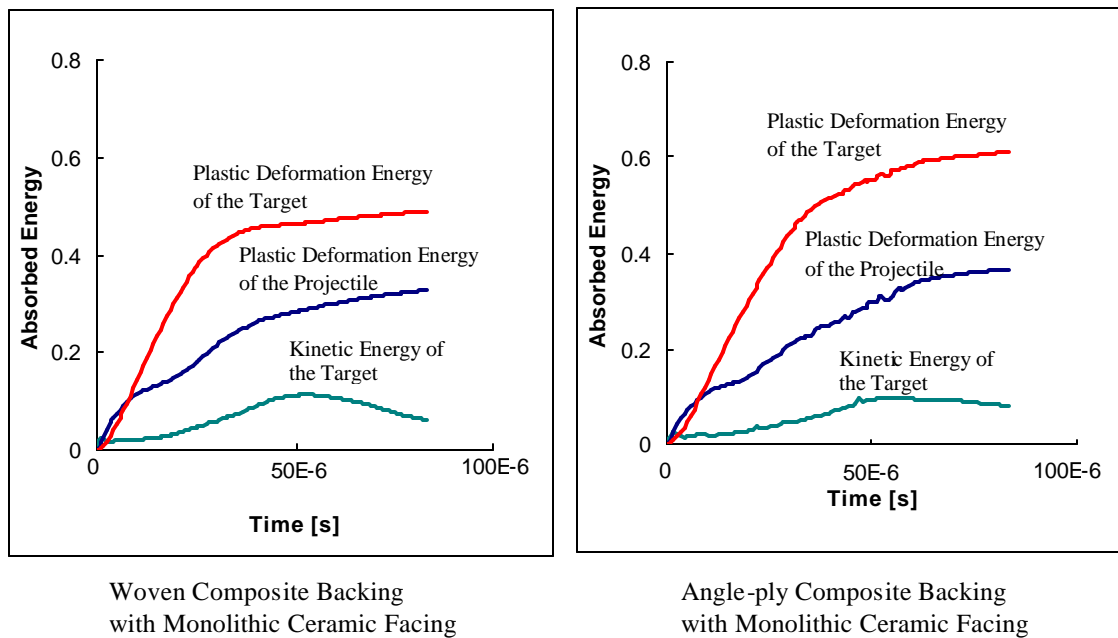


Figure 8.19: The Influence of Textile Architecture on Energy Time History

An angle-ply composite backing showed to have higher plastic deformation energy of the target and slightly higher plastic deformation energy of the projectile, which contributes to its better ballistic resistance.

Impact energy absorption for the models with different ceramic facing is also explored. Figure 8.20 shows that a monolithic ceramic facing backed with an angle-ply composite absorbs higher energy than the corresponding facing with ceramic spheres with the same areal density, which will result in better energy transfer on backing plate, leading to better overall ballistic resistance comparable to that of the armor with a spherical ceramic facing layer.

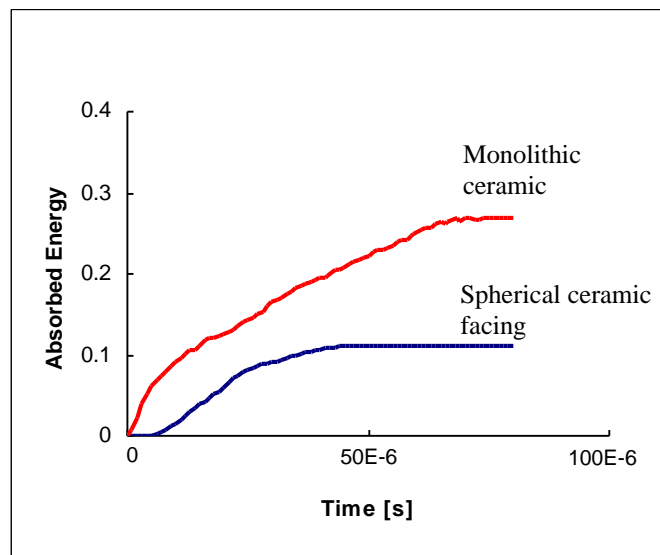


Figure 8.20: The Influence of Ceramic Facings on their Energy Dissipation Capability

8.1 Comparison of Experimental and Numerical Results

In order to validate the numerical models and results, high velocity impact tests on integral multiphase composite plates were carried out at the Center of Excellence for Advanced Materials (CEAM) at University of California at San Diego, Department of Aeronautical and Mechanical Engineering [8.8]. At the CEAM impact laboratory (Figure 8.21), a single stage 25.4mm (1”) bore gas gun is used to propel a Tungsten, heavy

alloy projectile. After the projectile perforates the target, it is recovered. The residual velocity and the residual mass of the projectile are measured. The difference in the initial and final kinetic energy gives the energy absorbed by the target and hence is a measure of ballistic efficiency. The impact test setup is presented in Figure 8.22.

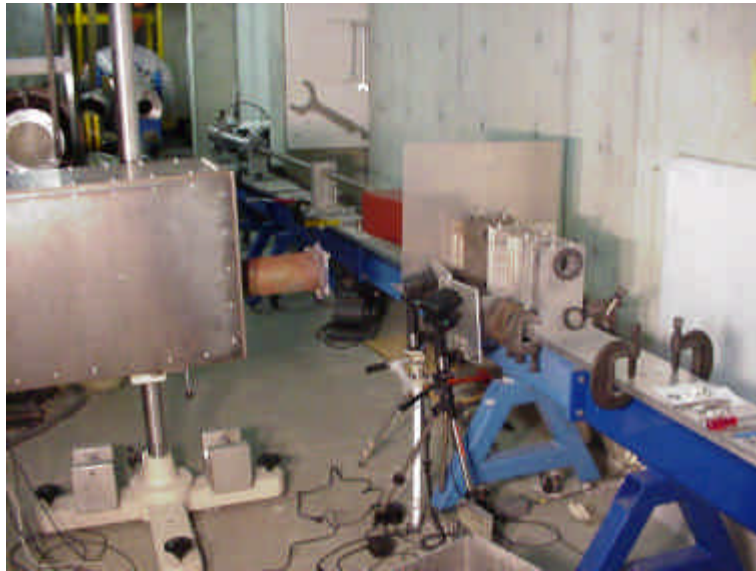


Figure 8.21: Ballistic Testing Lab

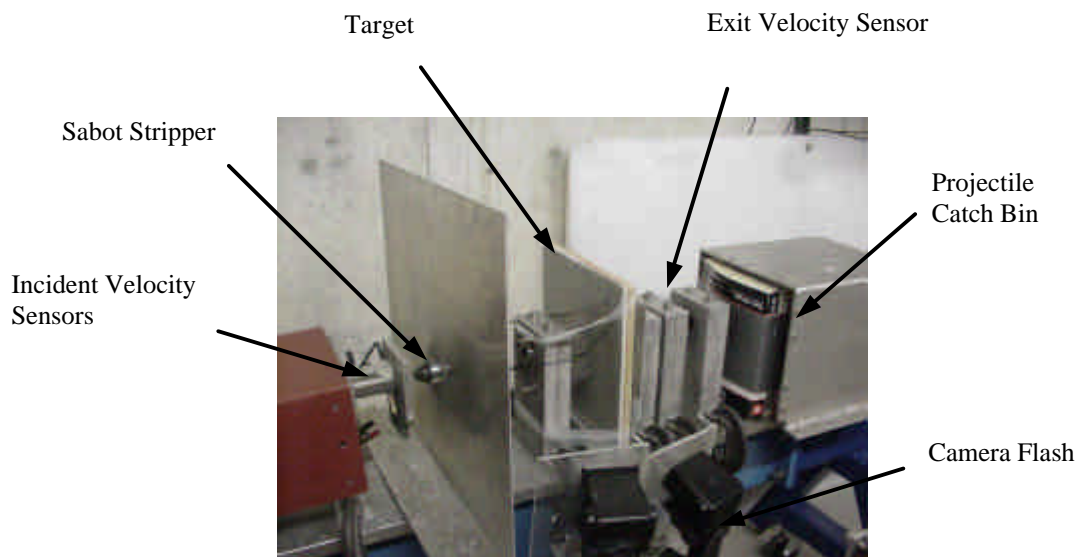


Figure 8.22: Impact Test Setup

The backing plate of the target panel was a 16mm thick angle-ply (0/90) Spectra[®] reinforced composite, and the facing was made of 6.35mm (1/4") ceramic spheres embedded in light epoxy (Figure 8.23). The panel dimensions are 30.5cmx30.5cmx2.3cm (12"x12"x0.9") with a mass of 2867.6g.

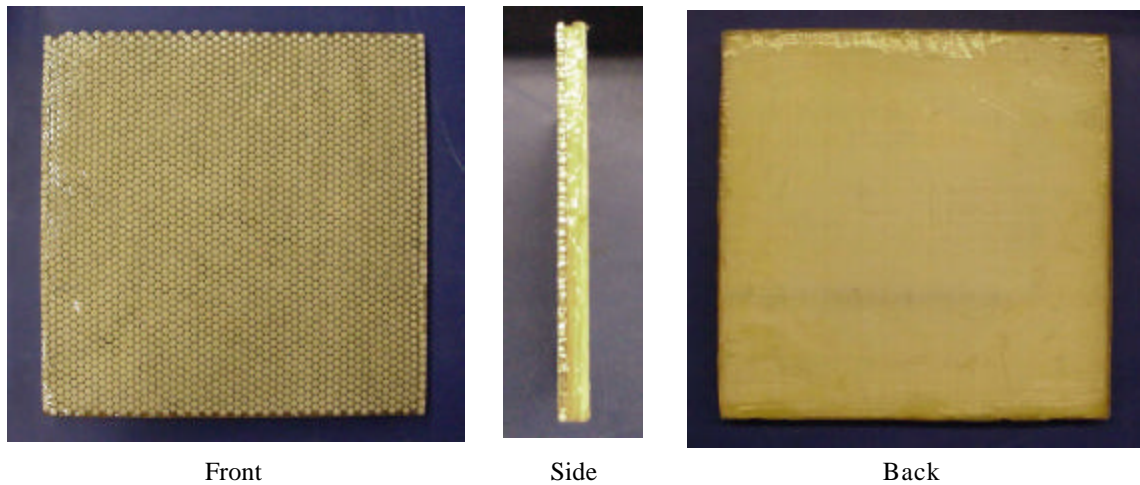


Figure 8. 23: Armor Sample: Pre-test

The initial velocity of the cylindrical, flat-ended, Tungsten, heavy alloy projectile with the mass of 10.712g was 920m/s, and the measured residual velocity after complete penetration was 735m/s. Figure 8.24 shows the armor sample after the test was complete.

Characteristics of the material model used for the WHA projectile are listed in Table 8.3.

Table 8.3: Material Properties of a WHA Projectile

Property	ρ [kg/m ³]	E [GPa]	ν	σ_y [GPa]	σ_{uts} [GPa]
WHA	17700	310	0.3	0.655	0.862

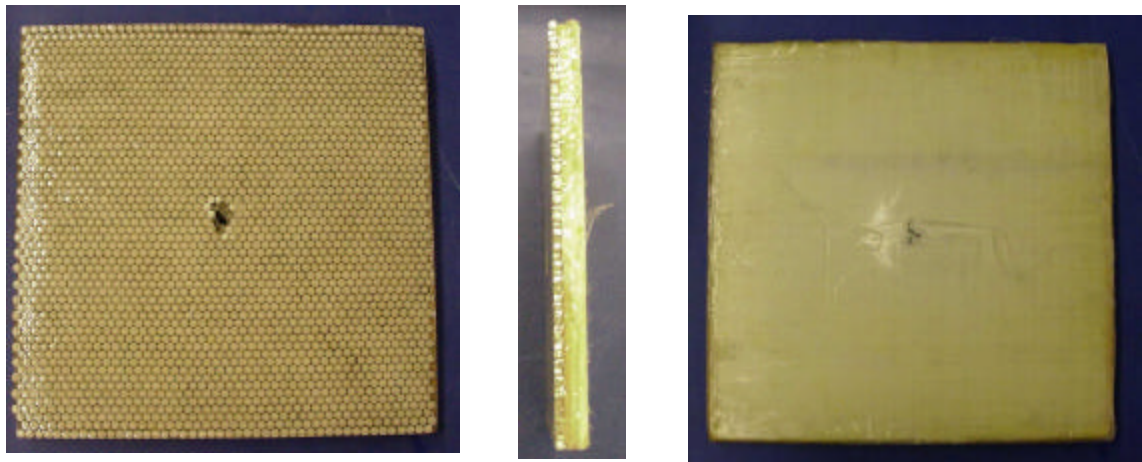


Figure 8.24: Armor Sample: Post-test

The mechanism by which the projectile fails during penetration also influences the ballistic performance. During previous ceramic armor tests at CEAM, it was observed through flash radiography that WHA failed by erosion due to shearing of the mushroom head. That failure mechanism is more effective than comparatively brittle projectiles that fail by shattering. The angle of projectile entry also affects the penetration resistance, thus high-speed photography is used to confirm that the impact is normal to the surface (Figure 8.25). The time interval between frames was $5\mu\text{sec}$.

Based on experimental results, a finite element model is made with the same combination of materials: 6.35mm alumina spherical facing (tetragonal arrangement), and 16mm thick, $0^\circ/90^\circ$ angle-ply Spectra[®]/epoxy backing ($V_f=50\%$), with the areal density corresponding to that of the armor sample. Figure 8.26 shows the FE model during impact simulation with $10\mu\text{sec}$ step difference.

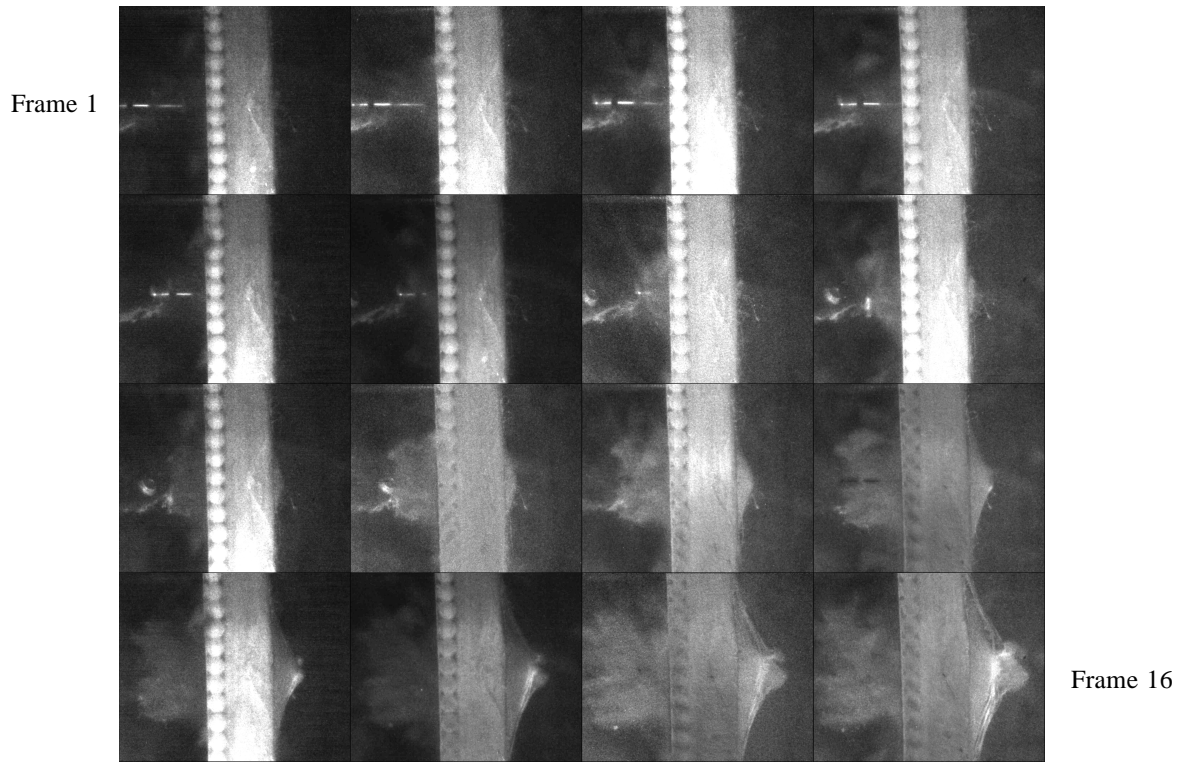


Figure 8.25: High-speed Photograph of the Ballistic Impact

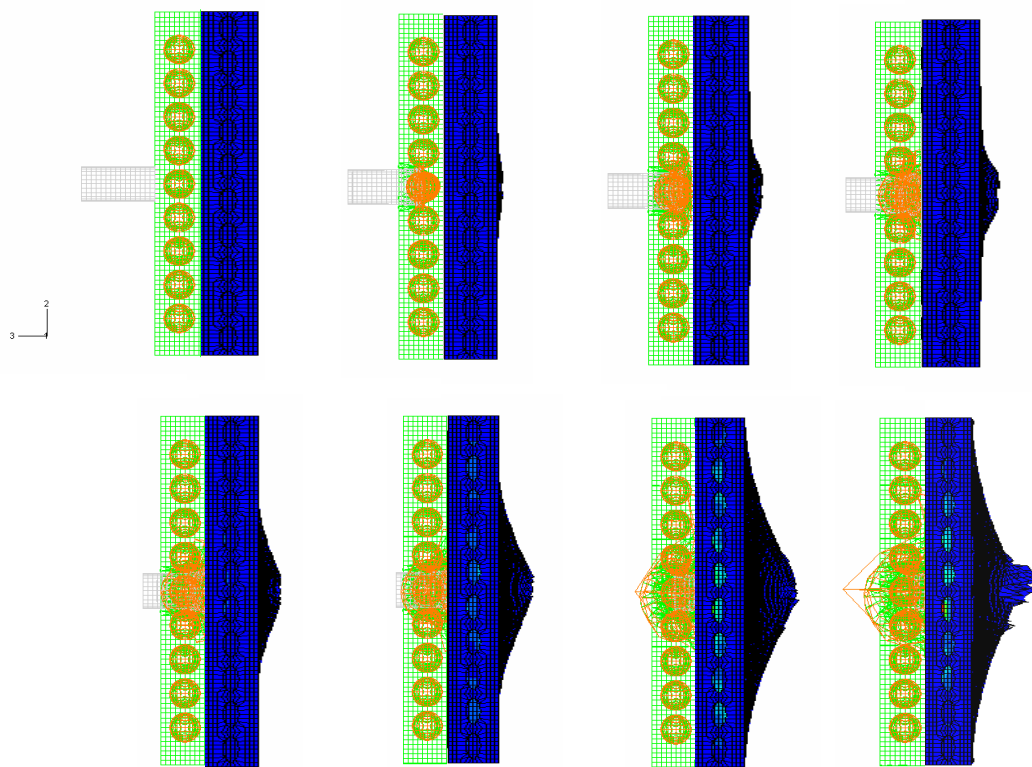


Figure 8.26: Material Damage in Different Phases of Target During Impact Simulation

It is important to note that due to the complexity of the model and the limitations in terms of the level of discretization, in order to limit the CPU time of a modern PC Pentium 4 machine, the adopted MDC model has a different packing factor of ceramic facing compared to that of a tested sample. Thus, the given results and comparisons, as a first approximation, have only a qualitative character.

Compared with the high-speed photograph of the ballistic test, the simulation accurately predicts projectile penetration and the both level and shape of the backing plate deformation. During the simulation, the shattering of ceramic spheres behind the penetrating projectile could also be visualized.

High-speed photography and residual velocity data (obtained from magneto coil sensors) indicate that the projectile did indeed tumble during perforation through the target. This is probably a result of the projectiles successfully being deflected off the aluminum spheres. The recovered projectile confirms that it underwent erosion during penetration. However, there is also an indication of shattering on the sides of the projectile, which again could be a result of oblique penetration due to tumbling.

Results of the ballistic test indicate a residual kinetic energy of 56%, with the areal density of 30.8kg/m^2 .

Numerical results showed to be in good correlation with experimental findings, even with different packing of ceramic spheres in the facing plate. Figure 8.27 shows Von-Mises stress distribution in the armor plate in the final stage of the projectile perforation. The locally damaged section corresponds well to that of the ballistic test (see Figure 8.24).

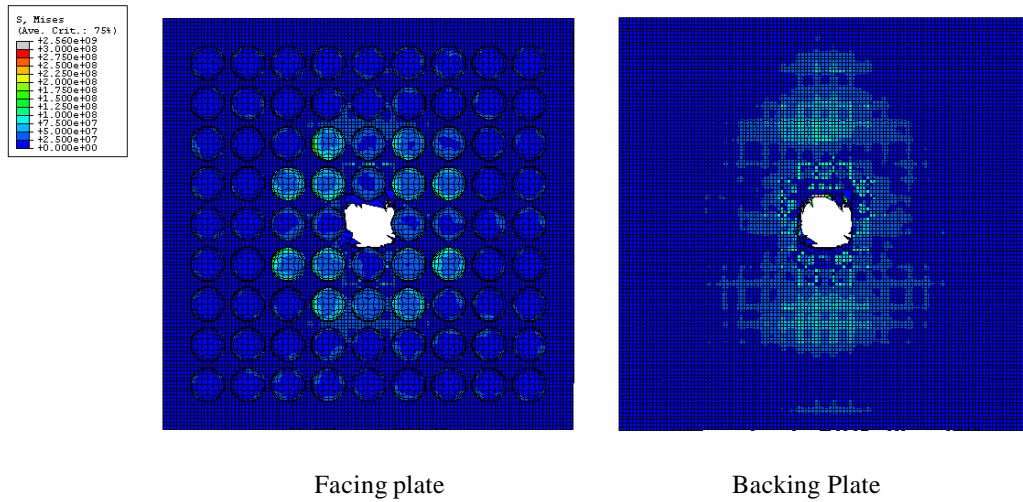


Figure 8.27: Contours of Von Mises Stress at $t=60\mu\text{sec}$ During Simulation of Ballistic Impact Test

The predicted residual velocity of 756m/s also is close to the one measured in the test, as shown on the velocity time history in Figure 8.28. It can be concluded that a developed engineering design tool, based on finite element modeling, gives a good prediction of ballistic behavior even for complex system such as multi-layered design composite armors.

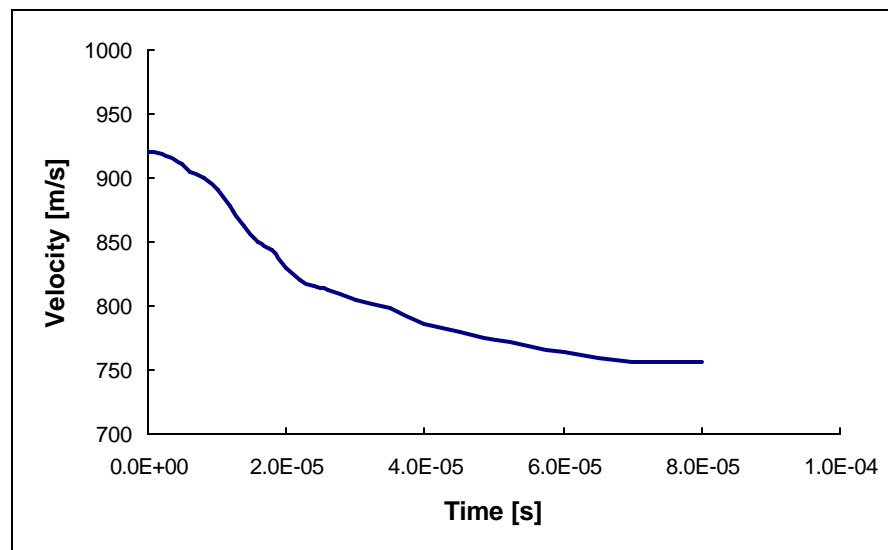


Figure 8.28: Velocity Time History of a Simulated Ballistic Test

Ballistic resistance of MDC with a facing layer of ceramic spheres embedded in epoxy is shown to be lower than that of a solid ceramic tile. However, using the presented engineering tool, further parametric studies combined with experiments would result in optimized structures for ballistic application.

9. CONCLUSIONS

A modeling tool that generates the unit cell geometries for different textile composites discretized in a structured, hexahedral finite element mesh is developed. The only inputs required of this robust tool are the unit cell dimensions and the mathematical description of the fiber reinforcement geometry.

Using a developed algorithm, a parametric study of the influence of fabric architecture on the mechanical properties of textile composites is presented. It is found that unidirectional, angle-ply, plain woven, 3D braided, and knitted composites offer a spectrum of elastic properties and allow for tailoring to the particular application.

Taking advantage of this tool's ability to represent faithfully the textile geometry, a study of the effect of fiber crimp and flattening, on in-plane modulus of a woven composite is presented. The results show that substantial changes of the modulus can originate from the variation of these two parameters.

Moreover, given that a large displacements-large strains analysis can be easily performed by the model developed, a discussion on some aspects of the non-linear elastic behavior of textile composites is presented.

This modeling tool has excellent potential for exploring the processing effects, as well as other important properties such as strength, viscoelasticity, failure and ballistic performance of textile composites.

Using this modeling tool, the ballistic resistance of two commonly used textile reinforced composites, woven and angle-ply, was compared.

Although the accuracy of the model is not completely established (at least in the case of multi-ply composites), the results are in agreement with experimental observations. A detailed examination of the stress and damage history in the composites compared showed that the lower in-plane modulus of the woven composites together with the presence of damage in crossover points resulted in their lower impact energy absorption.

Despite the apparent need for further improvements, this work offers a clear advantage over prior numerical analyses that were based on homogenized properties of composites.

It is shown that detailed descriptions of the reinforcing structures enable the characterization and understanding the failure modes, which could complement and guide the necessary experimental evaluation of such heterogeneous material structures.

The impact resistance of multiphase/multi-layered design composite (MDC) armors was evaluated. The performance of the monolithic ceramic tile is compared to that of the facing layer composed of ceramic spheres embedded in epoxy.

It is shown that mutual contribution of both the textile architecture and the ceramic facing layer influences the ballistic performance of the specific armor structure.

The armor plate with a facing layer of ceramic spheres embedded in epoxy is shown to have a lower ballistic resistance to that of a solid ceramic tile. However, presented simulations showed that with further optimization and parametric studies, especially of spherical size and their packing factor, ceramic spheres offer the potential to

replace the conventional ceramic tiles to reduce weight and cost without sacrificing its ballistic effectiveness.

Simulations have predicted that the proposed ceramic sphere/epoxy system offers an interesting inhomogeneity in ballistic response, which was shown to induce tumbling of the projectile, lowering its penetration effectiveness, allowing in the same time the optimization of such a multi-layer/multiphase system.

Finally, a preliminary comparison of the simulation with experimental results showed clearly that the numerical modeling of the impact process captures the major aspects of the physical phenomena, providing even more information on the behavior of different target constituents during ballistic impact.

There is no doubt that computer simulations represent an important step towards better understanding of different geometric and material effects in armor ballistic resistance, and opens the possibility of advanced parametric and sensitivity studies critical for advancement in the field of modern armor protective systems.

10. FUTURE WORK (RECOMMENDATIONS)

This work is meant to be a first step in the development of an Engineering Design Tool capable of accurate modeling and prediction of both the static and dynamic behavior of textile composites and hybrid, multi-layered/multiphase armor materials.

The next step in modeling of textile composites would be to establish relationships between processing variables and geometric parameters, which would give true model-to-manufacturing optimized textile composite configurations for their structural application.

Together with experimental validation, this will lead to the development of a reliable database, which will be important in the practical design and manufacturing of textile composite based structures for variety of applications.

With the computer code developed in this work even more detailed geometry of the textile composite should be modeled, especially in the vicinity of the impact site. A possible approach would be to include two different mesh refinements: one, very fine, around the impact, and second, coarser elsewhere. This would give a more reliable prediction of failure initiation and propagation during ballistic impact, addressing more specifically the role of the interface, matrix cracking, fiber de-bonding and fracture.

The role of the type and character of the interface in ballistic resistance of textile based composite materials has to be examined. The presented analysis tool com-

bined with experimental tests could be used to facilitate developing of the material's interface for maximum impact energy dissipation.

This study has shown the need for better and more reliable material models for different applications over a range of velocities. The description of the dynamic response of solids, to high-velocity, large deformation loadings, requires a mathematical description for the material behavior. The conditions encountered involve strains between 0% and 200%, strain rates from 0.01/s to 10,000,000/s, and temperatures from 300K to the melting point. Nonlinear, finite deformation, anisotropic material response, including strain-rate dependence, thermal softening, and failure, must be accurately modeled. For good correlation with experiments, it is crucial that the material parameters be determined from wave propagation experiments. Only with such an improved constitutive models capable of capturing the behavior of both traditional and advanced materials in a variety of loading regimes can a true design tool for ballistic applications be attainable.

There is no doubt that an ability to transfer energy rapidly away from the point of impact is the most desirable quality for ballistic efficiency. The energy absorption characteristics during the high velocity impact of Multi-layered Design Composite materials are influenced by the microstructural variables of both the projectile and target. The fundamental question to be tackled is how mechanical waves propagate and interact with the multiphase anisotropic media of the Multi-layered Design Composite Materials. The influence of the material impedance mismatch on stress wave propagation is to be examined and as a result, select the combination of the facing/backing plate materials

according to their ability to transfer the impact energy as fast as it is possible from the impact site.

Using the procedure developed here, initiated armor optimization study, combined with well designed experiments should be further extended toward a better understanding of what fiber type and what type of fabric, sheet or panel combined with ceramic facing, gives the highest protection level for the lowest weight for a specific application.

Bibliography

- [1.1] Herakovich, C.T.: "Mechanics of Fibrous Composites." *John Wiley & Sons. Inc.* New York, 1998.
- [2.1] Abusafieh, A., and Kalidindi, S.R.: "Longitudinal and Transverse Moduli and Strengths of Low Angle 3-D Braided Composites." *Journal of Composite Materials*, 30, pp. 885-905, 1996.
- [2.2] Anderson, C., and Bodner, S.: "Ballistic Impact: The Status of Analytical and Numerical Modeling." *Int. J. of Impact Engineering*. Vol. 7, No.1, pp. 9-35, 1988.
- [2.3] Backman, M., and Goldsmith W.: "The Mechanics of Penetration of Projectiles Into Targets." *Int. J. of Engineering Science*. Vol.16, pp.1-99, 1978.
- [2.4] Chou, T.W.: "Microstructural Design of Fiber Composites." *Cambridge University Press*. Cambridge, UK, 1992.
- [2.5] Cortes, R., Navarro, C., Martinez, A., Rodriguez, J., and Sanchez-Galvez, V.: "Numerical Modeling of Normal Impact on Ceramic Composite Armors." *Int. J. of Impact Engineering*, Vol.12, pp.639-651, 1992.
- [2.6] Cox, B.N., Carter, W.C., and Fleck, N.A.: "A Binary Model of Textile Composites-I. Formulation." *Acta Metall. Mater.*, Vol. 42, No. 10, pp. 3463-3479, 1994.
- [2.7] Crane, R.M., and Camponeschi, E.T.: "A Model for Fiber Geometry and Stiffness of Multi-directionally Braided Composites." *3-D Composite Materials, NASA Conference Publication #2420*, 1986.
- [2.8] Dasgupta, A., Bhandarkar, S., Pecht, M., and Barkar, D.: "Thermo-elastic properties of Woven-fabric Composites Using Homogenization Techniques." In Proc. *American Society for Composites 5th Technical Conference*, Lansing, MI. Technomic, Lancaster, PA, pp. 1001-1110, 1990.
- [2.9] Dasgupta, A., Agarwal, R.K., and Bhandarkar, S.M.: "Three-dimensional Modeling of Woven-fabric Composites for Effective Thermo-Mechanical and Thermal Properties." *Composites Science and Technology*, Vol.56, pp.209-223, 1996.
- [2.10] Dow, N.F., et al: "New Concept for Multiple Directional Fabric Formation." *21st. International SAMPE Technical Conference*, Sep. 25-28, pp. 558, 1989.

- [2.11] Florence, A.L.: "Interaction of Projectiles and Composite Armor plate." *Stanford Research Institute*, Menlo Park, CA, USA., AMMRG-CR-69-15, August, 1969.
- [2.12] Franco, E.: "Finite Element Simulation of the Micromechanical Behavior of Three-dimensionally Braided Composite Materials." *M.S. Thesis, Drexel University*, Philadelphia, 1995.
- [2.13] Hahn, H.T., and Pandey, R.: "A Micromechanics Model for Thermoelastic Properties of Plain Weave Fabric Composites." *Journal of Engineering Materials and Technology*, Vol.116, pp.517-523, 1994.
- [2.14] Hetherington, J.G. and Rajagopalan, B.P.: "An Investigation Into the Energy Absorbed During Ballistic Perforation of Composite Armors." *Int. J. Impact Engineering*. Vol. 11, pp. 33-40, 1991.
- [2.15] Ishikawa, T., and Chou, T.W.: "One Dimensional Micro-mechanical Analysis of Woven Fabric Composites." *AIAA Journal*, Vol. 21, No. 12, pp. 1714, 1983.
- [2.16] Jovicic, J., Zavaliangos, A. and Ko, F.: "Modeling of the Ballistic Behavior of Gradient Design Composite Armors." *Special issue of Composite Part A: Applied Science and Manufacturing*, Elsevier Science. Vol.31 (8), pp.773-784, August 2000.
- [2.17] Kalidindi, S. and Franco, E.: "Numerical Evaluation of Isostrain and Weighted-average Models for Elastic Modulus of Three-dimensional Composites." *Composite Science and Technology*, Vol.57, pp. 293-305, 1997.
- [2.18] Ko, F.K., and Wang, A.S.D.: "Finite Cell Modeling for 3-D Braided Composites." *ASME, Material Division*, MD. VOL. 5, pp. 45-55, 1988.
- [2.19] Ko, F.: "Preform Fiber Architecture for Composites." *Ceramic Bulletin*, Vol.68, No.2, pp.402-408, 1989.
- [2.20] Ko, F.K.: "Three Dimensional Fabric for Composites." *Textile Structural Composites*, Chou, T.W., and Ko, F.K. editors, Elsevier, New York, 1989.
- [2.21] Ko, F.K., Pastore, C.M., Young, J.M., and Chou, T.W.: "Structure and Properties of Multilayer Multidirectional Warp Knit Fabric Reinforced Composites." *In Proceedings of the 3rd Japan-US Conference*, pp.21-28, Tokyo, 1986.
- [2.22] Ko, F.K., Sun, W., Zavaliangos, A., Jovicic, J. El-Shiekh, A., and Song, J.: "Integrated Design for Manufacturing of Composite Helmets." *The Design and Integration of Helmet Systems, US Army Natick Symposium*, Framingham, MA, 1997.

- [2.23] Kostar, T.D. and Chou, T.W.: "Design and Automated Fabrication of 3-D Braided Preforms for Advanced Structural Composites." *Computer Aided Design in Composite Material Technology III*, Elsevier science, pp.63-78, 1992.
- [2.24] Lei, C., Cai, Y.J., and Ko, F.K.: "Finite Element Analysis of 3-D Braided composites." *Advances in Engineering Software*, Vol.14, pp.187-194, 1992.
- [2.25] Li, W.: "Structural Analysis of 3-D Braided Preforms for Composites." *J. Text. Inst.*, Vol. 81, No.40, pp. 491-514, 1990.
- [2.26] Ma, C.L., Yang, J.M., and Chou, T.W.: "Elastic Stiffness of Three Dimensional Braided Textile Structure Composites, Composite Materials: Testing and Design." (Seventh Conference), *ASTM STP 893*, American Society for Testing and Materials, Philadelphia, pp. 404-421, 1986.
- [2.27] Mahfuz, H., et al: "Investigation of High-velocity Impact on Integral Armor Using Finite Element Method." *Int. J. Impact Engineering*, Vol. 24, pp. 203-217, 2000.
- [2.28] Masters, J.E., Foye, R.L., et al: "Mechanical Properties of Triaxially Braided Composites: Experimental and Analytical Results." *Journal of Composite Technology and Research*, Vol. 15, No. 2, pp. 112-122, 1993.
- [2.29] Mayselless, M., Goldsmith, W., Virostek, P. and Finnegan, A.: "Impact on Ceramic Faced Targets." *Journal of Applied Mechanics*, Vol. 54, 1987.
- [2.30] Mukherjee, N., and Sinha, P.K.: "Three-Dimensional Thermo-structural Analysis of Multidirectional Fibrous Composite Plates." *Composite Structures*, Vol.28, pp.333-346, 1994.
- [2.31] Naik, R.A.: "Analysis of Woven and Braided Fabric Reinforced Composites." *NASA CR-194930*, National Aeronautics and Space Administration, Washington, DC, 1994.
- [2.32] Pandey, R.: "Micromechanics Based Computer-aided Design and Analysis of Two-dimensional and Three-dimensional Fabric Composites." *Ph.D. Thesis in Engineering Science and Mechanics*, The Pennsylvania State University, August 1995.
- [2.33] Pandey, R., and Hahn, H.T.: "Visualization of Representative Volume Elements for Three-dimensional 4-Step Braided Composites." *Composites Science and Technology*, Vol.56, pp.161-170, 1996.
- [2.34] Pandey, R., and Hahn, H.T.: "Designing with 4-Step Braided Fabric Composites." *Composites Science and Technology*, Vol.56, pp.623-634, 1996.

- [2.35] Pastore, C.M., and Ko, F.K.: "Modeling of Textile Structural Composites, Part I: Processing-science Model for Three-dimensional Braiding." *Journal of Textile Institute*, Vol.81, No.4, pp. 480-490, 1990.
- [2.36] Ramakrishna, S., and Hull, D.: "Tensile Behavior of Knitted Carbon Fiber/Epoxy Laminates: Prediction of Tensile Properties." *Composites Science and Technology*, Vol.50, 249-258, 1994.
- [2.37] Ravid, M., Bodner, S.R., and Holcman: "I. Application of Two-dimensional Analytic Models of Ballistic Penetration to Ceramic Armor." *Proceedings 11th. International Symposium on Ballistics*. Brussels, Belgium, 1989.
- [2.38] Reijer, P.C.: "Impact on Ceramic Faced Armor." *Ph.D. Thesis*, Delft University of Technology, Delft, The Netherlands, 1991.
- [2.39] Ruiz, C.: "Overview of Impact Properties of Monolithic Ceramics." *International Journal of Fracture Mechanics*, Vol.29, pp101, 1985.
- [2.40] Sedgwick, R.T., et al: "Numerical Investigations in Penetration Mechanics." *Int. J. of Engineering Science*, Vol.16, pp.859-869, 1978.
- [2.41] Sherman, D.: "Impact Failure Mechanisms in Alumina Tiles on Finite Thickness Support and the Effect of Confinement." *Int. J. of Impact Engineering*, Vol.24, pp. 313-328, 2000.
- [2.42] Song, J.W., Geshury, A., and Ko, F.K.: "Behavior of Gradient Designed Composites Under Ballistic Impact." *Proceedings, Eleventh International Conference on Composite Materials*, Gold Coast, Australia, July 14-18, 1997.
- [2.43] Sun, W., Lin, F., and Hu, X.: "Computer Aided Design and Modeling of Composite Unit Cells." *Composites Science and Technology*. Vol. 61, pp. 289-299, 2001.
- [2.44] Tan, P., Tong, L., and Steven, G.P.: "Modeling for Predicting the Mechanical Properties of Textile Composites-A Review." *Composites Part A*, Vol.28A, pp.903-922, 1997.
- [2.45] Vandeurzen, P.: "Structure-Performance Modeling of Two-dimensional Woven Fabric Composites." *Ph.D. Thesis, Katholieke Universiteit Leuven, Belgium*, 1998.
- [2.46] Vandeurzen, P., Ivens, J., and Verpoest, I.: "A Three-dimensional Micromechanical Analysis of Woven-fabric Composites: I. Geometric Analysis." *Composites Science and Technology*, Vol.56, pp. 1303-1315, 1996.

- [2.47] Vandeurzen, P., Ivens, J., and Verpoest, I.: "A Three-dimensional Micromechanical Analysis of Woven-fabric Composites: II. Elastic Analysis." *Composites Science and Technology*, Vol.56, pp. 1317-1327, 1996.
- [2.48] Vandeurzen, P., Ivens, J., and Verpoest, I.: "Structure-performance Analysis of Two-dimensional Woven Fabric Composites." *Polymers & Polymer Composites*, Vol. 4, No.5, pp.361-367, 1996.
- [2.49] Wang, Y.Q. and Wang, A.S.D.: "On the Topological Yarn Structure of 3-D Rectangular and Tubular Braided Preforms." *Composites Science and Technology*, 51, pp.575-586, 1994.
- [2.50] Whitcomb, J., Chapman, C., and Tang, X.: "Simulation of Progressive Failure of Woven Composites." *V Int. Conference on Composites Engng.*, Las Vegas, Nevada, 5-11 July, 1998.
- [2.51] Whitcomb, J., Woo, K., and Gundapaneni, S.: "Macro Finite Element for Analysis of Textile Composites." *Journal of Composite Materials*, Vol.28, No.7, pp.607-617, 1994.
- [2.52] Wilkins, M.L.: "Mechanics of Penetration and Perforation." *Int. J. Eng. Sci.*, 16, pp.793-807, 1978.
- [2.53] Wilkins, M.L.: "Computer Simulation of Penetration Phenomena, in Ballistic Materials and Penetration Mechanics." Edited by Laible, R.C., pp. 225-252, *Elsevier Sci. Pub. Co.*, 1980.
- [2.54] Woo, K.: "A Finite Element Analysis of Thickness and Layer Shift Effects on the Mechanical Behavior of Woven Composites." *V Int. Conference on Composites Engng.*, Las Vegas, Nevada, 5-11 July, 1998.
- [2.55] Woodward, R.L., et al: "Energy Absorption in the Failure of Ceramic Composite Armors." *Materials Forum*, Vol.13, pp. 174-181, 1989.
- [2.56] Woodward, R.L.: "A Simple One-dimensional Approach to Modeling Ceramic Composite Armor Defeat." *Int. J. of Impact Engineering*, Vol.9, pp. 455-474, 1990.
- [2.57] Woodward R.L., et al: "A Study of Fragmentation in the Ballistic Impact of Ceramic." *Int. J. of Impact Engineering*, Vol.15, pp.605-618, 1994.
- [2.58] Yang, J.M.: "Modeling and Characterization of 2D and 3D Textile Structural Composites." *Ph.D. Dissertation*, University of Delaware, 1986.

- [2.59] Zaera, R., and Sanchez-Galvez, V.: "Analytical Modeling of Normal and Oblique Ballistic Impact on Ceramic/Metal Lightweight Armors." *Int. J. of Impact Engineering*. Vol.21, No.3, pp. 133-148, 1998.
- [3.1] Scheffler, D.R., and Zukas, J.A.: "Practical Aspects of Numerical Simulation of Dynamic Events: Material Interface." *Int. J. of Impact Engineering*. Vol.24, pp. 821-842, 2000.
- [3.2] Zukas, J.A.: "Impact Dynamics." *John Wiley & Sons*, New York, 1982.
- [3.3] Zukas, J.A., and Scheffler, D.R.: "Practical Aspects of Numerical Simulation of Dynamic Events: Effects of Meshing." *Int. J. of Impact Engineering*. Vol.24, pp. 924-945, 2000.
- [4.1] Benzley, Steven E., Ernest, P., Merkley, K., Clark, B., and Sjaardema, G.: "A Comparison of All-hexahedral and All-tetrahedral Finite Element Meshes for Elastic and Elasto-plastic Analysis." Proceedings, *4th International Meshing Roundtable*, Sandia National Laboratories, pp.179-191, October 1995.
- [4.2] Chamis, C.C.: "Simplified Composite Micromechanics Equations for Hygral, Thermal, and Mechanical Properties." *SAMPE Quarterly*, April 14-23, 1984.
- [4.3] Huang, Z.M., and Ramakrishna, S.: "Micromechanical Modeling Approaches for the Stiffness and Strength of Knitted Fabric Composites: a Review and Comparative Study." *Composite Part A: Applied Science and Manufacturing*, Elsevier Science. Vol.31, pp.479-501, August 2000.
- [4.4] Keefe, M., Edwards, D.C., and Yang, J.: "Solid Modeling of Yarn and Fiber Assemblies." *Journal of Textile Institute*. Vol. 83 No. 2, pp. 185-196, 1992.
- [4.5] Keefe, M.: "Geometric Modeling of Yarn and Fiber Assemblies." Chapter 4, *Microstructural Characterization of Fiber-reinforced Composites*, edited by John Summerscales, Woodhead Publishing, CRC Press, 1998.
- [4.6] Lam, H., and Ko, F.K.: "Composite Manufacturing by the Braidtrusion Process." *33rd International SAMPE Technical Conference*, Seattle, Washington, 4-8 November 2001.
- [4.7] Leaf, G.A.V., and Glaskin, A.: "The Geometry of a Plain Knitted Loop." *Journal of Textile Institute*, Vol. 45, T587-605, 1955.
- [4.8] Liao, T., and Adanur, S.: "A Novel Approach to Three-Dimensional Modeling of Interlaced Fabric Structures." *Textile Research Journal*. Vol.68 No. 11 pp. 841-847, 1998.

- [4.9] Owen, S.J.: "A Survey of Unstructured Mesh Generation Technology." Proceedings, 7th *International Meshing Roundtable*, Sandia National Laboratories, pp.239-267, October 1998.
- [4.10] Paumelle, P., Hassim, A. and Lene, F., "Composites With Woven Reinforcements: Calculation and Parametric Analysis of the Properties of the Homogeneous Equivalent." *La Recherche Aerospaciale*, 1, 1990.
- [4.11] Peirce, F.T.: "The Geometry of Cloth Structure." *Journal of Textile Institute*, Vol. 28, T45, 1937.
- [4.12] Rogers, D.F., and Adams, A.J.: "Mathematical Elements for Computer Graphics." *McGraw-Hill Publishing Company*, New York 1990.
- [4.13] Sun, H.Y, and Qiao, X.: "Prediction of the Mechanical Properties of Three-Dimensionally Braided Composites." *Composites Science and Technology*. Vol.57. pp. 632-629, Elsevier Science, 1997.
- [5.1] Barsoum, M.: "Fundamentals of Ceramics." *McGraw Hill Inc.*,1996.
- [5.2] Crisfield, MA.: "Snap-Through and Snap Back Response in Concrete Structures and the Dangers of Under-Integration." *Int. J. for Numerical Methods in Engineering*, Vol.22, pp. 751-767, 1986.
- [5.3] Graham, R.A. Editor: "High-Pressure Shock Compression of Solids II." *Springer-Verlag*, New York 1995.
- [5.4] Hilleborg, A., Modeer, M., and Petersson, P.: "Analysis of Crack Formation and Crack Growth in Concrete by Means of Fracture Mechanics and Finite Elements." *Cement and Concrete Research*, Vol.6, pp. 773-782, 1976.
- [5.5] Lekhnitskii, S.G.: "Theory of Elasticity of an Anisotropic Body." *MIR Publisher*, Moscow, 1981.
- [5.6] Prevorsek, D.C., et al: "Strain Rate Effects in Ultrastrong Polyethylene Fibers and Composites." *Journal of Applied Polymer Science*. Vol. 47, pp. 45-66, 1991.
- [5.7] Roeder, B., and Sun, C.T.: "Dynamic Penetration of Alumina/Aluminum Laminates: Experiment and Modeling." *International Journal of Impact Engineering*. Vol. 25, pp.169-185, 2000.
- [5.8] Sherman, D.: "Impact Failure Mechanisms in Alumina Tiles on Finite Thickness Support and the Effect of Confinement." *International Journal of Impact Engineering*. Vol. 24, pp. 313-328, 2000.

- [6.1] Backman, M.E., and Goldsmith, W.: "The Mechanics of Penetration of Projectiles Into Targets." *Int. J. Engng. Sci.* Vol. 16, pp. 1-99. Pergamon Press, 1978.
- [7.1] Abrate, S.: "Impact on Composite Structures." *Academic Press*, 1998.
- [7.2] Cunnif, P.: "An Analysis of the System Effects in Woven Fabric Under Ballistic Impact." *Textile Research Journal*, 62, pp. 495-509, 1992.
- [7.3] Flanagan, M.P, and Zikry, M.A.: "An Experimental Investigation of High Velocity Impact and Penetration Failure Modes in Textile Composites." *Journal of Composite Materials*, Vol.33, No. 12/1999.
- [7.4] Jovicic, J. Zavaliangos, A., and Ko, F.: "Fiber Architecture Based Computer Modeling of Textile Composites." Poster Presentation on the *Fifth International Conference on Textile Composites (TEXCOMP 5)*, Katholieke Universiteit Leuven, Belgium, September 18-20, 2000.
- [7.5] Karaoglan, L., Noor, A.: "Frictional Contact/Impact Response of Textile Composite Structure." *Composite Structures*, Vol. 37, pp. 269-280, 1997.
- [7.6] Laible, R. C.: "Ballistic Materials and Penetration Mechanics. Method and Phenomena: Their Applications in Science and Technology", Vol. 5. *Elsevier*, Amsterdam, 1980.
- [7.7] Lim, C.T., Shim, V.P.W., Ng, Y.H.: "Finite-element Modeling of the Ballistic Impact of Fabric Armor." *Int. J. Impact Engineering*, in press, 2002.
- [7.8] Lindemulder, J.L, and Beugels, J.: "Bullet Resistant Light Helmets." *Technical Usage Textiles*, No.29, Vol.3. SIBL/MAB-M, 1998.
- [7.9] Shim, V.P.W., Lim, C.T., and Foo, K.J.: "Dynamic Mechanical Properties of Fabric Armour." *Intl. Journal of Impact Engineering*, Vol. 25, pp. 1-15, 2001.
- [7.10] Tan, V.B.C, Lim, C.T. and Cheong, C.H.: "Perforation of High-strength Fabric by Projectiles of Different Geometry." *Int. J. Impact Engineering*. In press, 2002.
- [8.1] Curran, D.R., Seaman, L., Cooper, T., and Shockey, D.A.: "Micromechanical Model for Comminution and Granular Flow of Brittle Material Under High Strain Rate Application to Penetration of Ceramic Targets." *Int. J. Impact Engineering*, Vol.13, pp.53-83, 1993.

- [8.2] Fellows, N.A., Barton, P.C.: "Development of Impact Model for Ceramic-faced Semi-infinite Armour." *Intl. Journal of Impact Engineering*, Vol. 22, pp.793-811, 1999.
- [8.3] Graham, R.A.: "Solids Under High-Pressure Shock Compression." *Springer-Verlag*, New York, 1993.
- [8.4] Graham, R. A. (editor): "High-Pressure Shock Compression of Solids II." *Springer-Verlag*, New York 1995.
- [8.5] Horsfall, I., Austina, S.J., and Bishop, W.: "Structural Ballistic Armour for Transport Aircraft." *Materials and Design*. Vol.21, pp.19-25, 2000.
- [8.6] Jovicic, J., Zavaliangos, A., and Ko, F.: "Numerical Modeling and Analysis of Dynamic Behavior of Gradient Design Composites." Presented at *The ICCM 13*. Beijing, China, June 25-29, 2001.
- [8.7] Lundberg, P., Renstrook, R., and Lundberg, B.: "Impact of Metallic Projectiles on Ceramic Targets: Transition Between Interface Defeat and Penetration." *Intl. Journal of Impact Engineering*, Vol. 24, pp259-275, 2000.
- [8.8] Nemat-Nasser, S., Isaacs, J., Sarva, S. and Plaisted, T.: Results of Ballistic Test Performed at UCSD's Center of Excellence for Advanced Materials (CEAM) facilities, San Diego, July 2002.
- [8.9] Wang, B., and Lu, G.: "On the Optimization of Two-component Plates Against Ballistic Impact." *Journal of Materials Processing Technology*, Vol.57, pp.141-145, 1996.
- [8.10] Wang, B., Lu, G., and Lim, M.K.: "Experimental and Numerical Analysis of the Response of Aluminium Oxide Tiles to Impact Loading." *Journal of Materials Processing Technology*, Vol. 51, pp.321-345, 1995.
- [8.11] Wilkins, M.L.: "Ball Materials and Penetration Mechanics." *Elsevier Scientific Publisher*, Liabe, R.C. editor, pp. 225-252, 1980.

Appendix A: Computer Code Example

COMPUTER-BASED MODELING OF THE TEXTILE REINFORCED COMPOSITE STRUCTURE

WOVEN UNIT CELL

```
restart;with(plots):
setoptions3d(title=`Woven Unit Cell`,style=PATCH, axes=BOXED);
```

1. MATHEMATICAL DEFINITION OF THE TEXTILE REINFORCEMENT

1.1 Define the unit cell dimensions (L x W x H)- and element resolution
(number of elements per side-NL x NW x NH)

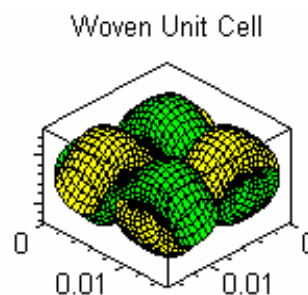
```
H:=0.00635: L:=0.015: W:=0.015:
NH:=12: NL:=16: NW:=16:
a:=0.0028: b:=0.0009: c:=0.001:
```

1.2 Define the reinforcement (yarn) architecture parametrically

```
f1p:=[L/4+a*sin(t),y,H/2+c*sin(2*Pi*y/W)+b*cos(t)]:
f2p:=[3*L/4+a*sin(t),y,H/2+c*sin(2*Pi*y/W+Pi)+b*cos(t)]:
f3p:=[x,3*W/4+a*sin(t),H/2+c*sin(2*Pi*x/L)+b*cos(t)]:
f4p:=[x,W/4+a*sin(t),H/2+c*sin(2*Pi*x/L+Pi)+b*cos(t)]:
```

1.3 Plot the unit cell

```
fiber1:=plot3d([f1p[1],f1p[2],f1p[3]],y=0..W,t=0..2*Pi,color=green):
fiber2:=plot3d([f2p[1],f2p[2],f2p[3]],y=0..W,t=0..2*Pi,color=green):
fiber3:=plot3d([f3p[1],f3p[2],f3p[3]],x=0..L,t=0..2*Pi,color=yellow):
fiber4:=plot3d([f4p[1],f4p[2],f4p[3]],x=0..L,t=0..2*Pi,color=yellow):
display(fiber1,fiber2,fiber3,fiber4);
```



2. DEFINE THE SURFACES AS INEQUALITIES

For a point (x,y,z) if $f_{lineq} < 0$ then it is inside the fiber, else outside.

```
flineq:=((x-L/4)/a)^2+((z-(H/2+c*sin(2*Pi*y/W)))/b)^2-1:
f2lineq:=((x-3*L/4)/a)^2+((z-(H/2+c*sin(2*Pi*y/W+Pi)))/b)^2-1:
f3lineq:=((y-3*W/4)/a)^2+((z-(H/2+c*sin(2*Pi*x/L)))/b)^2-1:
f4lineq:=((y-W/4)/a)^2+((z-(H/2+c*sin(2*Pi*x/L+Pi)))/b)^2-1:
```

3. GENERATE THE ELEMENT PROPERTIES

For each element find: its nodes, whether its center belongs to any of the yarns, and determine.

```
elements:=array(1..NL*NW*NH):
for E from 1 to NL*NW*NH do elements[E]:=0 od:
ELEMENT:=array(1..NL,1..NW,1..NH):
for i from 1 to NL do
for j from 1 to NW do
for k from 1 to NH do
ELEMENT[i,j,k]:=0
od:od:od:
nodes:=array(1..NL*NW*NH):
X:=array(1..(NL+1),1..(NW+1),1..(NH+1)):
for i from 1 to NL+1 do
for j from 1 to NW+1 do
for k from 1 to NH+1 do
X[i,j,k]:=(i-1)*L/NL:
od:od:od:
Y:=array(1..(NL+1),1..(NW+1),1..(NH+1)):
for i from 1 to NL+1 do
for j from 1 to NW+1 do
for k from 1 to NH+1 do
Y[i,j,k]:=(j-1)*W/NW:
od:od:od:
Z:=array(1..(NL+1),1..(NW+1),1..(NH+1)):
for i from 1 to NL+1 do
for j from 1 to NW+1 do
for k from 1 to NH+1 do
Z[i,j,k]:=(k-1)*H/NH:
od:od:od:
```

Defining the Elements and Setting the Tolerance

```
for i from 1 to NL do
for j from 1 to NW do
for k from 1 to NH do
EL_NUM:=i+(j-1)*NL+(k-1)*NW*NL;
nodes[EL_NUM]:=[i+(j-1)*(NL+1)+(k-1)*(NW+1)*(NL+1),
(i+1)+(j-1)*(NL+1)+(k-1)*(NW+1)*(NL+1),
(i+1)+j*(NL+1)+(k-1)*(NW+1)*(NL+1),
i+j*(NL+1)+(k-1)*(NW+1)*(NL+1),
i+(j-1)*(NL+1)+k*(NW+1)*(NL+1),
(i+1)+(j-1)*(NL+1)+k*(NW+1)*(NL+1),
(i+1)+j*(NL+1)+k*(NW+1)*(NL+1),
i+j*(NL+1)+k*(NW+1)*(NL+1)];
XCEN:=(i-1/2)*L/NL;
YCEN:=(j-1/2)*W/NW;
ZCEN:=(k-1/2)*H/NH;
TOL:=(L*H*W)^(1/3)/(NL*NW*NH);
```

```

if(evalf(subs(x=XCEN,y=YCEN,z=ZCEN,f1ineq))<TOL) then
elements[EL_NUM]:=1 fi;
if(evalf(subs(x=XCEN,y=YCEN,z=ZCEN,f2ineq))<TOL) then
elements[EL_NUM]:=2 fi;
if(evalf(subs(x=XCEN,y=YCEN,z=ZCEN,f3ineq))<TOL) then
elements[EL_NUM]:=3 fi;
if(evalf(subs(x=XCEN,y=YCEN,z=ZCEN,f4ineq))<TOL) then
elements[EL_NUM]:=4 fi;
od: od: od:

```

4) SOLID MODEL VALIDATION

- a) Testing for possible self-intersections.
- b) Volume fraction
- c) Number of nodes
- d) Number of elements

```

SUM:=0; for E from 1 to NL*NW*NH do
if (elements[E]=0) then SUM:=evalf (SUM)+1;
fi;
od;
Vf:=1-SUM/NL/NW/NH;
Nnum:=(NL+1)*(NW+1)*(NH+1);
Enum:=NL*NW*NH;

```

SUM := 0

Vf := .35

Nnum := 3757

Enum := 3072

5) DEFINING THE INTERFACE

Number of interesections between the matrix and the reinforcement

```

for i from 1 to NL do
for j from 1 to NW do
for k from 1 to NH do
NINTS:=0;
I1:=i; I2:=i+1; I3:=i+1; I4:=i; J1:=j; J2:=j; J3:=j+1; J4:=j+1; K1:=k;
K2:=k; K3:=k; K4:=k;
I5:=i; I6:=i+1; I7:=i+1; I8:=i; J5:=j; J6:=j; J7:=j+1; J8:=j+1;
K5:=k+1; K6:=k+1; K7:=k+1; K8:=k+1;

if(evalf(subs(x=X[I1,J1,K1],y=Y[I1,J1,K1],z=Z[I1,J1,K1],f1ineq))<TOL)
then
NINTS:=NINTS+1; fi:

if(evalf(subs(x=X[I2,J2,K2],y=Y[I2,J2,K2],z=Z[I2,J2,K2],f1ineq))<TOL)
then
NINTS:=NINTS+1; fi:

if(evalf(subs(x=X[I3,J3,K3],y=Y[I3,J3,K3],z=Z[I3,J3,K3],f1ineq))<TOL)
then
NINTS:=NINTS+1; fi:

```



```

if(evalf(subs(x=X[I4,J4,K4],y=Y[I4,J4,K4],z=Z[I4,J4,K4],f1ineq))<TOL)
then
    NINTS:=NINTS+1; fi:

if(evalf(subs(x=X[I5,J5,K5],y=Y[I5,J5,K5],z=Z[I5,J5,K5],f1ineq))<TOL)
then
    NINTS:=NINTS+1; fi:

if(evalf(subs(x=X[I6,J6,K6],y=Y[I6,J6,K6],z=Z[I6,J6,K6],f1ineq))<TOL)
then
    NINTS:=NINTS+1; fi:

if(evalf(subs(x=X[I7,J7,K7],y=Y[I7,J7,K7],z=Z[I7,J7,K7],f1ineq))<TOL)
then
    NINTS:=NINTS+1; fi:

if(evalf(subs(x=X[I8,J8,K8],y=Y[I8,J8,K8],z=Z[I8,J8,K8],f1ineq))<TOL)
then
    NINTS:=NINTS+1; fi:
    ELEMENT1[i,j,k]:=NINTS;
od;od;od;

for i from 1 to NL do
for j from 1 to NW do
for k from 1 to NH do
    NINTS:=0;
    I1:=i; I2:=i+1; I3:=i+1; I4:=i; J1:=j; J2:=j; J3:=j+1; J4:=j+1;
    K1:=k; K2:=k; K3:=k; K4:=k;
    I5:=i; I6:=i+1; I7:=i+1; I8:=i; J5:=j; J6:=j; J7:=j+1; J8:=j+1;
    K5:=k+1; K6:=k+1; K7:=k+1; K8:=k+1;

if(evalf(subs(x=X[I1,J1,K1],y=Y[I1,J1,K1],z=Z[I1,J1,K1],f2ineq))<TOL)
then
    NINTS:=NINTS+1; fi:

if(evalf(subs(x=X[I2,J2,K2],y=Y[I2,J2,K2],z=Z[I2,J2,K2],f2ineq))<TOL)
then
    NINTS:=NINTS+1; fi:

if(evalf(subs(x=X[I3,J3,K3],y=Y[I3,J3,K3],z=Z[I3,J3,K3],f2ineq))<TOL)
then
    NINTS:=NINTS+1; fi:

if(evalf(subs(x=X[I4,J4,K4],y=Y[I4,J4,K4],z=Z[I4,J4,K4],f2ineq))<TOL)
then
    NINTS:=NINTS+1; fi:

if(evalf(subs(x=X[I5,J5,K5],y=Y[I5,J5,K5],z=Z[I5,J5,K5],f2ineq))<TOL)
then
    NINTS:=NINTS+1; fi:

if(evalf(subs(x=X[I6,J6,K6],y=Y[I6,J6,K6],z=Z[I6,J6,K6],f2ineq))<TOL)
then
    NINTS:=NINTS+1; fi:

if(evalf(subs(x=X[I7,J7,K7],y=Y[I7,J7,K7],z=Z[I7,J7,K7],f2ineq))<TOL)
then

```

```

        NINTS:=NINTS+1; fi:

if(evalf(subs(x=X[I8,J8,K8],y=Y[I8,J8,K8],z=Z[I8,J8,K8],f2ineq))<TOL)
then
        NINTS:=NINTS+1; fi:
        ELEMENT2[i,j,k]:=NINTS;
        od;od;od;

for i from 1 to NL do
for j from 1 to NW do
for k from 1 to NH do
        NINTS:=0;
        I1:=i; I2:=i+1; I3:=i+1; I4:=i; J1:=j; J2:=j; J3:=j+1; J4:=j+1;
        K1:=k; K2:=k; K3:=k; K4:=k;
        I5:=i; I6:=i+1; I7:=i+1; I8:=i; J5:=j; J6:=j; J7:=j+1; J8:=j+1;
        K5:=k+1; K6:=k+1; K7:=k+1; K8:=k+1;

if(evalf(subs(x=X[I1,J1,K1],y=Y[I1,J1,K1],z=Z[I1,J1,K1],f3ineq))<TOL)
then
        NINTS:=NINTS+1; fi:

if(evalf(subs(x=X[I2,J2,K2],y=Y[I2,J2,K2],z=Z[I2,J2,K2],f3ineq))<TOL)
then
        NINTS:=NINTS+1; fi:

if(evalf(subs(x=X[I3,J3,K3],y=Y[I3,J3,K3],z=Z[I3,J3,K3],f3ineq))<TOL)
then
        NINTS:=NINTS+1; fi:

if(evalf(subs(x=X[I4,J4,K4],y=Y[I4,J4,K4],z=Z[I4,J4,K4],f3ineq))<TOL)
then
        NINTS:=NINTS+1; fi:

if(evalf(subs(x=X[I5,J5,K5],y=Y[I5,J5,K5],z=Z[I5,J5,K5],f3ineq))<TOL)
then
        NINTS:=NINTS+1; fi:

if(evalf(subs(x=X[I6,J6,K6],y=Y[I6,J6,K6],z=Z[I6,J6,K6],f3ineq))<TOL)
then
        NINTS:=NINTS+1; fi:

if(evalf(subs(x=X[I7,J7,K7],y=Y[I7,J7,K7],z=Z[I7,J7,K7],f3ineq))<TOL)
then
        NINTS:=NINTS+1; fi:

if(evalf(subs(x=X[I8,J8,K8],y=Y[I8,J8,K8],z=Z[I8,J8,K8],f3ineq))<TOL)
then
        NINTS:=NINTS+1; fi:
        ELEMENT3[i,j,k]:=NINTS;
        od;od;od;

for i from 1 to NL do
for j from 1 to NW do
for k from 1 to NH do
        NINTS:=0;
        I1:=i; I2:=i+1; I3:=i+1; I4:=i; J1:=j; J2:=j; J3:=j+1; J4:=j+1;
        K1:=k; K2:=k; K3:=k; K4:=k;

```

```

    I5:=i; I6:=i+1; I7:=i+1; I8:=i; J5:=j; J6:=j; J7:=j+1; J8:=j+1;
    K5:=k+1; K6:=k+1; K7:=k+1; K8:=k+1;

    if(evalf(subs(x=X[I1,J1,K1],y=Y[I1,J1,K1],z=Z[I1,J1,K1],f4ineq))<TOL)
    then
        NINTS:=NINTS+1; fi:

    if(evalf(subs(x=X[I2,J2,K2],y=Y[I2,J2,K2],z=Z[I2,J2,K2],f4ineq))<TOL)
    then
        NINTS:=NINTS+1; fi:

    if(evalf(subs(x=X[I3,J3,K3],y=Y[I3,J3,K3],z=Z[I3,J3,K3],f4ineq))<TOL)
    then
        NINTS:=NINTS+1; fi:

    if(evalf(subs(x=X[I4,J4,K4],y=Y[I4,J4,K4],z=Z[I4,J4,K4],f4ineq))<TOL)
    then
        NINTS:=NINTS+1; fi:

    if(evalf(subs(x=X[I5,J5,K5],y=Y[I5,J5,K5],z=Z[I5,J5,K5],f4ineq))<TOL)
    then
        NINTS:=NINTS+1; fi:

    if(evalf(subs(x=X[I6,J6,K6],y=Y[I6,J6,K6],z=Z[I6,J6,K6],f4ineq))<TOL)
    then
        NINTS:=NINTS+1; fi:

    if(evalf(subs(x=X[I7,J7,K7],y=Y[I7,J7,K7],z=Z[I7,J7,K7],f4ineq))<TOL)
    then
        NINTS:=NINTS+1; fi:

    if(evalf(subs(x=X[I8,J8,K8],y=Y[I8,J8,K8],z=Z[I8,J8,K8],f4ineq))<TOL)
    then
        NINTS:=NINTS+1; fi:
        ELEMENT4[i,j,k]:=NINTS;
        od;od;od;

Defining the minimum functions, g
    minimum1:=proc(x,yp,z)
    MIND:=10^100;
    MMT=-100;
    MMY=-100;
    M:=20;
    for mm from 0 to M do
    for nn from 0 to M do
    tm:=(mm/M)*2*evalf(Pi);
    ym:=(nn/M)*W;
    dist:=evalf((x-subs(t=tm,flp[1]))^2+
                (yp-subs(y=ym,flp[2]))^2+
                (z-subs(y=ym,t=tm,flp[3]))^2);
    if(dist<MIND) then
    MIND:=dist;
    MMT:=tm;
    MMY:=ym;
    fi;
    od;od;
    RETURN (evalf(subs(t=MMT,flp[1])),

```

```

evalf(subs(y=MMY,f1p[2])),
evalf(subs(y=MMY,t=MMT,f1p[3]));
end:
g1:=minimum1;

minimum2:=proc(x,yp,z)
MIND:=10^100;
MMT=-100;
MMY=-100;
M:=20;
for mm from 0 to M do
for nn from 0 to M do
tm:=(mm/M)*2*evalf(Pi);
ym:=(nn/M)*L;
dist:=evalf((x-subs(t=tm,f2p[1]))^2+
              (yp-subs(y=ym,f2p[2]))^2+
              (z-subs(y=ym,t=tm,f2p[3]))^2);
if(dist<MIND) then
MIND:=dist;
MMT:=tm;
MMY:=ym;
fi;
od;od;
RETURN (evalf(subs(t=MMT,f2p[1])),
        evalf(subs(y=MMY,f2p[2])),
        evalf(subs(y=MMY,t=MMT,f2p[3])));
end:
g2:=minimum2;

minimum3:=proc(xp,y,z)
MIND:=10^100;
MMT=-100;
MMX=-100;
M:=20;
for mm from 0 to M do
for nn from 0 to M do
tm:=(mm/M)*2*evalf(Pi);
xm:=(nn/M)*L;
dist:=evalf((xp-subs(x=xm,f3p[1]))^2+
              (y-subs(t=tm,f3p[2]))^2+
              (z-subs(x=xm,t=tm,f3p[3]))^2);
if(dist<MIND) then
MIND:=dist;
MMT:=tm;
MMX:=xm;
fi;
od;od;
RETURN (evalf(subs(x=MMX,f3p[1])),
        evalf(subs(t=MMT,f3p[2])),
        evalf(subs(x=MMX,t=MMT,f3p[3])));
end:
g3:=minimum3;

minimum4:=proc(xp,y,z)
MIND:=10^100;
MMT=-100;

```

```

MMX:=-100;
M:=20;
for mm from 0 to M do
for nn from 0 to M do
tm:=(mm/M)*2*evalf(Pi);
xm:=(nn/M)*L;
dist:=evalf((xp-subs(x=xm,f4p[1]))^2+
            (y-subs(t=tm,f4p[2]))^2+
            (z-subs(x=xm,t=tm,f4p[3]))^2);
if(dist<MIND) then
MIND:=dist;
MMT:=tm;
MMX:=xm;
fi;
od;od;
RETURN (evalf(subs(x=MMX,f4p[1])),
evalf(subs(t=MMT,f4p[2])),
evalf(subs(x=MMX,t=MMT,f4p[3])));
end:
g4:=minimum4;

```

6) BORDER NODES ADJUSTMENT

(1) Procedure for elements with four points in

```

<><><><>Yarn one<><><><>
for i from 1 to NL do
for j from 1 to NW do
for k from 1 to NH do
    if (ELEMENT1[i,j,k]=4) then
        I1:=i; I2:=i+1; I3:=i+1; I4:=i; J1:=j; J2:=j; J3:=j+1; J4:=j+1;
        K1:=k; K2:=k; K3:=k; K4:=k;
        I5:=i; I6:=i+1; I7:=i+1; I8:=i; J5:=j; J6:=j; J7:=j+1; J8:=j+1;
        K5:=k+1; K6:=k+1; K7:=k+1; K8:=k+1;

if(evalf(subs(x=X[I1,J1,K1],y=Y[I1,J1,K1],z=Z[I1,J1,K1],f1lineq))>TOL)
then
    sol1:=g1(X[I1,J1,K1],Y[I1,J1,K1],Z[I1,J1,K1]);
    X[I1,J1,K1]:=sol1[1]; Y[I1,J1,K1]:=sol1[2];
    Z[I1,J1,K1]:=sol1[3]; fi:

if(evalf(subs(x=X[I2,J2,K2],y=Y[I2,J2,K2],z=Z[I2,J2,K2],f1lineq))>TOL)
then
    sol2:=g1(X[I2,J2,K2],Y[I2,J2,K2],Z[I2,J2,K2]);
    X[I2,J2,K2]:=sol2[1]; Y[I2,J2,K2]:=sol2[2];
    Z[I2,J2,K2]:=sol2[3]; fi:

if(evalf(subs(x=X[I3,J3,K3],y=Y[I3,J3,K3],z=Z[I3,J3,K3],f1lineq))>TOL)
then
    sol3:=g1(X[I3,J3,K3],Y[I3,J3,K3],Z[I3,J3,K3]);
    X[I3,J3,K3]:=sol3[1]; Y[I3,J3,K3]:=sol3[2];
    Z[I3,J3,K3]:=sol3[3]; fi:
if(evalf(subs(x=X[I4,J4,K4],y=Y[I4,J4,K4],z=Z[I4,J4,K4],f1lineq))>TOL)
then

```

```

        sol4:=g1(X[I4,J4,K4],Y[I4,J4,K4],Z[I4,J4,K4]);
        X[I4,J4,K4]:=sol4[1]; Y[I4,J4,K4]:=sol4[2];
Z[I4,J4,K4]:=sol4[3]; fi:

if(evalf(subs(x=X[I5,J5,K5],y=Y[I5,J5,K5],z=Z[I5,J5,K5],f1ineq))>TOL)
then
        sol5:=g1(X[I5,J5,K5],Y[I5,J5,K5],Z[I5,J5,K5]);
        X[I5,J5,K5]:=sol5[1]; Y[I5,J5,K5]:=sol5[2];
Z[I5,J5,K5]:=sol5[3]; fi:

if(evalf(subs(x=X[I6,J6,K6],y=Y[I6,J6,K6],z=Z[I6,J6,K6],f1ineq))>TOL)
then
        sol6:=g1(X[I6,J6,K6],Y[I6,J6,K6],Z[I6,J6,K6]);
        X[I6,J6,K6]:=sol6[1]; Y[I6,J6,K6]:=sol6[2];
Z[I6,J6,K6]:=sol6[3]; fi:

if(evalf(subs(x=X[I7,J7,K7],y=Y[I7,J7,K7],z=Z[I7,J7,K7],f1ineq))>TOL)
then
        sol7:=g1(X[I7,J7,K7],Y[I7,J7,K7],Z[I7,J7,K7]);
        X[I7,J7,K7]:=sol7[1]; Y[I7,J7,K7]:=sol7[2];
Z[I7,J7,K7]:=sol7[3]; fi:

if(evalf(subs(x=X[I8,J8,K8],y=Y[I8,J8,K8],z=Z[I8,J8,K8],f1ineq))>TOL)
then
        sol8:=g1(X[I8,J8,K8],Y[I8,J8,K8],Z[I8,J8,K8]);
        X[I8,J8,K8]:=sol8[1]; Y[I8,J8,K8]:=sol8[2];
Z[I8,J8,K8]:=sol8[3]; fi:
        fi;
        od;od;od;

<><><><>Yarn two<><><><>
for i from 1 to NL do
for j from 1 to NW do
for k from 1 to NH do
        if (ELEMENT2[i,j,k]=4) then
                I1:=i; I2:=i+1; I3:=i+1; I4:=i; J1:=j; J2:=j; J3:=j+1; J4:=j+1;
K1:=k; K2:=k; K3:=k; K4:=k;
                I5:=i; I6:=i+1; I7:=i+1; I8:=i; J5:=j; J6:=j; J7:=j+1; J8:=j+1;
K5:=k+1; K6:=k+1; K7:=k+1; K8:=k+1;

if(evalf(subs(x=X[I1,J1,K1],y=Y[I1,J1,K1],z=Z[I1,J1,K1],f2ineq))>TOL)
then
        sol1:=g2(X[I1,J1,K1],Y[I1,J1,K1],Z[I1,J1,K1]);
        X[I1,J1,K1]:=sol1[1]; Y[I1,J1,K1]:=sol1[2];
Z[I1,J1,K1]:=sol1[3]; fi:

if(evalf(subs(x=X[I2,J2,K2],y=Y[I2,J2,K2],z=Z[I2,J2,K2],f2ineq))>TOL)
then
        sol2:=g2(X[I2,J2,K2],Y[I2,J2,K2],Z[I2,J2,K2]);
        X[I2,J2,K2]:=sol2[1]; Y[I2,J2,K2]:=sol2[2];
Z[I2,J2,K2]:=sol2[3]; fi:

if(evalf(subs(x=X[I3,J3,K3],y=Y[I3,J3,K3],z=Z[I3,J3,K3],f2ineq))>TOL)
then
        sol3:=g2(X[I3,J3,K3],Y[I3,J3,K3],Z[I3,J3,K3]);

```

```

        X[I3,J3,K3]:=sol3[1]; Y[I3,J3,K3]:=sol3[2];
Z[I3,J3,K3]:=sol3[3]; fi:

if(evalf(subs(x=X[I4,J4,K4],y=Y[I4,J4,K4],z=Z[I4,J4,K4],f2ineq))>TOL)
then
    sol4:=g2(X[I4,J4,K4],Y[I4,J4,K4],Z[I4,J4,K4]);
    X[I4,J4,K4]:=sol4[1]; Y[I4,J4,K4]:=sol4[2];
Z[I4,J4,K4]:=sol4[3]; fi:

if(evalf(subs(x=X[I5,J5,K5],y=Y[I5,J5,K5],z=Z[I5,J5,K5],f2ineq))>TOL)
then
    sol5:=g2(X[I5,J5,K5],Y[I5,J5,K5],Z[I5,J5,K5]);
    X[I5,J5,K5]:=sol5[1]; Y[I5,J5,K5]:=sol5[2];
Z[I5,J5,K5]:=sol5[3]; fi:

if(evalf(subs(x=X[I6,J6,K6],y=Y[I6,J6,K6],z=Z[I6,J6,K6],f2ineq))>TOL)
then
    sol6:=g2(X[I6,J6,K6],Y[I6,J6,K6],Z[I6,J6,K6]);
    X[I6,J6,K6]:=sol6[1]; Y[I6,J6,K6]:=sol6[2];
Z[I6,J6,K6]:=sol6[3]; fi:

if(evalf(subs(x=X[I7,J7,K7],y=Y[I7,J7,K7],z=Z[I7,J7,K7],f2ineq))>TOL)
then
    sol7:=g2(X[I7,J7,K7],Y[I7,J7,K7],Z[I7,J7,K7]);
    X[I7,J7,K7]:=sol7[1]; Y[I7,J7,K7]:=sol7[2];
Z[I7,J7,K7]:=sol7[3]; fi:

if(evalf(subs(x=X[I8,J8,K8],y=Y[I8,J8,K8],z=Z[I8,J8,K8],f2ineq))>TOL)
then
    sol8:=g2(X[I8,J8,K8],Y[I8,J8,K8],Z[I8,J8,K8]);
    X[I8,J8,K8]:=sol8[1]; Y[I8,J8,K8]:=sol8[2];
Z[I8,J8,K8]:=sol8[3]; fi:
    fi;
    od;od;od;

<><><><>Yarn three<><><><>
for i from 1 to NL do
for j from 1 to NW do
for k from 1 to NH do
    if (ELEMENT3[i,j,k]=4) then
        I1:=i; I2:=i+1; I3:=i+1; I4:=i; J1:=j; J2:=j; J3:=j+1; J4:=j+1;
K1:=k; K2:=k; K3:=k; K4:=k;
        I5:=i; I6:=i+1; I7:=i+1; I8:=i; J5:=j; J6:=j; J7:=j+1; J8:=j+1;
K5:=k+1; K6:=k+1; K7:=k+1;
        K8:=k+1;

if(evalf(subs(x=X[I1,J1,K1],y=Y[I1,J1,K1],z=Z[I1,J1,K1],f3ineq))>TOL)
then
    sol1:=g3(X[I1,J1,K1],Y[I1,J1,K1],Z[I1,J1,K1]);
    X[I1,J1,K1]:=sol1[1]; Y[I1,J1,K1]:=sol1[2];
Z[I1,J1,K1]:=sol1[3]; fi:

if(evalf(subs(x=X[I2,J2,K2],y=Y[I2,J2,K2],z=Z[I2,J2,K2],f3ineq))>TOL)
then
    sol2:=g3(X[I2,J2,K2],Y[I2,J2,K2],Z[I2,J2,K2]);

```

```

        X[I2,J2,K2]:=sol2[1]; Y[I2,J2,K2]:=sol2[2];
Z[I2,J2,K2]:=sol2[3]; fi:

if(evalf(subs(x=X[I3,J3,K3],y=Y[I3,J3,K3],z=Z[I3,J3,K3],f3ineq))>TOL)
then
    sol3:=g3(X[I3,J3,K3],Y[I3,J3,K3],Z[I3,J3,K3]);
    X[I3,J3,K3]:=sol3[1]; Y[I3,J3,K3]:=sol3[2];
Z[I3,J3,K3]:=sol3[3]; fi:

if(evalf(subs(x=X[I4,J4,K4],y=Y[I4,J4,K4],z=Z[I4,J4,K4],f3ineq))>TOL)
then
    sol4:=g3(X[I4,J4,K4],Y[I4,J4,K4],Z[I4,J4,K4]);
    X[I4,J4,K4]:=sol4[1]; Y[I4,J4,K4]:=sol4[2];
Z[I4,J4,K4]:=sol4[3]; fi:

if(evalf(subs(x=X[I5,J5,K5],y=Y[I5,J5,K5],z=Z[I5,J5,K5],f3ineq))>TOL)
then
    sol5:=g3(X[I5,J5,K5],Y[I5,J5,K5],Z[I5,J5,K5]);
    X[I5,J5,K5]:=sol5[1]; Y[I5,J5,K5]:=sol5[2];
Z[I5,J5,K5]:=sol5[3]; fi:

if(evalf(subs(x=X[I6,J6,K6],y=Y[I6,J6,K6],z=Z[I6,J6,K6],f3ineq))>TOL)
then
    sol6:=g3(X[I6,J6,K6],Y[I6,J6,K6],Z[I6,J6,K6]);
    X[I6,J6,K6]:=sol6[1]; Y[I6,J6,K6]:=sol6[2];
Z[I6,J6,K6]:=sol6[3]; fi:

if(evalf(subs(x=X[I7,J7,K7],y=Y[I7,J7,K7],z=Z[I7,J7,K7],f3ineq))>TOL)
then
    sol7:=g3(X[I7,J7,K7],Y[I7,J7,K7],Z[I7,J7,K7]);
    X[I7,J7,K7]:=sol7[1]; Y[I7,J7,K7]:=sol7[2];
Z[I7,J7,K7]:=sol7[3]; fi:

if(evalf(subs(x=X[I8,J8,K8],y=Y[I8,J8,K8],z=Z[I8,J8,K8],f3ineq))>TOL)
then
    sol8:=g3(X[I8,J8,K8],Y[I8,J8,K8],Z[I8,J8,K8]);
    X[I8,J8,K8]:=sol8[1]; Y[I8,J8,K8]:=sol8[2];
Z[I8,J8,K8]:=sol8[3]; fi:
    fi;
    od;od;od;

<<<<<<>Yarn four<><<<<<<
for i from 1 to NL do
for j from 1 to NW do
for k from 1 to NH do
    if (ELEMENT4[i,j,k]=4) then
        I1:=i; I2:=i+1; I3:=i+1; I4:=i; J1:=j; J2:=j; J3:=j+1; J4:=j+1;
K1:=k; K2:=k; K3:=k; K4:=k;
        I5:=i; I6:=i+1; I7:=i+1; I8:=i; J5:=j; J6:=j; J7:=j+1; J8:=j+1;
K5:=k+1; K6:=k+1; K7:=k+1;
        K8:=k+1;

if(evalf(subs(x=X[I1,J1,K1],y=Y[I1,J1,K1],z=Z[I1,J1,K1],f4ineq))>TOL)
then
    sol1:=g4(X[I1,J1,K1],Y[I1,J1,K1],Z[I1,J1,K1]);

```



```

        X[I1,J1,K1]:=sol1[1]; Y[I1,J1,K1]:=sol1[2];
Z[I1,J1,K1]:=sol1[3]; fi:

if(evalf(subs(x=X[I2,J2,K2],y=Y[I2,J2,K2],z=Z[I2,J2,K2],f4ineq))>TOL)
then
        sol2:=g4(X[I2,J2,K2],Y[I2,J2,K2],Z[I2,J2,K2]);
        X[I2,J2,K2]:=sol2[1]; Y[I2,J2,K2]:=sol2[2];
Z[I2,J2,K2]:=sol2[3]; fi:

if(evalf(subs(x=X[I3,J3,K3],y=Y[I3,J3,K3],z=Z[I3,J3,K3],f4ineq))>TOL)
then
        sol3:=g4(X[I3,J3,K3],Y[I3,J3,K3],Z[I3,J3,K3]);
        X[I3,J3,K3]:=sol3[1]; Y[I3,J3,K3]:=sol3[2];
Z[I3,J3,K3]:=sol3[3]; fi:

if(evalf(subs(x=X[I4,J4,K4],y=Y[I4,J4,K4],z=Z[I4,J4,K4],f4ineq))>TOL)
then
        sol4:=g4(X[I4,J4,K4],Y[I4,J4,K4],Z[I4,J4,K4]);
        X[I4,J4,K4]:=sol4[1]; Y[I4,J4,K4]:=sol4[2];
Z[I4,J4,K4]:=sol4[3]; fi:

if(evalf(subs(x=X[I5,J5,K5],y=Y[I5,J5,K5],z=Z[I5,J5,K5],f4ineq))>TOL)
then
        sol5:=g4(X[I5,J5,K5],Y[I5,J5,K5],Z[I5,J5,K5]);
        X[I5,J5,K5]:=sol5[1]; Y[I5,J5,K5]:=sol5[2];
Z[I5,J5,K5]:=sol5[3]; fi:

if(evalf(subs(x=X[I6,J6,K6],y=Y[I6,J6,K6],z=Z[I6,J6,K6],f4ineq))>TOL)
then
        sol6:=g4(X[I6,J6,K6],Y[I6,J6,K6],Z[I6,J6,K6]);
        X[I6,J6,K6]:=sol6[1]; Y[I6,J6,K6]:=sol6[2];
Z[I6,J6,K6]:=sol6[3]; fi:

if(evalf(subs(x=X[I7,J7,K7],y=Y[I7,J7,K7],z=Z[I7,J7,K7],f4ineq))>TOL)
then
        sol7:=g4(X[I7,J7,K7],Y[I7,J7,K7],Z[I7,J7,K7]);
        X[I7,J7,K7]:=sol7[1]; Y[I7,J7,K7]:=sol7[2];
Z[I7,J7,K7]:=sol7[3]; fi:

if(evalf(subs(x=X[I8,J8,K8],y=Y[I8,J8,K8],z=Z[I8,J8,K8],f4ineq))>TOL)
then
        sol8:=g4(X[I8,J8,K8],Y[I8,J8,K8],Z[I8,J8,K8]);
        X[I8,J8,K8]:=sol8[1]; Y[I8,J8,K8]:=sol8[2];
Z[I8,J8,K8]:=sol8[3]; fi:
fi;
od;od;od;

```

(2) Procedure for elements with three points in

```

<<<<<<>Yarn one<><<<<<<
for i from 1 to NL do
for j from 1 to NW do
for k from 1 to NH do
        if (ELEMENT1[i,j,k]=3) then

```

```

      I1:=i; I2:=i+1; I3:=i+1; I4:=i; J1:=j; J2:=j; J3:=j+1; J4:=j+1;
      K1:=k; K2:=k; K3:=k; K4:=k;
      I5:=i; I6:=i+1; I7:=i+1; I8:=i; J5:=j; J6:=j; J7:=j+1; J8:=j+1;
      K5:=k+1; K6:=k+1; K7:=k+1; K8:=k+1;

      if(evalf(subs(x=X[I1,J1,K1],y=Y[I1,J1,K1],z=Z[I1,J1,K1],flineq))>TOL)
      then
          sol1:=g1(X[I1,J1,K1],Y[I1,J1,K1],Z[I1,J1,K1]);
          X[I1,J1,K1]:=sol1[1]; Y[I1,J1,K1]:=sol1[2];
          Z[I1,J1,K1]:=sol1[3]; fi:

      if(evalf(subs(x=X[I2,J2,K2],y=Y[I2,J2,K2],z=Z[I2,J2,K2],flineq))>TOL)
      then
          sol2:=g1(X[I2,J2,K2],Y[I2,J2,K2],Z[I2,J2,K2]);
          X[I2,J2,K2]:=sol2[1]; Y[I2,J2,K2]:=sol2[2];
          Z[I2,J2,K2]:=sol2[3]; fi:

      if(evalf(subs(x=X[I3,J3,K3],y=Y[I3,J3,K3],z=Z[I3,J3,K3],flineq))>TOL)
      then
          sol3:=g1(X[I3,J3,K3],Y[I3,J3,K3],Z[I3,J3,K3]);
          X[I3,J3,K3]:=sol3[1]; Y[I3,J3,K3]:=sol3[2];
          Z[I3,J3,K3]:=sol3[3]; fi:

      if(evalf(subs(x=X[I4,J4,K4],y=Y[I4,J4,K4],z=Z[I4,J4,K4],flineq))>TOL)
      then
          sol4:=g1(X[I4,J4,K4],Y[I4,J4,K4],Z[I4,J4,K4]);
          X[I4,J4,K4]:=sol4[1]; Y[I4,J4,K4]:=sol4[2];
          Z[I4,J4,K4]:=sol4[3]; fi:

      if(evalf(subs(x=X[I5,J5,K5],y=Y[I5,J5,K5],z=Z[I5,J5,K5],flineq))>TOL)
      then
          sol5:=g1(X[I5,J5,K5],Y[I5,J5,K5],Z[I5,J5,K5]);
          X[I5,J5,K5]:=sol5[1]; Y[I5,J5,K5]:=sol5[2];
          Z[I5,J5,K5]:=sol5[3]; fi:

      if(evalf(subs(x=X[I6,J6,K6],y=Y[I6,J6,K6],z=Z[I6,J6,K6],flineq))>TOL)
      then
          sol6:=g1(X[I6,J6,K6],Y[I6,J6,K6],Z[I6,J6,K6]);
          X[I6,J6,K6]:=sol6[1]; Y[I6,J6,K6]:=sol6[2];
          Z[I6,J6,K6]:=sol6[3]; fi:

      if(evalf(subs(x=X[I7,J7,K7],y=Y[I7,J7,K7],z=Z[I7,J7,K7],flineq))>TOL)
      then
          sol7:=g1(X[I7,J7,K7],Y[I7,J7,K7],Z[I7,J7,K7]);
          X[I7,J7,K7]:=sol7[1]; Y[I7,J7,K7]:=sol7[2];
          Z[I7,J7,K7]:=sol7[3]; fi:

      if(evalf(subs(x=X[I8,J8,K8],y=Y[I8,J8,K8],z=Z[I8,J8,K8],flineq))>TOL)
      then
          sol8:=g1(X[I8,J8,K8],Y[I8,J8,K8],Z[I8,J8,K8]);
          X[I8,J8,K8]:=sol8[1]; Y[I8,J8,K8]:=sol8[2];
          Z[I8,J8,K8]:=sol8[3]; fi:
      ELEMENT1[i,j,k]=8
      fi;
      od;od;od;

```

```

<><><><>Yarn two<><><><>
for i from 1 to NL do
for j from 1 to NW do
for k from 1 to NH do
    if (ELEMENT2[i,j,k]=3) then
        I1:=i; I2:=i+1; I3:=i+1; I4:=i; J1:=j; J2:=j; J3:=j+1; J4:=j+1;
        K1:=k; K2:=k; K3:=k; K4:=k;
        I5:=i; I6:=i+1; I7:=i+1; I8:=i; J5:=j; J6:=j; J7:=j+1; J8:=j+1;
        K5:=k+1; K6:=k+1; K7:=k+1; K8:=k+1;

if(evalf(subs(x=X[I1,J1,K1],y=Y[I1,J1,K1],z=Z[I1,J1,K1],f2ineq))>TOL)
then
    sol1:=g2(X[I1,J1,K1],Y[I1,J1,K1],Z[I1,J1,K1]);
    X[I1,J1,K1]:=sol1[1]; Y[I1,J1,K1]:=sol1[2];
Z[I1,J1,K1]:=sol1[3]; fi:

if(evalf(subs(x=X[I2,J2,K2],y=Y[I2,J2,K2],z=Z[I2,J2,K2],f2ineq))>TOL)
then
    sol2:=g2(X[I2,J2,K2],Y[I2,J2,K2],Z[I2,J2,K2]);
    X[I2,J2,K2]:=sol2[1]; Y[I2,J2,K2]:=sol2[2];
Z[I2,J2,K2]:=sol2[3]; fi:

if(evalf(subs(x=X[I3,J3,K3],y=Y[I3,J3,K3],z=Z[I3,J3,K3],f2ineq))>TOL)
then
    sol3:=g2(X[I3,J3,K3],Y[I3,J3,K3],Z[I3,J3,K3]);
    X[I3,J3,K3]:=sol3[1]; Y[I3,J3,K3]:=sol3[2];
Z[I3,J3,K3]:=sol3[3]; fi:

if(evalf(subs(x=X[I4,J4,K4],y=Y[I4,J4,K4],z=Z[I4,J4,K4],f2ineq))>TOL)
then
    sol4:=g2(X[I4,J4,K4],Y[I4,J4,K4],Z[I4,J4,K4]);
    X[I4,J4,K4]:=sol4[1]; Y[I4,J4,K4]:=sol4[2];
Z[I4,J4,K4]:=sol4[3]; fi:

if(evalf(subs(x=X[I5,J5,K5],y=Y[I5,J5,K5],z=Z[I5,J5,K5],f2ineq))>TOL)
then
    sol5:=g2(X[I5,J5,K5],Y[I5,J5,K5],Z[I5,J5,K5]);
    X[I5,J5,K5]:=sol5[1]; Y[I5,J5,K5]:=sol5[2];
Z[I5,J5,K5]:=sol5[3]; fi:

if(evalf(subs(x=X[I6,J6,K6],y=Y[I6,J6,K6],z=Z[I6,J6,K6],f2ineq))>TOL)
then
    sol6:=g2(X[I6,J6,K6],Y[I6,J6,K6],Z[I6,J6,K6]);
    X[I6,J6,K6]:=sol6[1]; Y[I6,J6,K6]:=sol6[2];
Z[I6,J6,K6]:=sol6[3]; fi:

if(evalf(subs(x=X[I7,J7,K7],y=Y[I7,J7,K7],z=Z[I7,J7,K7],f2ineq))>TOL)
then
    sol7:=g2(X[I7,J7,K7],Y[I7,J7,K7],Z[I7,J7,K7]);
    X[I7,J7,K7]:=sol7[1]; Y[I7,J7,K7]:=sol7[2];
Z[I7,J7,K7]:=sol7[3]; fi:

if(evalf(subs(x=X[I8,J8,K8],y=Y[I8,J8,K8],z=Z[I8,J8,K8],f2ineq))>TOL)
then
    sol8:=g2(X[I8,J8,K8],Y[I8,J8,K8],Z[I8,J8,K8]);
    X[I8,J8,K8]:=sol8[1]; Y[I8,J8,K8]:=sol8[2];
Z[I8,J8,K8]:=sol8[3]; fi:

```

```

fi;
od;od;od;

<><><><>Yarn three<><><><>
for i from 1 to NL do
for j from 1 to NW do
for k from 1 to NH do
    if (ELEMENT3[i,j,k]=3) then
        I1:=i; I2:=i+1; I3:=i+1; I4:=i; J1:=j; J2:=j; J3:=j+1; J4:=j+1;
K1:=k; K2:=k; K3:=k; K4:=k;
        I5:=i; I6:=i+1; I7:=i+1; I8:=i; J5:=j; J6:=j; J7:=j+1; J8:=j+1;
K5:=k+1; K6:=k+1; K7:=k+1;
        K8:=k+1;

if(evalf(subs(x=X[I1,J1,K1],y=Y[I1,J1,K1],z=Z[I1,J1,K1],f3ineq))>TOL)
then
    sol1:=g3(X[I1,J1,K1],Y[I1,J1,K1],Z[I1,J1,K1]);
    X[I1,J1,K1]:=sol1[1]; Y[I1,J1,K1]:=sol1[2];
Z[I1,J1,K1]:=sol1[3]; fi:

if(evalf(subs(x=X[I2,J2,K2],y=Y[I2,J2,K2],z=Z[I2,J2,K2],f3ineq))>TOL)
then
    sol2:=g3(X[I2,J2,K2],Y[I2,J2,K2],Z[I2,J2,K2]);
    X[I2,J2,K2]:=sol2[1]; Y[I2,J2,K2]:=sol2[2];
Z[I2,J2,K2]:=sol2[3]; fi:

if(evalf(subs(x=X[I3,J3,K3],y=Y[I3,J3,K3],z=Z[I3,J3,K3],f3ineq))>TOL)
then
    sol3:=g3(X[I3,J3,K3],Y[I3,J3,K3],Z[I3,J3,K3]);
    X[I3,J3,K3]:=sol3[1]; Y[I3,J3,K3]:=sol3[2];
Z[I3,J3,K3]:=sol3[3]; fi:

if(evalf(subs(x=X[I4,J4,K4],y=Y[I4,J4,K4],z=Z[I4,J4,K4],f3ineq))>TOL)
then
    sol4:=g3(X[I4,J4,K4],Y[I4,J4,K4],Z[I4,J4,K4]);
    X[I4,J4,K4]:=sol4[1]; Y[I4,J4,K4]:=sol4[2];
Z[I4,J4,K4]:=sol4[3]; fi:

if(evalf(subs(x=X[I5,J5,K5],y=Y[I5,J5,K5],z=Z[I5,J5,K5],f3ineq))>TOL)
then
    sol5:=g3(X[I5,J5,K5],Y[I5,J5,K5],Z[I5,J5,K5]);
    X[I5,J5,K5]:=sol5[1]; Y[I5,J5,K5]:=sol5[2];
Z[I5,J5,K5]:=sol5[3]; fi:

if(evalf(subs(x=X[I6,J6,K6],y=Y[I6,J6,K6],z=Z[I6,J6,K6],f3ineq))>TOL)
then
    sol6:=g3(X[I6,J6,K6],Y[I6,J6,K6],Z[I6,J6,K6]);
    X[I6,J6,K6]:=sol6[1]; Y[I6,J6,K6]:=sol6[2];
Z[I6,J6,K6]:=sol6[3]; fi:

if(evalf(subs(x=X[I7,J7,K7],y=Y[I7,J7,K7],z=Z[I7,J7,K7],f3ineq))>TOL)
then
    sol7:=g3(X[I7,J7,K7],Y[I7,J7,K7],Z[I7,J7,K7]);
    X[I7,J7,K7]:=sol7[1]; Y[I7,J7,K7]:=sol7[2];
Z[I7,J7,K7]:=sol7[3]; fi:

```

```

if(evalf(subs(x=X[I8,J8,K8],y=Y[I8,J8,K8],z=Z[I8,J8,K8],f3ineq))>TOL)
then
    sol8:=g3(X[I8,J8,K8],Y[I8,J8,K8],Z[I8,J8,K8]);
    X[I8,J8,K8]:=sol8[1]; Y[I8,J8,K8]:=sol8[2];
Z[I8,J8,K8]:=sol8[3]; fi:
    fi;
    od;od;od;

<><><><>Yarn four<><><><>
for i from 1 to NL do
for j from 1 to NW do
for k from 1 to NH do
    if (ELEMENT4[i,j,k]=3) then
        I1:=i; I2:=i+1; I3:=i+1; I4:=i; J1:=j; J2:=j; J3:=j+1; J4:=j+1;
K1:=k; K2:=k; K3:=k; K4:=k;
        I5:=i; I6:=i+1; I7:=i+1; I8:=i; J5:=j; J6:=j; J7:=j+1; J8:=j+1;
K5:=k+1; K6:=k+1; K7:=k+1;
        K8:=k+1;

if(evalf(subs(x=X[I1,J1,K1],y=Y[I1,J1,K1],z=Z[I1,J1,K1],f4ineq))>TOL)
then
    sol1:=g4(X[I1,J1,K1],Y[I1,J1,K1],Z[I1,J1,K1]);
    X[I1,J1,K1]:=sol1[1]; Y[I1,J1,K1]:=sol1[2];
Z[I1,J1,K1]:=sol1[3]; fi:

if(evalf(subs(x=X[I2,J2,K2],y=Y[I2,J2,K2],z=Z[I2,J2,K2],f4ineq))>TOL)
then
    sol2:=g4(X[I2,J2,K2],Y[I2,J2,K2],Z[I2,J2,K2]);
    X[I2,J2,K2]:=sol2[1]; Y[I2,J2,K2]:=sol2[2];
Z[I2,J2,K2]:=sol2[3]; fi:

if(evalf(subs(x=X[I3,J3,K3],y=Y[I3,J3,K3],z=Z[I3,J3,K3],f4ineq))>TOL)
then
    sol3:=g4(X[I3,J3,K3],Y[I3,J3,K3],Z[I3,J3,K3]);
    X[I3,J3,K3]:=sol3[1]; Y[I3,J3,K3]:=sol3[2];
Z[I3,J3,K3]:=sol3[3]; fi:

if(evalf(subs(x=X[I4,J4,K4],y=Y[I4,J4,K4],z=Z[I4,J4,K4],f4ineq))>TOL)
then
    sol4:=g4(X[I4,J4,K4],Y[I4,J4,K4],Z[I4,J4,K4]);
    X[I4,J4,K4]:=sol4[1]; Y[I4,J4,K4]:=sol4[2];
Z[I4,J4,K4]:=sol4[3]; fi:

if(evalf(subs(x=X[I5,J5,K5],y=Y[I5,J5,K5],z=Z[I5,J5,K5],f4ineq))>TOL)
then
    sol5:=g4(X[I5,J5,K5],Y[I5,J5,K5],Z[I5,J5,K5]);
    X[I5,J5,K5]:=sol5[1]; Y[I5,J5,K5]:=sol5[2];
Z[I5,J5,K5]:=sol5[3]; fi:

if(evalf(subs(x=X[I6,J6,K6],y=Y[I6,J6,K6],z=Z[I6,J6,K6],f4ineq))>TOL)
then
    sol6:=g4(X[I6,J6,K6],Y[I6,J6,K6],Z[I6,J6,K6]);
    X[I6,J6,K6]:=sol6[1]; Y[I6,J6,K6]:=sol6[2];
Z[I6,J6,K6]:=sol6[3]; fi:
if(evalf(subs(x=X[I7,J7,K7],y=Y[I7,J7,K7],z=Z[I7,J7,K7],f4ineq))>TOL)
then

```

```

        sol7:=g4(X[I7,J7,K7],Y[I7,J7,K7],Z[I7,J7,K7]);
        X[I7,J7,K7]:=sol7[1]; Y[I7,J7,K7]:=sol7[2];
Z[I7,J7,K7]:=sol7[3]; fi:

if(evalf(subs(x=X[I8,J8,K8],y=Y[I8,J8,K8],z=Z[I8,J8,K8],f4ineq))>TOL)
then
        sol8:=g4(X[I8,J8,K8],Y[I8,J8,K8],Z[I8,J8,K8]);
        X[I8,J8,K8]:=sol8[1]; Y[I8,J8,K8]:=sol8[2];
Z[I8,J8,K8]:=sol8[3]; fi:
        fi;
        od;od;od;

```

(3) Procedure for elements with two points in

```

<><><><>Yarn one<><><><>
for i from 1 to NL do
for j from 1 to NW do
for k from 1 to NH do
        if (ELEMENT1[i,j,k]=2) then
                I1:=i; I2:=i+1; I3:=i+1; I4:=i; J1:=j; J2:=j; J3:=j+1; J4:=j+1;
K1:=k; K2:=k; K3:=k; K4:=k;
                I5:=i; I6:=i+1; I7:=i+1; I8:=i; J5:=j; J6:=j; J7:=j+1; J8:=j+1;
K5:=k+1; K6:=k+1; K7:=k+1; K8:=k+1;

if(evalf(subs(x=X[I1,J1,K1],y=Y[I1,J1,K1],z=Z[I1,J1,K1],f1ineq))>TOL)
then
        sol1:=g1(X[I1,J1,K1],Y[I1,J1,K1],Z[I1,J1,K1]);
        X[I1,J1,K1]:=sol1[1]; Y[I1,J1,K1]:=sol1[2];
Z[I1,J1,K1]:=sol1[3]; fi:

if(evalf(subs(x=X[I2,J2,K2],y=Y[I2,J2,K2],z=Z[I2,J2,K2],f1ineq))>TOL)
then
        sol2:=g1(X[I2,J2,K2],Y[I2,J2,K2],Z[I2,J2,K2]);
        X[I2,J2,K2]:=sol2[1]; Y[I2,J2,K2]:=sol2[2];
Z[I2,J2,K2]:=sol2[3]; fi:

if(evalf(subs(x=X[I3,J3,K3],y=Y[I3,J3,K3],z=Z[I3,J3,K3],f1ineq))>TOL)
then
        sol3:=g1(X[I3,J3,K3],Y[I3,J3,K3],Z[I3,J3,K3]);
        X[I3,J3,K3]:=sol3[1]; Y[I3,J3,K3]:=sol3[2];
Z[I3,J3,K3]:=sol3[3]; fi:

if(evalf(subs(x=X[I4,J4,K4],y=Y[I4,J4,K4],z=Z[I4,J4,K4],f1ineq))>TOL)
then
        sol4:=g1(X[I4,J4,K4],Y[I4,J4,K4],Z[I4,J4,K4]);
        X[I4,J4,K4]:=sol4[1]; Y[I4,J4,K4]:=sol4[2];
Z[I4,J4,K4]:=sol4[3]; fi:

if(evalf(subs(x=X[I5,J5,K5],y=Y[I5,J5,K5],z=Z[I5,J5,K5],f1ineq))>TOL)
then
        sol5:=g1(X[I5,J5,K5],Y[I5,J5,K5],Z[I5,J5,K5]);
        X[I5,J5,K5]:=sol5[1]; Y[I5,J5,K5]:=sol5[2];
Z[I5,J5,K5]:=sol5[3]; fi:

if(evalf(subs(x=X[I6,J6,K6],y=Y[I6,J6,K6],z=Z[I6,J6,K6],f1ineq))>TOL)
then

```

```

        sol6:=g1(X[I6,J6,K6],Y[I6,J6,K6],Z[I6,J6,K6]);
        X[I6,J6,K6]:=sol6[1]; Y[I6,J6,K6]:=sol6[2];
Z[I6,J6,K6]:=sol6[3]; fi:

if(evalf(subs(x=X[I7,J7,K7],y=Y[I7,J7,K7],z=Z[I7,J7,K7],f1ineq))>TOL)
then
        sol7:=g1(X[I7,J7,K7],Y[I7,J7,K7],Z[I7,J7,K7]);
        X[I7,J7,K7]:=sol7[1]; Y[I7,J7,K7]:=sol7[2];
Z[I7,J7,K7]:=sol7[3]; fi:

if(evalf(subs(x=X[I8,J8,K8],y=Y[I8,J8,K8],z=Z[I8,J8,K8],f1ineq))>TOL)
then
        sol8:=g1(X[I8,J8,K8],Y[I8,J8,K8],Z[I8,J8,K8]);
        X[I8,J8,K8]:=sol8[1]; Y[I8,J8,K8]:=sol8[2];
Z[I8,J8,K8]:=sol8[3]; fi:
        ELEMENT1[i,j,k]=8
        fi;
        od;od;od;

<><><><>Yarn two<><><><>
for i from 1 to NL do
for j from 1 to NW do
for k from 1 to NH do
        if (ELEMENT2[i,j,k]=2) then
                I1:=i; I2:=i+1; I3:=i+1; I4:=i; J1:=j; J2:=j; J3:=j+1; J4:=j+1;
K1:=k; K2:=k; K3:=k; K4:=k;
                I5:=i; I6:=i+1; I7:=i+1; I8:=i; J5:=j; J6:=j; J7:=j+1; J8:=j+1;
K5:=k+1; K6:=k+1; K7:=k+1; K8:=k+1;

if(evalf(subs(x=X[I1,J1,K1],y=Y[I1,J1,K1],z=Z[I1,J1,K1],f2ineq))>TOL)
then
        sol1:=g2(X[I1,J1,K1],Y[I1,J1,K1],Z[I1,J1,K1]);
        X[I1,J1,K1]:=sol1[1]; Y[I1,J1,K1]:=sol1[2];
Z[I1,J1,K1]:=sol1[3]; fi:

if(evalf(subs(x=X[I2,J2,K2],y=Y[I2,J2,K2],z=Z[I2,J2,K2],f2ineq))>TOL)
then
        sol2:=g2(X[I2,J2,K2],Y[I2,J2,K2],Z[I2,J2,K2]);
        X[I2,J2,K2]:=sol2[1]; Y[I2,J2,K2]:=sol2[2];
Z[I2,J2,K2]:=sol2[3]; fi:

if(evalf(subs(x=X[I3,J3,K3],y=Y[I3,J3,K3],z=Z[I3,J3,K3],f2ineq))>TOL)
then
        sol3:=g2(X[I3,J3,K3],Y[I3,J3,K3],Z[I3,J3,K3]);
        X[I3,J3,K3]:=sol3[1]; Y[I3,J3,K3]:=sol3[2];
Z[I3,J3,K3]:=sol3[3]; fi:

if(evalf(subs(x=X[I4,J4,K4],y=Y[I4,J4,K4],z=Z[I4,J4,K4],f2ineq))>TOL)
then
        sol4:=g2(X[I4,J4,K4],Y[I4,J4,K4],Z[I4,J4,K4]);
        X[I4,J4,K4]:=sol4[1]; Y[I4,J4,K4]:=sol4[2];
Z[I4,J4,K4]:=sol4[3]; fi:

if(evalf(subs(x=X[I5,J5,K5],y=Y[I5,J5,K5],z=Z[I5,J5,K5],f2ineq))>TOL)
then
        sol5:=g2(X[I5,J5,K5],Y[I5,J5,K5],Z[I5,J5,K5]);

```

```

        X[I5,J5,K5]:=sol5[1]; Y[I5,J5,K5]:=sol5[2];
Z[I5,J5,K5]:=sol5[3]; fi:

if(evalf(subs(x=X[I6,J6,K6],y=Y[I6,J6,K6],z=Z[I6,J6,K6],f2ineq))>TOL)
then
    sol6:=g2(X[I6,J6,K6],Y[I6,J6,K6],Z[I6,J6,K6]);
    X[I6,J6,K6]:=sol6[1]; Y[I6,J6,K6]:=sol6[2];
Z[I6,J6,K6]:=sol6[3]; fi:

if(evalf(subs(x=X[I7,J7,K7],y=Y[I7,J7,K7],z=Z[I7,J7,K7],f2ineq))>TOL)
then
    sol7:=g2(X[I7,J7,K7],Y[I7,J7,K7],Z[I7,J7,K7]);
    X[I7,J7,K7]:=sol7[1]; Y[I7,J7,K7]:=sol7[2];
Z[I7,J7,K7]:=sol7[3]; fi:

if(evalf(subs(x=X[I8,J8,K8],y=Y[I8,J8,K8],z=Z[I8,J8,K8],f2ineq))>TOL)
then
    sol8:=g2(X[I8,J8,K8],Y[I8,J8,K8],Z[I8,J8,K8]);
    X[I8,J8,K8]:=sol8[1]; Y[I8,J8,K8]:=sol8[2];
Z[I8,J8,K8]:=sol8[3]; fi:
    fi;
    od;od;od;

<<<<<<Yarn three<<<<<<
for i from 1 to NL do
for j from 1 to NW do
for k from 1 to NH do
    if (ELEMENT3[i,j,k]=2) then
        I1:=i; I2:=i+1; I3:=i+1; I4:=i; J1:=j; J2:=j; J3:=j+1; J4:=j+1;
K1:=k; K2:=k; K3:=k; K4:=k;
        I5:=i; I6:=i+1; I7:=i+1; I8:=i; J5:=j; J6:=j; J7:=j+1; J8:=j+1;
K5:=k+1; K6:=k+1; K7:=k+1;
        K8:=k+1;

if(evalf(subs(x=X[I1,J1,K1],y=Y[I1,J1,K1],z=Z[I1,J1,K1],f3ineq))>TOL)
then
    sol1:=g3(X[I1,J1,K1],Y[I1,J1,K1],Z[I1,J1,K1]);
    X[I1,J1,K1]:=sol1[1]; Y[I1,J1,K1]:=sol1[2];
Z[I1,J1,K1]:=sol1[3]; fi:

if(evalf(subs(x=X[I2,J2,K2],y=Y[I2,J2,K2],z=Z[I2,J2,K2],f3ineq))>TOL)
then
    sol2:=g3(X[I2,J2,K2],Y[I2,J2,K2],Z[I2,J2,K2]);
    X[I2,J2,K2]:=sol2[1]; Y[I2,J2,K2]:=sol2[2];
Z[I2,J2,K2]:=sol2[3]; fi:

if(evalf(subs(x=X[I3,J3,K3],y=Y[I3,J3,K3],z=Z[I3,J3,K3],f3ineq))>TOL)
then
    sol3:=g3(X[I3,J3,K3],Y[I3,J3,K3],Z[I3,J3,K3]);
    X[I3,J3,K3]:=sol3[1]; Y[I3,J3,K3]:=sol3[2];
Z[I3,J3,K3]:=sol3[3]; fi:

if(evalf(subs(x=X[I4,J4,K4],y=Y[I4,J4,K4],z=Z[I4,J4,K4],f3ineq))>TOL)
then
    sol4:=g3(X[I4,J4,K4],Y[I4,J4,K4],Z[I4,J4,K4]);

```



```

        X[I4,J4,K4]:=sol4[1]; Y[I4,J4,K4]:=sol4[2];
Z[I4,J4,K4]:=sol4[3]; fi:

if(evalf(subs(x=X[I5,J5,K5],y=Y[I5,J5,K5],z=Z[I5,J5,K5],f3ineq))>TOL)
then
    sol5:=g3(X[I5,J5,K5],Y[I5,J5,K5],Z[I5,J5,K5]);
    X[I5,J5,K5]:=sol5[1]; Y[I5,J5,K5]:=sol5[2];
Z[I5,J5,K5]:=sol5[3]; fi:

if(evalf(subs(x=X[I6,J6,K6],y=Y[I6,J6,K6],z=Z[I6,J6,K6],f3ineq))>TOL)
then
    sol6:=g3(X[I6,J6,K6],Y[I6,J6,K6],Z[I6,J6,K6]);
    X[I6,J6,K6]:=sol6[1]; Y[I6,J6,K6]:=sol6[2];
Z[I6,J6,K6]:=sol6[3]; fi:

if(evalf(subs(x=X[I7,J7,K7],y=Y[I7,J7,K7],z=Z[I7,J7,K7],f3ineq))>TOL)
then
    sol7:=g3(X[I7,J7,K7],Y[I7,J7,K7],Z[I7,J7,K7]);
    X[I7,J7,K7]:=sol7[1]; Y[I7,J7,K7]:=sol7[2];
Z[I7,J7,K7]:=sol7[3]; fi:

if(evalf(subs(x=X[I8,J8,K8],y=Y[I8,J8,K8],z=Z[I8,J8,K8],f3ineq))>TOL)
then
    sol8:=g3(X[I8,J8,K8],Y[I8,J8,K8],Z[I8,J8,K8]);
    X[I8,J8,K8]:=sol8[1]; Y[I8,J8,K8]:=sol8[2];
Z[I8,J8,K8]:=sol8[3]; fi:
    fi;
    od;od;od;

<><><><>Yarn four<><><><>
for i from 1 to NL do
for j from 1 to NW do
for k from 1 to NH do
    if (ELEMENT4[i,j,k]=2) then
        I1:=i; I2:=i+1; I3:=i+1; I4:=i; J1:=j; J2:=j; J3:=j+1; J4:=j+1;
K1:=k; K2:=k; K3:=k; K4:=k;
        I5:=i; I6:=i+1; I7:=i+1; I8:=i; J5:=j; J6:=j; J7:=j+1; J8:=j+1;
K5:=k+1; K6:=k+1; K7:=k+1;
        K8:=k+1;

if(evalf(subs(x=X[I1,J1,K1],y=Y[I1,J1,K1],z=Z[I1,J1,K1],f4ineq))>TOL)
then
    sol1:=g4(X[I1,J1,K1],Y[I1,J1,K1],Z[I1,J1,K1]);
    X[I1,J1,K1]:=sol1[1]; Y[I1,J1,K1]:=sol1[2];
Z[I1,J1,K1]:=sol1[3]; fi:

if(evalf(subs(x=X[I2,J2,K2],y=Y[I2,J2,K2],z=Z[I2,J2,K2],f4ineq))>TOL)
then
    sol2:=g4(X[I2,J2,K2],Y[I2,J2,K2],Z[I2,J2,K2]);
    X[I2,J2,K2]:=sol2[1]; Y[I2,J2,K2]:=sol2[2];
Z[I2,J2,K2]:=sol2[3]; fi:

if(evalf(subs(x=X[I3,J3,K3],y=Y[I3,J3,K3],z=Z[I3,J3,K3],f4ineq))>TOL)
then
    sol3:=g4(X[I3,J3,K3],Y[I3,J3,K3],Z[I3,J3,K3]);

```

```

        X[I3,J3,K3]:=sol3[1]; Y[I3,J3,K3]:=sol3[2];
Z[I3,J3,K3]:=sol3[3]; fi:

if(evalf(subs(x=X[I4,J4,K4],y=Y[I4,J4,K4],z=Z[I4,J4,K4],f4ineq))>TOL)
then
    sol4:=g4(X[I4,J4,K4],Y[I4,J4,K4],Z[I4,J4,K4]);
    X[I4,J4,K4]:=sol4[1]; Y[I4,J4,K4]:=sol4[2];
Z[I4,J4,K4]:=sol4[3]; fi:

if(evalf(subs(x=X[I5,J5,K5],y=Y[I5,J5,K5],z=Z[I5,J5,K5],f4ineq))>TOL)
then
    sol5:=g4(X[I5,J5,K5],Y[I5,J5,K5],Z[I5,J5,K5]);
    X[I5,J5,K5]:=sol5[1]; Y[I5,J5,K5]:=sol5[2];
Z[I5,J5,K5]:=sol5[3]; fi:

if(evalf(subs(x=X[I6,J6,K6],y=Y[I6,J6,K6],z=Z[I6,J6,K6],f4ineq))>TOL)
then
    sol6:=g4(X[I6,J6,K6],Y[I6,J6,K6],Z[I6,J6,K6]);
    X[I6,J6,K6]:=sol6[1]; Y[I6,J6,K6]:=sol6[2];
Z[I6,J6,K6]:=sol6[3]; fi:

if(evalf(subs(x=X[I7,J7,K7],y=Y[I7,J7,K7],z=Z[I7,J7,K7],f4ineq))>TOL)
then
    sol7:=g4(X[I7,J7,K7],Y[I7,J7,K7],Z[I7,J7,K7]);
    X[I7,J7,K7]:=sol7[1]; Y[I7,J7,K7]:=sol7[2];
Z[I7,J7,K7]:=sol7[3]; fi:

if(evalf(subs(x=X[I8,J8,K8],y=Y[I8,J8,K8],z=Z[I8,J8,K8],f4ineq))>TOL)
then
    sol8:=g4(X[I8,J8,K8],Y[I8,J8,K8],Z[I8,J8,K8]);
    X[I8,J8,K8]:=sol8[1]; Y[I8,J8,K8]:=sol8[2];
Z[I8,J8,K8]:=sol8[3]; fi:
fi;
od;od;od;

```

(4) Procedure for elements with one point in

```

<><><><>Yarn one<><><><>
for i from 1 to NL do
for j from 1 to NW do
for k from 1 to NH do
    if (ELEMENT1[i,j,k]=1) then
        I1:=i; I2:=i+1; I3:=i+1; I4:=i; J1:=j; J2:=j; J3:=j+1; J4:=j+1;
K1:=k; K2:=k; K3:=k; K4:=k;
        I5:=i; I6:=i+1; I7:=i+1; I8:=i; J5:=j; J6:=j; J7:=j+1; J8:=j+1;
K5:=k+1; K6:=k+1; K7:=k+1; K8:=k+1;

if(evalf(subs(x=X[I1,J1,K1],y=Y[I1,J1,K1],z=Z[I1,J1,K1],f1ineq))>TOL)
then
    sol1:=g1(X[I1,J1,K1],Y[I1,J1,K1],Z[I1,J1,K1]);
    X[I1,J1,K1]:=sol1[1]; Y[I1,J1,K1]:=sol1[2];
Z[I1,J1,K1]:=sol1[3]; fi:

if(evalf(subs(x=X[I2,J2,K2],y=Y[I2,J2,K2],z=Z[I2,J2,K2],f1ineq))>TOL)
then
    sol2:=g1(X[I2,J2,K2],Y[I2,J2,K2],Z[I2,J2,K2]);

```

```

        X[I2,J2,K2]:=sol2[1]; Y[I2,J2,K2]:=sol2[2];
Z[I2,J2,K2]:=sol2[3]; fi:

if(evalf(subs(x=X[I3,J3,K3],y=Y[I3,J3,K3],z=Z[I3,J3,K3],f1ineq))>TOL)
then
        sol3:=g1(X[I3,J3,K3],Y[I3,J3,K3],Z[I3,J3,K3]);
        X[I3,J3,K3]:=sol3[1]; Y[I3,J3,K3]:=sol3[2];
Z[I3,J3,K3]:=sol3[3]; fi:

if(evalf(subs(x=X[I4,J4,K4],y=Y[I4,J4,K4],z=Z[I4,J4,K4],f1ineq))>TOL)
then
        sol4:=g1(X[I4,J4,K4],Y[I4,J4,K4],Z[I4,J4,K4]);
        X[I4,J4,K4]:=sol4[1]; Y[I4,J4,K4]:=sol4[2];
Z[I4,J4,K4]:=sol4[3]; fi:

if(evalf(subs(x=X[I5,J5,K5],y=Y[I5,J5,K5],z=Z[I5,J5,K5],f1ineq))>TOL)
then
        sol5:=g1(X[I5,J5,K5],Y[I5,J5,K5],Z[I5,J5,K5]);
        X[I5,J5,K5]:=sol5[1]; Y[I5,J5,K5]:=sol5[2];
Z[I5,J5,K5]:=sol5[3]; fi:

if(evalf(subs(x=X[I6,J6,K6],y=Y[I6,J6,K6],z=Z[I6,J6,K6],f1ineq))>TOL)
then
        sol6:=g1(X[I6,J6,K6],Y[I6,J6,K6],Z[I6,J6,K6]);
        X[I6,J6,K6]:=sol6[1]; Y[I6,J6,K6]:=sol6[2];
Z[I6,J6,K6]:=sol6[3]; fi:

if(evalf(subs(x=X[I7,J7,K7],y=Y[I7,J7,K7],z=Z[I7,J7,K7],f1ineq))>TOL)
then
        sol7:=g1(X[I7,J7,K7],Y[I7,J7,K7],Z[I7,J7,K7]);
        X[I7,J7,K7]:=sol7[1]; Y[I7,J7,K7]:=sol7[2];
Z[I7,J7,K7]:=sol7[3]; fi:

if(evalf(subs(x=X[I8,J8,K8],y=Y[I8,J8,K8],z=Z[I8,J8,K8],f1ineq))>TOL)
then
        sol8:=g1(X[I8,J8,K8],Y[I8,J8,K8],Z[I8,J8,K8]);
        X[I8,J8,K8]:=sol8[1]; Y[I8,J8,K8]:=sol8[2];
Z[I8,J8,K8]:=sol8[3]; fi:
        ELEMENT1[i,j,k]=8
        fi;
        od;od;od;

<><><><>Yarn two<><><><>
for i from 1 to NL do
for j from 1 to NW do
for k from 1 to NH do
        if (ELEMENT2[i,j,k]=1) then
                I1:=i; I2:=i+1; I3:=i+1; I4:=i; J1:=j; J2:=j; J3:=j+1; J4:=j+1;
K1:=k; K2:=k; K3:=k; K4:=k;
                I5:=i; I6:=i+1; I7:=i+1; I8:=i; J5:=j; J6:=j; J7:=j+1; J8:=j+1;
K5:=k+1; K6:=k+1; K7:=k+1; K8:=k+1;

if(evalf(subs(x=X[I1,J1,K1],y=Y[I1,J1,K1],z=Z[I1,J1,K1],f2ineq))>TOL)
then
        sol1:=g2(X[I1,J1,K1],Y[I1,J1,K1],Z[I1,J1,K1]);

```

```

        X[I1,J1,K1]:=sol1[1]; Y[I1,J1,K1]:=sol1[2];
Z[I1,J1,K1]:=sol1[3]; fi:

if(evalf(subs(x=X[I2,J2,K2],y=Y[I2,J2,K2],z=Z[I2,J2,K2],f2ineq))>TOL)
then
    sol2:=g2(X[I2,J2,K2],Y[I2,J2,K2],Z[I2,J2,K2]);
    X[I2,J2,K2]:=sol2[1]; Y[I2,J2,K2]:=sol2[2];
Z[I2,J2,K2]:=sol2[3]; fi:

if(evalf(subs(x=X[I3,J3,K3],y=Y[I3,J3,K3],z=Z[I3,J3,K3],f2ineq))>TOL)
then
    sol3:=g2(X[I3,J3,K3],Y[I3,J3,K3],Z[I3,J3,K3]);
    X[I3,J3,K3]:=sol3[1]; Y[I3,J3,K3]:=sol3[2];
Z[I3,J3,K3]:=sol3[3]; fi:

if(evalf(subs(x=X[I4,J4,K4],y=Y[I4,J4,K4],z=Z[I4,J4,K4],f2ineq))>TOL)
then
    sol4:=g2(X[I4,J4,K4],Y[I4,J4,K4],Z[I4,J4,K4]);
    X[I4,J4,K4]:=sol4[1]; Y[I4,J4,K4]:=sol4[2];
Z[I4,J4,K4]:=sol4[3]; fi:

if(evalf(subs(x=X[I5,J5,K5],y=Y[I5,J5,K5],z=Z[I5,J5,K5],f2ineq))>TOL)
then
    sol5:=g2(X[I5,J5,K5],Y[I5,J5,K5],Z[I5,J5,K5]);
    X[I5,J5,K5]:=sol5[1]; Y[I5,J5,K5]:=sol5[2];
Z[I5,J5,K5]:=sol5[3]; fi:

if(evalf(subs(x=X[I6,J6,K6],y=Y[I6,J6,K6],z=Z[I6,J6,K6],f2ineq))>TOL)
then
    sol6:=g2(X[I6,J6,K6],Y[I6,J6,K6],Z[I6,J6,K6]);
    X[I6,J6,K6]:=sol6[1]; Y[I6,J6,K6]:=sol6[2];
Z[I6,J6,K6]:=sol6[3]; fi:

if(evalf(subs(x=X[I7,J7,K7],y=Y[I7,J7,K7],z=Z[I7,J7,K7],f2ineq))>TOL)
then
    sol7:=g2(X[I7,J7,K7],Y[I7,J7,K7],Z[I7,J7,K7]);
    X[I7,J7,K7]:=sol7[1]; Y[I7,J7,K7]:=sol7[2];
Z[I7,J7,K7]:=sol7[3]; fi:

if(evalf(subs(x=X[I8,J8,K8],y=Y[I8,J8,K8],z=Z[I8,J8,K8],f2ineq))>TOL)
then
    sol8:=g2(X[I8,J8,K8],Y[I8,J8,K8],Z[I8,J8,K8]);
    X[I8,J8,K8]:=sol8[1]; Y[I8,J8,K8]:=sol8[2];
Z[I8,J8,K8]:=sol8[3]; fi:
    fi;
    od;od;od;

<><><><>Yarn three<><><><>
for i from 1 to NL do
for j from 1 to NW do
for k from 1 to NH do
    if (ELEMENT3[i,j,k]=1) then
        I1:=i; I2:=i+1; I3:=i+1; I4:=i; J1:=j; J2:=j; J3:=j+1; J4:=j+1;
K1:=k; K2:=k; K3:=k; K4:=k;
        I5:=i; I6:=i+1; I7:=i+1; I8:=i; J5:=j; J6:=j; J7:=j+1; J8:=j+1;
K5:=k+1; K6:=k+1; K7:=k+1;

```

```

      K8:=k+1;

if(evalf(subs(x=X[I1,J1,K1],y=Y[I1,J1,K1],z=Z[I1,J1,K1],f3ineq))>TOL)
then
      sol1:=g3(X[I1,J1,K1],Y[I1,J1,K1],Z[I1,J1,K1]);
      X[I1,J1,K1]:=sol1[1]; Y[I1,J1,K1]:=sol1[2];
Z[I1,J1,K1]:=sol1[3]; fi:

if(evalf(subs(x=X[I2,J2,K2],y=Y[I2,J2,K2],z=Z[I2,J2,K2],f3ineq))>TOL)
then
      sol2:=g3(X[I2,J2,K2],Y[I2,J2,K2],Z[I2,J2,K2]);
      X[I2,J2,K2]:=sol2[1]; Y[I2,J2,K2]:=sol2[2];
Z[I2,J2,K2]:=sol2[3]; fi:

if(evalf(subs(x=X[I3,J3,K3],y=Y[I3,J3,K3],z=Z[I3,J3,K3],f3ineq))>TOL)
then
      sol3:=g3(X[I3,J3,K3],Y[I3,J3,K3],Z[I3,J3,K3]);
      X[I3,J3,K3]:=sol3[1]; Y[I3,J3,K3]:=sol3[2];
Z[I3,J3,K3]:=sol3[3]; fi:

if(evalf(subs(x=X[I4,J4,K4],y=Y[I4,J4,K4],z=Z[I4,J4,K4],f3ineq))>TOL)
then
      sol4:=g3(X[I4,J4,K4],Y[I4,J4,K4],Z[I4,J4,K4]);
      X[I4,J4,K4]:=sol4[1]; Y[I4,J4,K4]:=sol4[2];
Z[I4,J4,K4]:=sol4[3]; fi:

if(evalf(subs(x=X[I5,J5,K5],y=Y[I5,J5,K5],z=Z[I5,J5,K5],f3ineq))>TOL)
then
      sol5:=g3(X[I5,J5,K5],Y[I5,J5,K5],Z[I5,J5,K5]);
      X[I5,J5,K5]:=sol5[1]; Y[I5,J5,K5]:=sol5[2];
Z[I5,J5,K5]:=sol5[3]; fi:

if(evalf(subs(x=X[I6,J6,K6],y=Y[I6,J6,K6],z=Z[I6,J6,K6],f3ineq))>TOL)
then
      sol6:=g3(X[I6,J6,K6],Y[I6,J6,K6],Z[I6,J6,K6]);
      X[I6,J6,K6]:=sol6[1]; Y[I6,J6,K6]:=sol6[2];
Z[I6,J6,K6]:=sol6[3]; fi:

if(evalf(subs(x=X[I7,J7,K7],y=Y[I7,J7,K7],z=Z[I7,J7,K7],f3ineq))>TOL)
then
      sol7:=g3(X[I7,J7,K7],Y[I7,J7,K7],Z[I7,J7,K7]);
      X[I7,J7,K7]:=sol7[1]; Y[I7,J7,K7]:=sol7[2];
Z[I7,J7,K7]:=sol7[3]; fi:

if(evalf(subs(x=X[I8,J8,K8],y=Y[I8,J8,K8],z=Z[I8,J8,K8],f3ineq))>TOL)
then
      sol8:=g3(X[I8,J8,K8],Y[I8,J8,K8],Z[I8,J8,K8]);
      X[I8,J8,K8]:=sol8[1]; Y[I8,J8,K8]:=sol8[2];
Z[I8,J8,K8]:=sol8[3]; fi:
      fi;
      od;od;od;

<><><><>Yarn four<><><><>
for i from 1 to NL do
for j from 1 to NW do
for k from 1 to NH do

```

```

        if (ELEMENT4[i,j,k]=1) then
            I1:=i; I2:=i+1; I3:=i+1; I4:=i; J1:=j; J2:=j; J3:=j+1; J4:=j+1;
            K1:=k; K2:=k; K3:=k; K4:=k;
            I5:=i; I6:=i+1; I7:=i+1; I8:=i; J5:=j; J6:=j; J7:=j+1; J8:=j+1;
            K5:=k+1; K6:=k+1; K7:=k+1;
            K8:=k+1;

if(evalf(subs(x=X[I1,J1,K1],y=Y[I1,J1,K1],z=Z[I1,J1,K1],f4ineq))>TOL)
then
            sol1:=g4(X[I1,J1,K1],Y[I1,J1,K1],Z[I1,J1,K1]);
            X[I1,J1,K1]:=sol1[1]; Y[I1,J1,K1]:=sol1[2];
            Z[I1,J1,K1]:=sol1[3]; fi:

if(evalf(subs(x=X[I2,J2,K2],y=Y[I2,J2,K2],z=Z[I2,J2,K2],f4ineq))>TOL)
then
            sol2:=g4(X[I2,J2,K2],Y[I2,J2,K2],Z[I2,J2,K2]);
            X[I2,J2,K2]:=sol2[1]; Y[I2,J2,K2]:=sol2[2];
            Z[I2,J2,K2]:=sol2[3]; fi:

if(evalf(subs(x=X[I3,J3,K3],y=Y[I3,J3,K3],z=Z[I3,J3,K3],f4ineq))>TOL)
then
            sol3:=g4(X[I3,J3,K3],Y[I3,J3,K3],Z[I3,J3,K3]);
            X[I3,J3,K3]:=sol3[1]; Y[I3,J3,K3]:=sol3[2];
            Z[I3,J3,K3]:=sol3[3]; fi:

if(evalf(subs(x=X[I4,J4,K4],y=Y[I4,J4,K4],z=Z[I4,J4,K4],f4ineq))>TOL)
then
            sol4:=g4(X[I4,J4,K4],Y[I4,J4,K4],Z[I4,J4,K4]);
            X[I4,J4,K4]:=sol4[1]; Y[I4,J4,K4]:=sol4[2];
            Z[I4,J4,K4]:=sol4[3]; fi:

if(evalf(subs(x=X[I5,J5,K5],y=Y[I5,J5,K5],z=Z[I5,J5,K5],f4ineq))>TOL)
then
            sol5:=g4(X[I5,J5,K5],Y[I5,J5,K5],Z[I5,J5,K5]);
            X[I5,J5,K5]:=sol5[1]; Y[I5,J5,K5]:=sol5[2];
            Z[I5,J5,K5]:=sol5[3]; fi:

if(evalf(subs(x=X[I6,J6,K6],y=Y[I6,J6,K6],z=Z[I6,J6,K6],f4ineq))>TOL)
then
            sol6:=g4(X[I6,J6,K6],Y[I6,J6,K6],Z[I6,J6,K6]);
            X[I6,J6,K6]:=sol6[1]; Y[I6,J6,K6]:=sol6[2];
            Z[I6,J6,K6]:=sol6[3]; fi:

if(evalf(subs(x=X[I7,J7,K7],y=Y[I7,J7,K7],z=Z[I7,J7,K7],f4ineq))>TOL)
then
            sol7:=g4(X[I7,J7,K7],Y[I7,J7,K7],Z[I7,J7,K7]);
            X[I7,J7,K7]:=sol7[1]; Y[I7,J7,K7]:=sol7[2];
            Z[I7,J7,K7]:=sol7[3]; fi:

if(evalf(subs(x=X[I8,J8,K8],y=Y[I8,J8,K8],z=Z[I8,J8,K8],f4ineq))>TOL)
then
            sol8:=g4(X[I8,J8,K8],Y[I8,J8,K8],Z[I8,J8,K8]);
            X[I8,J8,K8]:=sol8[1]; Y[I8,J8,K8]:=sol8[2];
            Z[I8,J8,K8]:=sol8[3]; fi:
        fi;
    od;od;od;

```

7) MESH SMOOTHING

Laplacian mesh optimization (average of centers) for elements in the matrix

```

for i from 1 to NL-1 do
for j from 1 to NW-1 do
for k from 1 to NH-1 do
if(ELEMENT[i,j,k]+ELEMENT[i+1,j,k]+ELEMENT[i+1,j+1,k]+ELEMENT[i,j+1,k]+
ELEMENT[i,j,k+1]+ELEMENT[i+1,j,k+1]+ELEMENT[i+1,j+1,k+1]+ELEMENT[i,j+1,
k+1]=0)
then
X[i+1,j+1,k+1]:=evalf(X[i,j+1,k+1]+X[i+2,j+1,k+1]+X[i+1,j,k+1]+X[i+1,j+
2,k+1]+X[i+1,j+1,k]+X[i+1,j+1,k+2])/6;
Y[i+1,j+1,k+1]:=evalf(Y[i,j+1,k+1]+Y[i+2,j+1,k+1]+Y[i+1,j,k+1]+Y[i+1,j+
2,k+1]+Y[i+1,j+1,k]+Y[i+1,j+1,k+2])/6;
Z[i+1,j+1,k+1]:=evalf(Z[i,j+1,k+1]+Z[i+2,j+1,k+1]+Z[i+1,j,k+1]+Z[i+1,j+
2,k+1]+Z[i+1,j+1,k]+Z[i+1,j+1,k+2])/6;
fi;
od:od:od:

```

Laplacian optimization of mesh in the yarns

```

for i from 1 to NL-1 do
for j from 1 to NW-1 do
for k from 1 to NH-1 do
if(ELEMENT[i,j,k]*ELEMENT[i+1,j,k]*ELEMENT[i,j+1,k]*ELEMENT[i+1,j+1,k]*
ELEMENT[i,j,k+1]*ELEMENT[i+1,j,k+1]*ELEMENT[i+1,j+1,k+1]*ELEMENT[i,j+1,
k+1]=0)
then
X[i+1,j+1,k+1]:=evalf(X[i,j+1,k+1]+X[i+2,j+1,k+1]+X[i+1,j,k+1]+X[i+1,j+
2,k+1]+X[i+1,j+1,k]+X[i+1,j+1,k+2])/6;
Y[i+1,j+1,k+1]:=evalf(Y[i,j+1,k+1]+Y[i+2,j+1,k+1]+Y[i+1,j,k+1]+Y[i+1,j+
2,k+1]+Y[i+1,j+1,k]+Y[i+1,j+1,k+2])/6;
Z[i+1,j+1,k+1]:=evalf(Z[i,j+1,k+1]+Z[i+2,j+1,k+1]+Z[i+1,j,k+1]+Z[i+1,j+
2,k+1]+Z[i+1,j+1,k]+Z[i+1,j+1,k+2])/6;
fi;
od:od:od:

```

```

for i from 1 to NL-1 do
for j from 1 to NW-1 do
for k from 1 to NH-1 do

```

```

if(ELEMENT[i,j,k]*ELEMENT[i+1,j,k]*ELEMENT[i,j+1,k]*ELEMENT[i+1,j+1,k]*
ELEMENT[i,j,k+1]*ELEMENT[i+1,j,k+1]*ELEMENT[i+1,j+1,k+1]*ELEMENT[i+1,j+1,
k+1]>0)
then
X[i+1,j+1,k+1]:=evalf(X[i,j+1,k+1]+X[i+2,j+1,k+1]+X[i+1,j,k+1]+X[i+1,j+
2,k+1]+X[i+1,j+1,k]+X[i+1,j+1,k+2])/6;
Y[i+1,j+1,k+1]:=evalf(Y[i,j+1,k+1]+Y[i+2,j+1,k+1]+Y[i+1,j,k+1]+Y[i+1,j+
2,k+1]+Y[i+1,j+1,k]+Y[i+1,j+1,k+2])/6;
Z[i+1,j+1,k+1]:=evalf(Z[i,j+1,k+1]+Z[i+2,j+1,k+1]+Z[i+1,j,k+1]+Z[i+1,j+
2,k+1]+Z[i+1,j+1,k]+Z[i+1,j+1,k+2])/6;
fi;
od:od:od:

```

```

for i from 1 to NL-1 do
for j from 1 to NW-1 do
for k from 1 to NH-1 do

```

```

if (ELEMENT3[i,j,k]*ELEMENT3[i+1,j,k]*ELEMENT3[i,j+1,k]*ELEMENT3[i+1,j+1,
,k]*ELEMENT3[i,j,k+1]*ELEMENT3[i+1,j,k+1]*ELEMENT3[i,j+1,k+1]*ELEMENT3[
i+1,j+1,k+1]>0)
  then
X[i+1,j+1,k+1]:=evalf(X[i,j+1,k+1]+X[i+2,j+1,k+1]+X[i+1,j,k+1]+X[i+1,j+
2,k+1]+X[i+1,j+1,k]+X[i+1,j+1,k+2])/6;
Y[i+1,j+1,k+1]:=evalf(Y[i,j+1,k+1]+Y[i+2,j+1,k+1]+Y[i+1,j,k+1]+Y[i+1,j+
2,k+1]+Y[i+1,j+1,k]+Y[i+1,j+1,k+2])/6;
Z[i+1,j+1,k+1]:=evalf(Z[i,j+1,k+1]+Z[i+2,j+1,k+1]+Z[i+1,j,k+1]+Z[i+1,j+
2,k+1]+Z[i+1,j+1,k]+Z[i+1,j+1,k+2])/6;
  fi;
od:od:od:

for i from 1 to NL-1 do
for j from 1 to NW-1 do
for k from 1 to NH-1 do

if (ELEMENT4[i,j,k]*ELEMENT4[i+1,j,k]*ELEMENT4[i,j+1,k]*ELEMENT4[i+1,j+1,
,k]*ELEMENT4[i,j,k+1]*ELEMENT4[i+1,j,k+1]*ELEMENT4[i,j+1,k+1]*ELEMENT4[
i+1,j+1,k+1]>0)
  then
X[i+1,j+1,k+1]:=evalf(X[i,j+1,k+1]+X[i+2,j+1,k+1]+X[i+1,j,k+1]+X[i+1,j+
2,k+1]+X[i+1,j+1,k]+X[i+1,j+1,k+2])/6;
Y[i+1,j+1,k+1]:=evalf(Y[i,j+1,k+1]+Y[i+2,j+1,k+1]+Y[i+1,j,k+1]+Y[i+1,j+
2,k+1]+Y[i+1,j+1,k]+Y[i+1,j+1,k+2])/6;
Z[i+1,j+1,k+1]:=evalf(Z[i,j+1,k+1]+Z[i+2,j+1,k+1]+Z[i+1,j,k+1]+Z[i+1,j+
2,k+1]+Z[i+1,j+1,k]+Z[i+1,j+1,k+2])/6;
  fi;
od:od:od:

```

8) GENERATE ABAQUS CODE INPUT FILE

```

open(`wucell.inp`,WRITE);
writeto(`wucell.inp`);
print(`*HEADING`);
print(`Woven Unit Cell`);
print(`***NODE DEFINITION***`);
print(`*NODE, NSET=NALL`);
for i from 1 to NL+1 do
for j from 1 to NW+1 do
for k from 1 to NH+1 do
print(i+(j-1)*(NL+1)+(k-1)*(NW+1)*(NL+1),
X[i,j,k],Y[i,j,k],Z[i,j,k]);
od; od; od;
print(`***ELEMENT DEFINITION***`);
print(`***MATRIX***`);
print(`*ELEMENT, TYPE=C3D8, ELSET=MATRIX`);
for E from 1 to NL*NW*NH do
if (elements[E]=0) then
print(E,nodes[E][1],nodes[E][2],nodes[E][3],nodes[E][4],
nodes[E][5],nodes[E][6],nodes[E][7],nodes[E][8]);
fi;
od;
print(`***FIBERS***`);

```



```

print(`*ELEMENT, TYPE=C3D8, ELSET=FIBER1`);
for E from 1 to NL*NW*NH do
if (elements[E]=1) then
print(E,nodes[E][1],nodes[E][2],nodes[E][3],nodes[E][4],
nodes[E][5],nodes[E][6],nodes[E][7],nodes[E][8]);
fi;
od;
print(`*ELEMENT, TYPE=C3D8, ELSET=FIBER2`);
for E from 1 to NL*NW*NH do
if (elements[E]=2) then
print(E,nodes[E][1],nodes[E][2],nodes[E][3],nodes[E][4],
nodes[E][5],nodes[E][6],nodes[E][7],nodes[E][8]);
fi;
od;
print(`*ELEMENT, TYPE=C3D8, ELSET=FIBER3`);
for E from 1 to NL*NW*NH do
if (elements[E]=3) then
print(E,nodes[E][1],nodes[E][2],nodes[E][3],nodes[E][4],
nodes[E][5],nodes[E][6],nodes[E][7],nodes[E][8]);
fi;
od;
print(`*ELEMENT, TYPE=C3D8, ELSET=FIBER4`);
for E from 1 to NL*NW*NH do
if (elements[E]=4) then
print(E,nodes[E][1],nodes[E][2],nodes[E][3],nodes[E][4],
nodes[E][5],nodes[E][6],nodes[E][7],nodes[E][8]);
fi;
od;
print(`***MATERIAL DEFINITION***`);
print(`*MATERIAL, NAME=MMATRIX`);
print(`*ELASTIC,TYPE=ISOTROPIC`);
print(`3.45E+9,0.35`);
print(`*MATERIAL, NAME=MFIBER1`);
print(`*ELASTIC,TYPE=ENGINEERING CONSTANTS`);
print(`1.72E+11,4.72E+09,4.72E+09, 0.4, 0.4, 0.4,3.6E+10,3.6E+10`);
print(`3.6E+10`);
print(`*MATERIAL, NAME=MFIBER2`);
print(`*ELASTIC,TYPE=ENGINEERING CONSTANTS`);
print(`1.72E+11,4.72E+09,4.72E+09, 0.4, 0.4, 0.4,3.6E+10,3.6E+10`);
print(`3.6E+10`);
print(`*MATERIAL, NAME=MFIBER3`);
print(`*ELASTIC,TYPE=ENGINEERING CONSTANTS`);
print(`1.72E+11,4.72E+09,4.72E+09, 0.4, 0.4, 0.4,3.6E+10,3.6E+10`);
print(`3.6E+10`);
print(`*MATERIAL, NAME=MFIBER4`);
print(`*ELASTIC,TYPE=ENGINEERING CONSTANTS`);
print(`1.72E+11,4.72E+09,4.72E+09, 0.4, 0.4, 0.4,3.6E+10,3.6E+10`);
print(`3.6E+10`);
print(`*SOLID SECTION, ELSET=MATRIX, MATERIAL=MMATRIX`);
print(`*SOLID SECTION,
ELSET=FIBER1,MATERIAL=MFIBER1,ORIENTATION=FTRANS`);
print(`*SOLID SECTION,
ELSET=FIBER2,MATERIAL=MFIBER2,ORIENTATION=FTRANS`);
print(`*SOLID SECTION,
ELSET=FIBER3,MATERIAL=MFIBER3,ORIENTATION=FLONG`);
print(`*SOLID SECTION,
ELSET=FIBER4,MATERIAL=MFIBER4,ORIENTATION=FLONG`);

```

```

print(`*ORIENTATION,NAME=FLONG,SYSTEM=RECTANGULAR,DEFINITION=COORDINATE
S`);
print(`1.,0.,0.,0.,1.,0.`);
print(`*ORIENTATION,NAME=FTRANS,SYSTEM=RECTANGULAR,DEFINITION=COORDINAT
ES`);
print(`0.,1.,0.,-1.,0.,0.`);
print(`***NODE SETS***`);
print(`*NSET, NSET=BASE`);
IL:='IL':IW:='IW': IH:='IH':
for IW from 1 to NW+1 do
for IL from 1 to NL+1 do
print(subs(IH=1,IL+(IW-1)*(NL+1)+(IH-1)*(NW+1)*(NL+1))); od; od;
print(`*NSET, NSET=TOP`);
IL:='IL':IW:='IW': IH:='IH':
for IW from 1 to NW+1 do
for IL from 1 to NL+1 do
print(subs(IH=NH+1,IL+(IW-1)*(NL+1)+(IH-1)*(NW+1)*(NL+1))); od; od;
print(`*NSET, NSET=XMIN`);
IL:='IL':IW:='IW': IH:='IH':
for IW from 1 to NW+1 do
for IH from 1 to NH+1 do
print(subs(IL=1,IL+(IW-1)*(NL+1)+(IH-1)*(NW+1)*(NL+1))); od; od;
print(`*NSET, NSET=XMAX`);
IL:='IL':IW:='IW': IH:='IH':
for IW from 1 to NW+1 do
for IH from 1 to NH+1 do
print(subs(IL=NL+1,IL+(IW-1)*(NL+1)+(IH-1)*(NW+1)*(NL+1))); od; od;
print(`*NSET, NSET=YMIN`);
IL:='IL':IW:='IW': IH:='IH':
for IL from 1 to NL+1 do
for IH from 1 to NH+1 do
print(subs(IW=1,IL+(IW-1)*(NL+1)+(IH-1)*(NW+1)*(NL+1))); od; od;
print(`*NSET, NSET=YMAX`);
IL:='IL':IW:='IW': IH:='IH':
for IL from 1 to NL+1 do
for IH from 1 to NH+1 do
print(subs(IW=NW+1,IL+(IW-1)*(NL+1)+(IH-1)*(NW+1)*(NL+1))); od; od;
print(`*STEP, NLGEOM`);
print(`*STATIC`);
print(`*RESTART,WRITE,FREQ=1`);
print(`***BOUNDARY CONDITIONS***`);
print(`*BOUNDARY`);
print(`BASE,3,,0.`);
print(`TOP,3,,0.`);
print(`XMIN,1,,0.`);
print(`XMAX,1,,0.001`);
print(`YMIN,2,,0.`);
print(`YMAX,2,,0.`);
print(`***NODE SET DEFINITION***`);
print(`*ELSET, ELSET=ALLF`);
print(`FIBER1,FIBER2,FIBER3,FIBER4`);
print(`*END STEP`);
close(`wucell.inp`);

```

Vita

Jovan Jovicic was born in Belgrade, Yugoslavia on March 11, 1962. He received a Bachelor of Science Degree in Aeronautical Engineering from the University of Belgrade, Yugoslavia in June 1988 and the Master of Science in Aeronautical Engineering from the same University in February 1994. He was recipient of the prize for the best student in 1983 by the Faculty of Mechanical Engineering, Belgrade, Yugoslavia, as well as recipient of the prize for the best master's thesis in 1994 by the Belgrade Chamber of Commerce.

From September 1988 to September 1989, he worked as a researcher engineer in the Jet Propulsion Lab of the Department of Aeronautical Engineering at Belgrade University. From September 1989 to August 1996, Mr. Jovicic served as a lecturer at the Aeronautical Department of Belgrade University, teaching Theory of Elasticity and Aeroelasticity.

He enrolled at Drexel University, Department of Materials Engineering in October 1996 to pursue a Ph.D. degree. In May 1998, he received Second Presidential Award for Graduates from the Drexel University Chapter of Sigma Xi for the presentation entitled: "Modeling of the Dynamic Response of Ultra High Impact Resistant-Ultra Light Composites.

During his work at Drexel, Mr. Jovicic has published fourteen journal and conference papers in the field of mechanical behavior of composite materials.